Myelination and Synaptogenesis in Olfactory System White Matter Tracts

Lindsay Collins
Millers Creek, NC

B.A. Wake Forest University, 2012
M.A. University of Virginia, 2015

A Dissertation Presented to the Graduate
Faculty of the University of Virginia in Candidacy for the Degree of
Doctor of Philosophy

Department of Psychology

University of Virginia
September 2017

_____

_____

_____

_____

Abstract

The olfactory forebrain is interconnected through two large white matter tracts: the lateral olfactory tract (LOT) transfers information from the olfactory bulb to the ipsilateral olfactory cortex while the anterior commissure (AC) interconnects the left and right olfactory cortices. Chapter 2 provides a developmental characterization of myelination and oligodendrocyte maturation within these two tracts. Results demonstrate that the LOT develops significantly earlier than the AC, exhibits key structural differences in axonal composition and myelination, and responds differently to sensory deprivation. Chapter 3 examines the susceptibility of the LOT and AC to experimental demyelination and whether they might have the capacity to remyelinate, as suggested by their proximity to the subventricular zone. Lysolecithin-induced demyelination and remyelination was examined at multiple post-injection times with electron microscopy. Significant demyelination was seen 7 days post-injection (dpi) in both tracts and evidence of remyelination was observed earlier in the LOT than AC. These findings indicate that the olfactory system could be an important model for studies of myelin regulation and suggest important differences in the capacity to recover from damage between the two tracts. Finally, Chapter 4 provides a detailed analysis of the terminations of axons coursing through the AC and synapsing in the contralateral AON. Axons were visualized by anterograde tracer injections into the AON and synapses were analyzed using electron microscopy. Results demonstrate that synapse formation within regions receiving input from the LOT and AC occurs prior to myelination of the tracts. Together, these studies indicate significant developmental and structural differences between the two tracts that have functional implications.

TABLE OF CONTENTS

Chapter I

General Introduction

Sensory systems offer unique opportunities for gaining insight into neural processing and development. Years of psychophysics and neuroscience research have set the stage for the use of sensory systems as valuable research models with observable output (behavior) and easily manipulated input (sensory stimulation). Sensory systems are particularly useful for understanding neural development because cellular and molecular changes correspond to measurable changes in function. For instance, eye opening marks a significant point in early postnatal development that is accompanied by myriad changes in anatomy, physiology, and connectivity of the visual system (Katz and Shatz, 1996; Sengpiel and Kink, 2002). The following studies further our understanding of the olfactory system, a relatively unstudied sensory system. In particular, the work examines the two white matter tracts that transfer olfactory information by: 1) determining the timing of myelination onset and maturation, 2) testing the susceptibility of each tract to experimentally-induced demyelination and remyelination, and 3) characterizing the morphology and synaptology of axon terminals in a region receiving input from both tracts. After a brief introduction to the olfactory system, this chapter will expand upon each of these ideas in turn.

Overview of the olfactory system

The olfactory system allows mammals to recognize, discriminate, and ascribe significance to odorants. Odorant molecules in the environment bind to receptors located on cilia of olfactory sensory neurons (OSNs) within the nasal cavity. OSN axons project to the olfactory bulb (OB), the first center of olfactory processing in the brain

(Vassar et al., 1994). The OB projects directly to the olfactory peduncle, which encompasses a few distinct areas, the largest of which is the anterior olfactory nucleus (AON). Subsequent processing and integration occurs in the olfactory, or piriform, cortex as well as other regions that do not exclusively process olfactory information, such as the amygdala and hippocampus (Fig. 1).

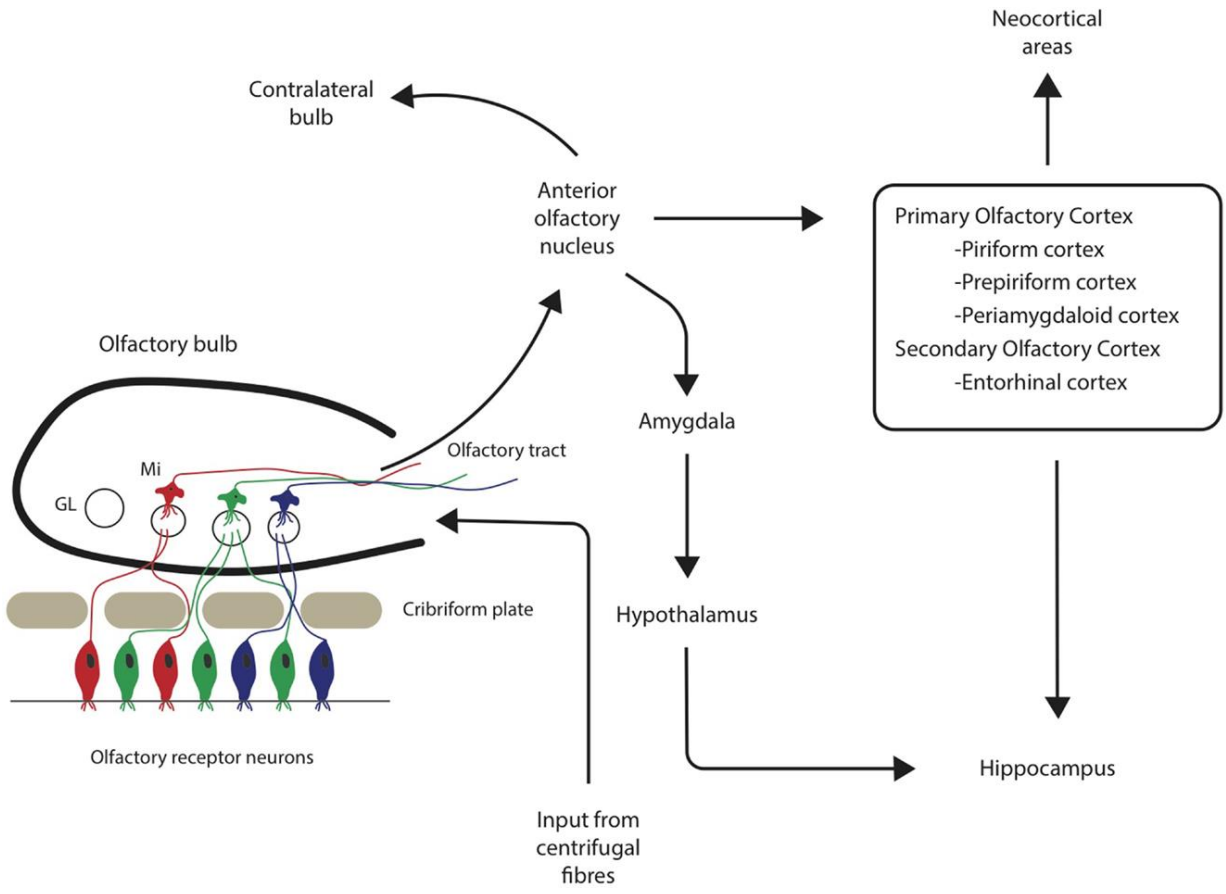

Figure 1 Olfactory system circuitry. Olfactory receptor neurons in the nasal epithelium project to specific glomeruli within the olfactory bulb (OB). Dendrites of mitral (Mi) and tufted cells synapse onto OSNs in the glomerular layer (GL). Axons from mitral and tufted cells project out of the OB, forming the lateral olfactory tract which projects to the anterior olfactory nucleus (AON) and olfactory cortices. Several projections arise from the AON, which transfer information to higher cortical processing centers, contralateral olfactory areas, and the amygdala. Figure taken from Franks et al., 2013.

Olfactory bulb

The OB is a stratified structure consisting of seven layers (Fig. 2b). The most superficial layer, the olfactory nerve layer, includes OSN axons and glial cells. OSN axons converge onto one medial and one lateral glomerulus within the OB (Xu et al., 2000; Meister & Bonhoeffer, 2001; Mori, 2014). Within a glomerulus, OSNs synapse onto projection (mitral and tufted [M/T]) and inhibitory (periglomerular) cells. A layer of plexiform space (external plexiform layer, EPL) separates the glomerular layer from the mitral cell layer, which consists of M/T cell bodies. M/T axons comprise an internal plexiform layer (IPL) and merge to form the lateral olfactory tract (LOT), which innervates the olfactory cortex (Haberly & Price, 1977). The granule cell layer, deep to the IPL, is comprised of GABAergic interneurons that allow for contrast enhancement by inhibiting mitral cells (Shepherd et al., 2007; Urban, 2002). Finally, the center of the OB contains the anterior extension of the rostral migratory stream (RMS). OB interneurons (granule and periglomerular cells) are continuously produced throughout life and migrate into the OB via the RMS (Lledo et al., 2008). For a review of olfactory bulb circuitry and processing, see Mori et al. 2014.

Anterior olfactory nucleus and olfactory cortex

The next level of olfactory processing occurs in the anterior olfactory nucleus (AON), which lies immediately caudal to the OB and surrounds the RMS and anterior limb of the anterior commissure (AC; Fig. 2C-E). Although the structure is termed a nucleus, the AON can be argued to be cortical in nature due to its laminated structure and the presence of pyramidal projection neurons. The AON has two components. Pars

principalis (pP) encircles the RMS and has been divided into pars lateralis, pars dorsalis, pars medialis, and pars ventroposterior on the basis of both location and differences in cytoarchitecture and connectivity (Haberly & Price, 1978a). Pars principalis consists of an outer plexiform layer (layer I) where OB axons terminate, and an inner cell-dense region (layer II). Pars externa lies dorsolateral to pP, emerging slightly anterior to the rostral-most tip of pP. Externa is unique from other AON subregions because it projects exclusively to the contralateral OB (Schwob & Price, 1984), a feature that allows it to play an important role in odor localization (Kikuta et al., 2010). For an extensive review of AON anatomy and connectivity, refer to Brunjes et al., 2005.

The posterior AON transitions into the anterior piriform cortex (PC, Fig. 2E-F), a three-layered cortical structure consisting of an outer plexiform layer (layer I), a high-density cell layer (layer II) and a deeper low-density cellular layer (layer III). The PC receives extensive input from the ipsilateral OB and AON that is segregated into distinct sublayers within layer I (Haberly & Price, 1978b). PC neurons in turn project back to the OB and AON and locally within the PC itself. The PC also projects to the nucleus of the olfactory tract, the amygdala, the periamygdaloid cortex, and the entorhinal cortex (Haberly & Price, 1978b).

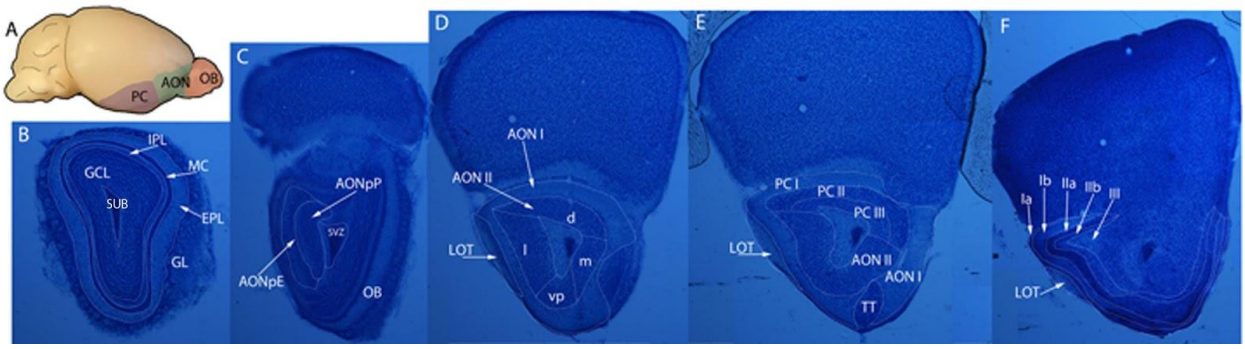

Figure 2 Anatomy of the olfactory system. (A) Lateral view of the mouse brain showing the location of the OB (orange), AON (green) and PC (purple). (B-F) Coronal sections stained with cresyl violet through the OB, AON, and PC. (B) The stratifications of the OB can be distinguished by cell density and organization. From superficial to deep, OB layers are: olfactory nerve layer, glomerular layer (GL), external plexiform layer (EPL), mitral cell layer (MC), internal plexiform layer (IPL), granule cell layer (GCL), and the subependymal layer (SUB), which contains the RMS. (C) Posterior to the OB, the AONpE emerges as a band of cells lateral to AONpP. SVZ=subventricular zone. (D) Continuing posteriorly, the AONpP can be seen as a ring of cells encircling the SVZ. l=pars lateralis, d=pars dorsalis, m=pars medialis, vp=pars ventroposterior. The LOT lies adjacent to pars lateralis. Note that the OB can still be seen on the medial side. (E) AON-PC transition zone. At this level the AONpP merges with the anterior PC, which is subdivided into three layers. The tenia tecta (TT) lies ventral to pars ventroposterior. (F) The piriform cortex is a three-layered structure deep to the LOT. Layers I and II can be further subdivided into Ia, Ib, IIa, and IIb based on cytoarchitecture.

Olfactory white matter tracts: overview

Two large white matter tracts exist within the olfactory system, allowing for mass information transfer between olfactory processing areas (Fig. 3A). As previously referenced, the LOT consists of mitral and tufted cell axons exiting the OB and innervating all areas of the ipsilateral olfactory cortex. In coronal sections, the LOT can be seen emerging from the OB and continuing through the AON to the caudal most region of the PC. The LOT is present as a band along the lateral edge of the AON and wraps around to the dorsal side underneath the frontal cortex (Fig. 2D). In the posterior AON the LOT coalesces to form a discrete bundle along the ventrolateral surface of the brain, which continues as far posterior as the amygdala.

Contralaterally-projecting axons arise in the AON and anterior PC and travel across the midline via the AC. The AC can be seen at the level of bregma as a thick band of myelinated axons (Fig. 3C). The AC is comprised of an anterior (or olfactory) limb, a posterior limb that connects the amygdala in each hemisphere, and the commissural portion of the stria terminalis. The focus of the work presented here is on the anterior limb of the AC, which courses alongside the RMS and lateral to the subventricular zone in coronal AON sections (Fig. 3B). Axons in the AC project to the contralateral AON, anterior PC, and granule cell layer of the OB (Haberly and Price, 1978a; Haberly and Price, 1978b; Schwob and Price, 1984).

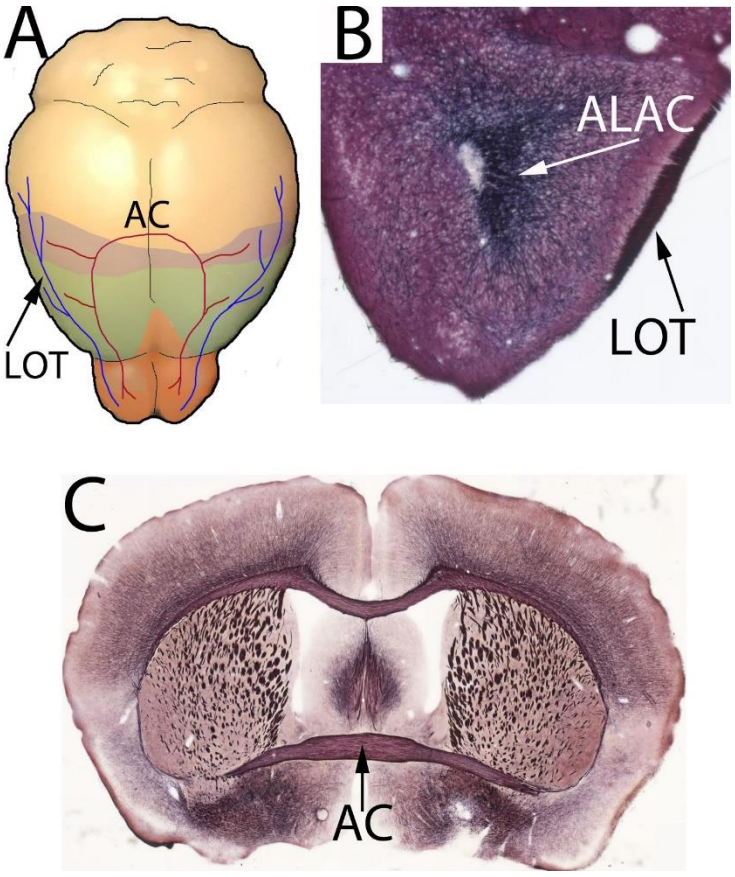

Figure 3 White matter tracts of the olfactory system. (A) The LOT (blue) originates in the OB (orange) from mitral and tufted cells. These axons project ipsilaterally, with collaterals innervating the AON (green) and olfactory cortex (purple). The AC (red) contains fibers arising from projection neurons in the AON and P. These fibers innervate the contralateral OB, AON, and PC, providing a pathway for interhemispheric communication in the olfactory system. (B) In a coronal section through the AON that has been stained for myelin, both the LOT and AC can be seen. At this point, the LOT forms a thin band along the ventrolateral surface of the brain. Fibers of the anterior limb of the AC can be seen lateral to the rostral migratory stream. Myelinated fibers can also be seen coursing laterally out of the ALAC into the AON. (C) In a myelin-stained coronal section taken slightly anterior to bregma, the AC can be seen as it crosses the midline, forming a thick band of braided myelinated fibers.

Chapter 2: Developmental myelination of the LOT and AC

Myelination is a complex process that requires the coordinated development of axons and glial cells (Aggarwal et al., 2011) and differs in timing between systems within the brain (Sampaio and Truwit, 2001; Foran and Peterson, 1992). Sensory systems develop faster than associational and motor circuits, and the LOT develops very early in comparison to other white matter tracts. The early development of the LOT contributes to a functional olfactory system at birth, which is necessary for survival (Logan et al., 2012). Using transgenic mice expressing GFP in M/T cells, Walz et al. (2006) demonstrated that axons of M/T cells emerge around embryonic day (E)12, not long after the formation of the telencephalic vesicle. Guidepost cells (or lot cells; Tomioka et al., 2000) provide a scaffolding for mitral and tufted cell axons that can be seen as early as E13 (Schwob and Price, 1984; Brunjes and Frazier, 1986). After axons are established myelination occurs, corresponding with an increase in conduction velocity (measured by electrically stimulating the OB and recording from the PC), and continues until after postnatal day (P)15 in rats (Schwob et al., 1984). A similar investigation of developmental conduction velocity changes in the LOT does not exist for mice.

While the literature on the development of the AC is scarce, it is apparent that it develops later than the LOT. An analogous structure to guidepost cells in commissural fiber tracts is a glial sling, formed by neurons originating in the lateral ganglionic eminence and migrating to form pathways on which commissural axons extend (Shu et al., 2003). The cells that form the glial sling of the corpus callosum and AC in mice begin migrating away from the lateral ventricle at E15, and form the callosal sling by

E17 (Silver et al., 1982). In mice, a significant increase in the number of axons making up the AC occurs from E16 to P11. The first evidence of myelination has been reported to be observed around P8, with a continuous increase in the percent of axons that are myelinated through life, although this percentage plateaus around P30. (Sturrock, 1975). Behavioral studies confirm that the AC develops later than the LOT. For example, rats that have been classically conditioned with one naris reversibly occluded cannot access trained olfactory memories from the contralateral side until P12, suggesting this time point as a significant milestone in the development of commissural fibers in the rat olfactory system (Kucharski and Hall, 1988).

Oligodendrocyte maturation

The maturation of oligodendrocytes, the myelin-forming cell of the central nervous system, has been extensively studied and well-characterized (Aggarwal et al., 2011). Oligodendrocyte maturation progresses in a stereotyped sequence of morphological and molecular changes (Fig. 4). As a result, well-established markers are available for most stages of oligodendrocyte maturation. Neural stem cells (NSCs) that will eventually become oligodendrocytes are first seen along the neural tube (Simons et al., 2007). During early embryologic development, these NSCs are found in the lateral, caudal, and medial ganglionic eminences and express specific transcription factors according to each cell's eventual destination and cellular fate. Platelet-derived growth factor α (PDGFα) along with sonic hedgehog and the transcription factor Olig1 are transiently expressed in order to allow for this migration as well as the differentiation of NSCs into oligodendrocyte precursor cells (OPCs; Balasubramaniyan et al., 2004; Dai et al., 2015; Vora et al., 2011). OPCs express neural/glial antigen 2 (NG2), an integral

membrane proteoglycan that is found in oligodendrocytes beginning during the progenitor period and extending through this early stage of post-differentiated oligodendrocyte maturation (Silbereis, 2010; Baumann & Pham-Dinh, 2001). Once the cell is no longer mitotically active, it is considered an immature oligodendrocyte. These pre-myelinating oligodendrocytes generate large amounts of plasma membrane (5-50x10^3 um^2/day; Miron et al., 2011) that extend to nearby axons (Fig. 5B). Molecular cues influenced by axonal activity help guide the myelin membranes to surrounding axons – as many as 40 different axonal segments per oligodendrocyte (Miron et al., 2011). Once there, myelin basic protein (MBP) as well as myelin-associated oligodendrocyte basic protein and proteolipid protein aids in compaction of the sheath and formation of functional subunits. At this point the oligodendrocyte is a fully mature, myelinating cell.

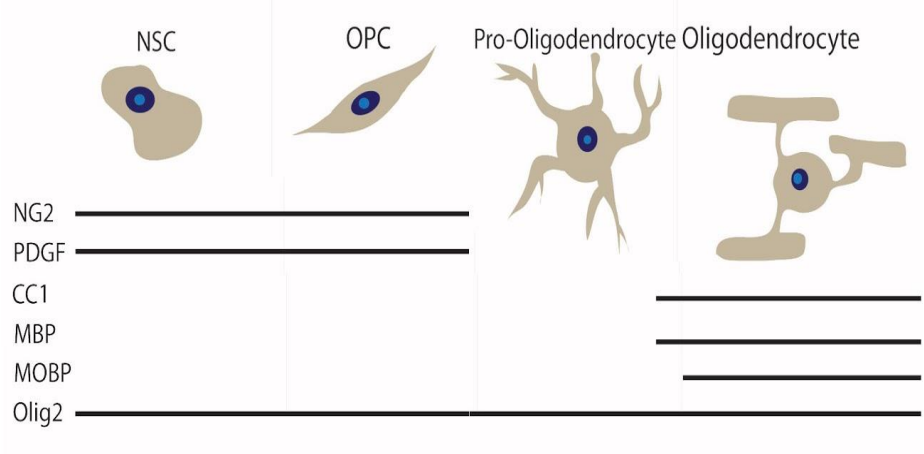

Figure 4 Molecular markers of oligodendrocyte maturation. Olig2 is a transcription factor expressed throughout oligodendrocyte development, and as such can be used as an indicator of the presence of oligodendrocyte populations at all stages of maturity. NG2 and PDGF are markers of early development. Both are expressed in many precursor cell types, including oligodendrocyte precursor cells. Mature oligodendrocytes express CC1 and mature myelin sheaths can be marked by the expression of MBP and MOBP.

While axonal development has been examined in the AC and LOT, myelination onset and development has not been well studied. Chapter 2 addresses these issues in two ways. First, the previously described molecular markers (Olig2, PDGF, NG2, CC1, MBP) are used to characterize the timing of oligodendrocyte maturation within the LOT and AC. The second study takes a closer look at developmental myelination using electron microscopy (EM). Additionally, unilateral sensory deprivation is used to assess the importance of sensory input on the initial myelination of the LOT and AC.

Electron microscopy

In the second study presented in Chapter 2, EM is used for a more accurate estimate of the percentage of axons that have begun myelination or that are fully myelinated at any given time point, as well as density and caliber of myelinated axons.

Oligodendrocytes can be distinguished in EM micrographs because of darkly stained cytoplasm and clumped chromatin (Peters et al., 1991). When an oligodendrocyte is seen contacting an axon but not yet completely wrapping around, the axon is considered pro-myelinated (Fig. 5A). Oligodendrocytes only remain in this stage of development for about twelve hours in mammals (Almeida and Lyons, 2014), so the presence of pro-myelinated axons indicates that myelination onset has recently occurred. The leading edge of the myelin membrane, which first makes contact with the axon, wraps around the axon and can be seen as an inner tongue (Fig. 5A, C). The myelin membrane initially wraps loosely around the axon; after a few wraps the cytoplasm is removed and the myelin membranes bind. This process is called compaction and is necessary for increasing conduction velocity (Salami et al., 2003).

When a myelinated axon is cross-sectioned, the myelin membrane can be seen wrapping around and forming intercalated darkly- and lightly- stained lines (Fig. 5C). The inner myelin membrane is brought together through the interaction of negatively charged cytoplasmic membranes and positively charged myelin basic protein (MBP), found in between the two membranes. This layer is electron-dense and shows up as dark bands in EM, so it is also referred to as the major dense line (MDL). The extracellular lipid layers that make up the outer membrane contain proteolipid protein (PLP), which attract other PLP molecules through homophilic interactions. Tryptophan is also found in this layer and interacts with opposing galactocerebrosides, bringing the myelin rings closer together. These proteins are electron-light and together are referred to as intraperiod lines (IPL). (Aggarwal et al., 2011; Barkovich, 2000)

Myelin sheaths form functionally and molecularly distinct segments (Fig. 5D-E). The internode makes up the majority of myelinated segments and consists of tightly compacted myelin, as described previously. Adjacent to the internode lies the juxtaparanode, which also consists of compact myelin. The juxtaparanode strongly adheres to the axon through the juxtaparanodal complex and forms a barrier between the internode and the paranode. The juxtaparanode is characteristically high in potassium channel expression. The paranode serves as a barrier between the potassium channels found in the juxtaparanode and the node of Ranvier. If this barrier breaks down, as is seen in mouse models of demyelination as well as multiple sclerosis (MS) in humans, the juxtaparanode comes into contact with the node of Ranvier and propogation down the axon is weakened. The node of Ranvier, flanked by paranodes, is a small break in myelination. At this point the axon aggregates a high concentration of

ion channels and transporters, providing the basis for saltatory conduction. (Zoupi et al., 2011)

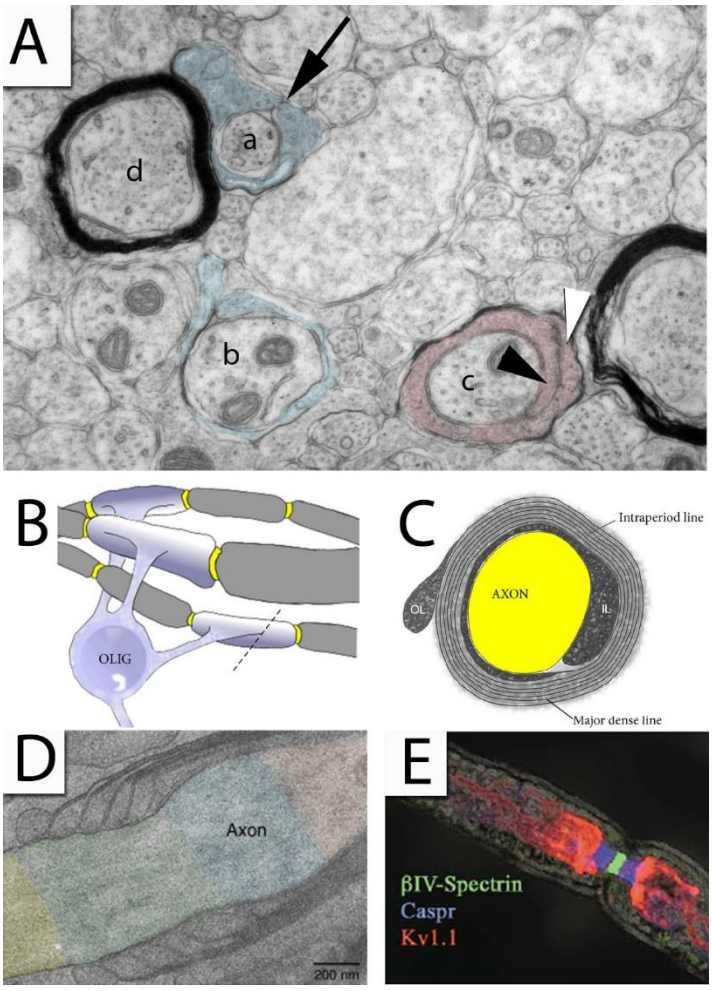

Figure 5 Ultrastructure of myelin sheaths. A) EM micrograph of the mouse AC at P15 taken at 10,000x. Multiple stages of oligodendrocyte development are visible. Axon (a) has been surrounded by an oligodendrocyte process. The process has tucked under, forming the inner tongue in axon (b). An inner and outer tongue is apparent in axon (c). The sheath surrounding this axon has yet to be compacted. Axon (d) is an example of a compacted myelinated axon. B) Oligodendrocytes have many projections that myelinate different axons or axonal segments. Image taken from Greer, 2013. C) The MDL is formed by the binding of the two layers of the bilayered myelin membrane. The point of contact between myelin membranes is seen as the IPL. Image taken from Greer, 2013. D) High pressure freezing-prepared EM micrograph showing functional subunits of the myelin sheath in a longitudinal section of a myelinated axon. The node (yellow) is an unmyelinated segment. The paranode (green) is the point of contact between the axon and myelin sheath. The juxtaparanode (blue) contains a high density of potassium channels, and the internode (pink) forms the center of each myelinated segment. Image adapted from Mobius et al., 2010. E) Immunofluorescence imaging of functional subunits of the myelin sheath. βIV-Spectrin aids in clustering of sodium channels at the node of ranvier. Caspr is a contactin-associated protein localized to paranodes that aids in adhesion of myelin membranes to axons. Kv1.1 labels potassium channels and is expressed in the juxtaparanodes. Image taken from Salzer, 2003.

Naris occlusion

In addition to characterizing normal myelination, unilateral naris occlusion is used as a sensory deprivation paradigm to assess the role of sensory activity on

developmental myelination of the LOT and AC. Unilateral naris occlusion is a well-established method in olfactory research that results in significant alterations to the development of the olfactory system, such as a 25% reduction in ipsilateral OB size and a 30% reduction in ipsilateral AON size (Brunjes, 1994; Brunjes et al., 2014; Coppola, 2012; Frazier & Brunjes, 1988). Unilateral naris occlusion does not affect the size of the LOT or number of mitral cells (Benson et al., 1984; Frazier & Brunjes, 1988) and a previous study did not observe any differences in staining for myelin in naris-occluded mice (Philpot et al., 1995). However, decreased neural activity has been correlated with alterations in myelination onset and maintenance in multiple central nervous system circuits. A particularly intriguing experiment compared myelination of the prefrontal cortex in normal and socially isolated mice pups. While the density of myelinated axons did not change, the myelinating oligodendrocytes were morphologically immature (Makinodan et al., 2012). In the optic nerve, sensory deprivation alters myelin formation as well as conduction velocity (Etxeberria et al. 2016). The mechanism underlying myelin plasticity in early life is likely dependent upon synaptic contacts between axons and OPCs such that more active neurons secrete molecules (i.e. glutamate, ATP, Fyn kinase) that signal surrounding OPCs to generate myelin sheaths and contact axons (Petersen and Monk, 2015). It is predicted that decreased sensory input due to naris occlusion will result in changes to myelination onset and/or oligodendrocyte maturation in the LOT and AC as a result of decreased sensory activity.

Chapter 3: Experimental Demyelination and Remyelination in the LOT and AC

Chapter 3 builds upon the first experiment by exploring demyelination and remyelination within the AC. Demyelinating disorders are particularly difficult to study

due to complex interactions between neurons, myelinating cells, and other glial cells (Franklin, 2002). The most common demyelinating disorder is MS, an autoimmune disease related to inflammation in which mature myelin sheaths degenerate. Symptoms caused by demyelination in MS include loss of vision, weakness of limbs, neuropathic pain, lack of coordination, and cognitive difficulties. MS affects ~400,000 people in the United States and 2.5 million people across the world (Tulman, 2013).

The causes of MS are unclear, although the disease has been strongly associated with neuroinflammation, genetic factors and environmental factors (Naegele and Martin, 2014). More recent evidence also suggests a role for microglial activation and axonal ion imbalance (Mahad et al., 2015). It is likely that these factors influence one another and come together to form MS pathology, each factor being most significant at a different time point of disease progression. At the onset of the disease, it is proposed that an immune response (possibly elicited by the presence of an infection) triggers microglial activation and oligodendrocyte degeneration. OPC cells have been found in higher quantities in areas surrounding lesions, so it is likely that the system is trying to compensate for cell degeneration. These OPCs do not reach maturity and remyelinate axons, but the factors preventing their maturity are not known.

Other less common demyelinating disorders include acute-disseminated encephalomyelitis, progressive multifocal leukencephalopathy, central myelinolysis and extrapontine myelinolysis, among others. These pathologies can be a result of many factors - from the presence of certain viruses (such as HIV) to alcoholism, cardiac arrest, or nerve compression. Abnormal myelination is also observed in schizophrenia (Takahashi et al., 2011), Alzheimer's disease (Gold et al., 2012), and cognitive decline

associated with aging (Peters, 2009). Taken together, demyelinating disorders represent a significant burden on public health and as such have received much scientific interest.

Several methods of experimentally inducing demyelination are currently available. To closely mimic the disease progression of autoimmune-mediated demyelinating disorders such as multiple sclerosis (MS), T-cell activating techniques can be used, such as experimental autoimmune encephalomyelitis (EAE). The EAE model has been useful in understanding interactions between the immune and nervous system, but does not allow for tight control of the location or extent of demyelination (Gold et al., 2006). To regulate demyelination without directly affecting immune cells, toxin-based methods can be used. Three commonly used demyelinating toxins are cuprizone, ethidium bromide, and lysolecithin. Cuprizone is a systemic toxin that is administered in the animal's food, resulting in widespread demyelination throughout the central nervous system. Ethidium bromide and lysolecithin are injectable toxins that selectively break down myelin membranes (although ethidium bromide has been shown to also damage nearby axons and astrocytes; Woodruff and Franklin, 1999).

In Chapter 3, the demyelinating agent lysolecithin is injected into the AC. Lysolecithin was chosen to provide 1) the ability to do localized injections and avoid widespread myelin damage and 2) the ability to examine both de- and remyelination, which occur about one week and one month post-injection, respectively. Lysolecithin has been used to study demyelination and remyelination in the mammalian corpus callosum (Etxeberria et al., 2010; Hoflich et al., 2016), optic tract (Pourabdolhossein et al., 2014; Dehghan et al., 2016), and spinal cord (Hall, 1972; Jeffrey and Blakemore,

1995; Keough et al., 2015; Ousman and David, 2000). However, no published work exists evaluating its effects within the olfactory system. Chapter 3 demonstrates that the LOT and AC both undergo extensive demyelination following lysolecithin administration and that recovery proceeds more quickly in the LOT.

Chapter 4: Synaptic characterization of AC projections

Developmental changes in myelination during early life increase the speed of signal processing in the LOT (Schwob et al., 1984) and other white matter tracts (Fields, 2008). Preliminary data presented in Chapter 2 have identified short (~72 hour) periods of rapid myelination in both the LOT and AC that are separated by 3-4 days. Ipsilateral and contralateral input into the AON is carried by the LOT and AC, respectively, which innervate distinct layers of the AON. If myelination onset is activity-dependent, then synaptic formation within layers receiving ipsilateral input from the LOT should precede that of layers receiving contralateral input via the AC. Therefore, chapter 4 is designed to test whether timing of rapid myelination of the LOT and AC corresponds with substantial alterations to the distribution of synapses formed in the AON.

AON anatomy and connectivity

As mentioned above, the AON is a cortical structure with strict lamination. The most superficial layer (layer I) is a plexiform, or molecular, layer largely consisting of neuropil with few neuronal and glial cell bodies. Layer I is often subdivided based on input patterns. Layer Ia lies immediately adjacent to the LOT and contains axon collaterals from the OB, while layer Ib lies deeper and contains association fibers from the PC and contralateral AON (Brunjes et al., 2005; Friedman and Price, 1984). Layer II is a cell-dense zone containing pyramidal cells that extend spiny apical dendrites into

layer I (Brunjes et al., 2005). Based on evidence of different neurochemical phenotypes and cell density, layer II has also been divided into superficial layer IIa and deeper IIb zones (Meyer et al., 2006).

Olfactory System Development

The olfactory system develops early, with neurogenesis of mitral cells in the OB initiated as early as embryonic day (E)10 (Lopez-Mascaraque and Castro, 2002; Bayer, 1983; Hinds, 1968), axons extending to form the LOT around E13 (Walz et al., 2006), and by birth substantial synaptogenesis has occurred in the OB and olfactory cortices (Hinds and Hinds, 1976). Development of the AON is substantially delayed. For example, neurogenesis largely occurs between E15 and 21 (Bayer, 1986). Interestingly, neurogenesis of the PC begins around the same time as the OB (E9.5-10; Lopez-Mascaraque and Castro, 2002), suggesting that neurogenesis in the AON and PC occurs independent of OB innervation. Around the time neurons are first seen forming the AON, axons emerge from AON and PC cells and begin to form the AC (~E16; Silver et al., 1982). Note that the initial formation of the AC is significantly later than that of the LOT.

Sensory systems typically develop in a trajectory that mirrors circuitry: primary sensory regions are established and reach maturity earlier than subsequent processing regions (Hooks and Chen, 2007; Sur and Leamey, 2001; Wong, 1999). The postnatal development of the olfactory system proceeds similarly, although within the PC and AON development proceeds in a caudal-rostral fashion (Schwob and Price, 1984). The development of olfactory pathways follows this developmental trend: Chapter 2 demonstrates that the LOT (connecting the OB to olfactory cortices) initiates myelination

around P7 while myelination in the AC (connecting olfactory cortices across hemispheres) is not apparent until P11.

Synapse Analysis

Increases in volumetric density of synapses can be used as a measure of circuit development. During development there is an overproduction of synapses, often followed by a period of synaptic pruning across brain regions (Andersen 2003; Elston et al., 2009; Levitt, 2003; Petanjek et al, 2011). Within layers of sensory cortices, most synapses are created around the same time (Rakic et al., 1986) and pruned if spontaneous and evoked neural activity is low (Hooks and Chen, 2006). In the visual system, large increases in rates of synaptogenesis are observed around the time of eye opening (Maslim and Stone, 1986; Vogel, 1978).

Synapses onto pyramidal cells of the PC have been previously examined using EM (opossum: Haberly and Feig, 1983; Haberly and Behan, 1983; rat: Westrum, 1975; Schikorski and Stevens, 1999; mouse: Derer et al., 1977; Fig. 6). Synapses in the pyramidal PC are numerous at birth, are largely asymmetric, and are made onto dendritic spines. Differences in synaptology between layers of the PC have also been reported. Schikorski and Stevens (1999) compared synapses in PC layer Ia (afferent projections from the OB) to layer Ib (recurrent connections from the olfactory cortex) and found a significantly lower density of docked and reserve vesicles in layer Ia (Fig. 6). The morphological differences between layer Ia and Ib correlate with physiology - Layer Ia shows paired-pulse facilitation, while Ib does not (Bower & Haberly, 1986). This difference is functionally relevant because paired-pulse facilitation indicates the capacity for presynaptic plasticity. Together, the morphological and electrophysiological

differences between layers suggest functional segregation of olfactory processing within the PC.

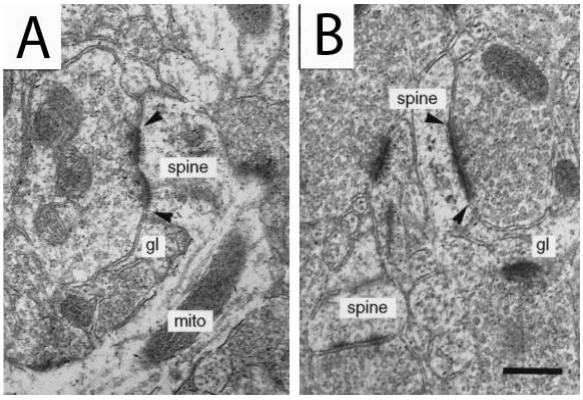

Figure 6 Visualization of PC synapses. EM micrographs of layer Ia (A) and layer Ib (B) of synapses onto dendritic spines in the mouse PC. In these asymmetric synapses, vesicles, a cleft, and a PSD (arrowheads) can be clearly seen. Note the high packing density of Ib terminals compared to that of Ia. The synapse depicted in (A) is perforated. Mitochondria (mito) and glial processes (gl) are also shown. Scale bar = 0.5μm. Image taken from Schikorski and Stevens, 1999.

Within the AON, differences in connectivity between layers suggests that functional segregation likely exists, but to date there have been no studies of the synaptic organization of the AON. Chapter 4 builds upon the results found in the previous two chapters by closely examining the developmental synaptology of the region in order to determine the temporal relationship between myelinogenesis in the AC and synaptogenesis in the AON. In the visual system, myelination and synaptogenesis occur at the same time, triggered by an explosive increase in neural activity at eye opening (Shepherd, 2003). The timing of these processes suggests that initiation of both myelination and synaptogenesis are activity-dependent. Findings presented in chapter 4 indicate that synaptogenesis within the AON occurs before the corresponding axons are myelinated, pointing to a role of synaptic activity in initiation of LOT and AC myelination.

Literature Cited

Aggarwal, S., Yurlova, L., Simons, M. (2011). Central nervous system myelin: structure, synthesis, and assembly. *Trends in Cell Biology. 21*(10)585-593.

Almeida, R. G., & Lyons, D. A. (2014). On the resemblance of synapse formation and CNS myelination. *Neuroscience*, *276*, 98-108.

Andersen, S. L. (2003). Trajectories of brain development: point of vulnerability or window of opportunity?. *Neuroscience & Biobehavioral Reviews*, *27*(1), 3-18.

Balasubramaniyan, V., Timmer, N., Kust, B., Boddeke, E., & Copray, S. (2004). Transient expression of Olig1 initiates the differentiation of neural stem cells into oligodendrocyte progenitor cells. *Stem Cells. 22*(6):878-882.

Barkovich, A. J. (2000). Concepts of myelin and myelination in neuroradiology. *American Journal of Neuroradiology*, *21*(6), 1099-1109.

Baumann, N. & Pham-Dinh, D. (2001). Biology of oligodendrocyte and myelin in the mammalian central nervous system. *Physiological Reviews. 81*(2):871-927.

Bayer, S. A. (1983). 3 H-thymidine-radiographic studies of neurogenesis in the rat olfactory bulb. *Experimental Brain Research*, *50*(2), 329-340.

Bayer, S. A. (1986). Neurogenesis in the rat primary olfactory cortex. *International journal of developmental neuroscience*, *4*(3), 251-271.

Benson, T. E., Ryugo, D. K., & Hinds, J. W. (1984). Effects of sensory deprivation on the developing mouse olfactory system: a light and electron microscopic, morphometric analysis. *Journal of Neuroscience*, *4*(3), 638-653.

Bower, J. M., & Haberly, L. B. (1986). Facilitating and nonfacilitating synapses on pyramidal cells: a correlation between physiology and morphology. *Proceedings*

of the National Academy of Sciences, *83*(4), 1115-1119.

Brunjes, P. C., & Frazier, L. L. (1986). Maturation and plasticity in the olfactory system of vertebrates. *Brain Research Reviews*, *11*(1), 1-45.

Brunjes, P. (1994). Unilateral naris closure and olfactory system development. *Brain Research Reviews. 19*(1): 146-160.

Brunjes, P. C., Illig, K. R., & Meyer, E. A. (2005). A field guide to the anterior olfactory nucleus (cortex). *Brain research reviews*, *50*(2), 305-335.

Brunjes, P., Collins, L., Osterberg, S., Phillips, A. (2014). The mouse olfactory peduncle. 3. Development of neurons, glia, and centrifugal afferents. *Frontiers in Neuroanatomy. 8*(4).

Coppola, D. (2012). Studies of olfactory system neural plasticity: the contribution of the unilateral naris occlusion technique. *Neural Plasticity. 2012.*

Dai, J., Bercury, K., Ahrendsen, J., & Macklin, W. (2015). Olig1 function is required for oligodendrocyte differentiation in the mouse brain. *The Journal of Neuroscience. 35*(10):4386-4402.

Dehghan, S., Hesaraki, M., Soleimani, M., Mirnajafi-Zadeh, J., Fathollahi, Y., & Javan, M. (2016). Oct4 transcription factor in conjunction with valproic acid accelerates myelin repair in demyelinated optic chiasm in mice. *Neuroscience*, *318*, 178-189.

Derer, P., Caviness, V. S., & Sidman, R. L. (1977). Early cortical histogenesis in the primary olfactory cortex of the mouse. *Brain research*, *123*(1), 27-40.

Elston, G. N., Oga, T., & Fujita, I. (2009). Spinogenesis and pruning scales across functional hierarchies. *Journal of Neuroscience*, *29*(10), 3271-3275.

Etxeberria, A., Mangin, J. M., Aguirre, A., & Gallo, V. (2010). Adult-born SVZ

progenitors receive transient synapses during remyelination in corpus callosum. *Nature neuroscience*, *13*(3), 287-289.

Etxeberria, A., Hokanson, K., Dao, D., Mayoral, S., Mei, F., Redmond, S., Ullian, E., Chan, J. (2016). Dynamic modulation of myelination in response to visual stimuli alters optic nerve conduction velocity. *The Journal of Neuroscience. 36*(26):6937-6948.

Fields RD. (2008). White matter in learning, cognition and psychiatric disorders. *Trends Neurosci* 30:361–70.

Foran, D. R., & Peterson, A. C. (1992). Myelin acquisition in the central nervous system of the mouse revealed by an MBP-Lac Z transgene. *Journal of Neuroscience*, *12*, 4890-4890.

Franklin, R. J. (2002). Why does remyelination fail in multiple sclerosis?. *Nature Reviews Neuroscience*, *3*(9), 705-714.

Frazier, L. & Brunjes, P. (1988). Unilateral odor deprivation: early postnatal changes in olfactory bulb cell density and number. *Journal of Comparative Neurology. 269*:355-370.

Friedman, B., & Price, J. L. (1984). Fiber systems in the olfactory bulb and cortex: a study in adult and developing rats, using the Timm method with the light and electron microscope. *Journal of Comparative Neurology*, *223*(1), 88-109.

Gold, R., Linington, C., & Lassmann, H. (2006). Understanding pathogenesis and therapy of multiple sclerosis via animal models: 70 years of merits and culprits in experimental autoimmune encephalomyelitis research. *Brain*, *129*(8), 1953-1971.

Gold, B. T., Jiang, Y., Powell, D. K., & Smith, C. D. (2012). Multimodal imaging

evidence for axonal and myelin deterioration in amnestic mild cognitive impairment. *Journal of Alzheimer's Disease*, *31*(s3), S19-S31.

Greer, J. M. (2013). Autoimmune T-cell reactivity to myelin proteolipids and glycolipids in multiple sclerosis. *Multiple sclerosis international*, *2013*.

Haberly, L., & Behan, M. (1983). Structure of the piriform cortex of the opossum. III. Ultrastructural characterization of synaptic terminals of association and olfactory bulb afferent fibers. *Journal of Comparative Neurology*, *219*(4), 448-460.

Haberly, L. B., & Feig, S. L. (1983). Structure of the piriform cortex of the opossum. II. Fine structure of cell bodies and neuropil. *Journal of Comparative Neurology*, *216*(1), 69-88.Haberly, L., & Price, J. (1977). The axonal projection patterns of the mitral and tufted cells of the olfactory bulb in the rat. *Brain Research. 129*(1):152-157.

Haberly, L. & Price, J. (1978). Association and commissural fiber systems of the olfactory cortex of the rat I. Systems originating in the piriform cortex and adjacent areas. *Journal of Comparative Neurology. 178 :* 711-740.

Haberly, L. & Price, J. (1978). Association and commissural fiber systems of the olfactory cortex of the rat II. Systems originating in the olfactory peduncle. *Journal of Comparative Neurology. 181:* 781-808.

Hall, S. (1972). The effect of injections of lysophosphatidyl choline into white matter of the adult mouse spinal cord. *Journal of cell science*, *10*(2), 535-546.

Hinds, J. W. (1968). Autoradiographic study of histogenesis in the mouse olfactory bulb Time of origin of neurons and neuroglia. *Journal of Comparative Neurology*, *134*(3), 287-304.

Hinds, J. W., & Hinds, P. L. (1976). Synapse formation in the mouse olfactory bulb. Quantitative studies. *Journal of Comparative Neurology*, *169*(1), 15-40.

Höflich, K. M., Beyer, C., Clarner, T., Schmitz, C., Nyamoya, S., Kipp, M., & Hochstrasser, T. (2016). Acute axonal damage in three different murine models of multiple sclerosis: A comparative approach. *Brain Research*, *1650*, 125-133.

Hooks, B. M., & Chen, C. (2006). Distinct roles for spontaneous and visual activity in remodeling of the retinogeniculate synapse. *Neuron*, *52*(2), 281-291.

Jeffery, N. D., & Blakemore, W. F. (1995). Remyelination of mouse spinal cord axons demyelinated by local injection of lysolecithin. *Journal of neurocytology*, *24*(10), 775-781.

Katz, L. C., & Shatz, C. J. (1996). Synaptic activity and the construction of cortical circuits. *Science*, *274*(5290), 1133.

Keough, M. B., Jensen, S. K., & Yong, V. W. (2015). Experimental demyelination and remyelination of murine spinal cord by focal injection of lysolecithin. *JoVE (Journal of Visualized Experiments)*, (97), e52679-e52679.

Kikuta, S., Sato, K., Kashiwadani, H., Tsunoda, K., Yamasoba, T., & Mori, K. (2010). Neurons in the anterior olfactory nucleus pars externa detect right or left localization of odor sources. *Proceedings of the National Academy of Sciences*, *107*(27), 12363-12368.

Kucharski, D. & Hall, W. (1988). Developmental change in the access to olfactory memories. *Behavioral Neuroscience. 102*(3):340-348.

Levitt, P. (2003). Structural and functional maturation of the developing primate brain. *The Journal of pediatrics*, *143*(4), 35-45.

Lledo, P. M., Merkle, F. T., & Alvarez-Buylla, A. (2008). Origin and function of olfactory bulb interneuron diversity. *Trends in neurosciences*, *31*(8), 392-400.

Logan, D., Brunet, L., Webb, W., Cutforth, T., Ngai, J., Stowers, L. (2012). Learned recognition of maternal signature odors mediates the first suckling episode in mice. *Current Biology. 22*(21)1998-2007.

Lopez-Mascaraque, L., & De Castro, F. (2002). The olfactory bulb as an independent developmental domain. *Cell death and differentiation*, *9*(12), 1279.

Mahad, D. H., Trapp, B. D., & Lassmann, H. (2015). Pathological mechanisms in progressive multiple sclerosis. *The Lancet Neurology*, *14*(2), 183-193.

Makinodan, M., Rosen, K., Ito, S., & Corfas, G. (2012). A critical period for social experience-dependent oligodendrocyte maturation and myelination. *Science. 337*:1357-1360.

Maslim, J., & Stone, J. (1986). Synaptogenesis in the retina of the cat. *Brain research*, *373*(1), 35-48.

Meister, M., & Bonhoeffer, T. (2001). Tuning and topography in an odor map on the rat olfactory bulb. *Journal of Neuroscience*, *21*(4), 1351-1360.

Meyer, E. A., Illig, K. R., & Brunjes, P. C. (2006). Differences in chemo-and cytoarchitectural features within pars principalis of the rat anterior olfactory nucleus suggest functional specialization. *Journal of Comparative Neurology*, *498*(6), 786-795.

Miron, V., Kuhlmann, T., & Antel, J. (2011). Cells of the oligodendroglial lineage, myelination, and remyelination. *Biochemica et Biophysica Acta (BBA) - Molecular Basis of Disease. 1812*(2):184-193.

Möbius, W., Cooper, B., Kaufmann, W. A., Imig, C., Ruhwedel, T., Snaidero, N., ... & Varoqueaux, F. (2010). Electron microscopy of the mouse central nervous system. *Methods in cell biology*, *96*, 475-512.

Mori, K. (2014). Odor Maps in the Olfactory Bulb. In *The Olfactory System* (pp. 59-69). Springer Japan.

Naegele, M., & Martin, R. (2014). The good and the bad of neuroinflammation in multiple sclerosis. *Handb Clin Neurol*, *122*, 59-87.

Ousman, S. S., & David, S. (2000). Lysophosphatidylcholine induces rapid recruitment and activation of macrophages in the adult mouse spinal cord. *Glia*, *30*(1), 92-104.

Petanjek, Z., Judaš, M., Šimić, G., Rašin, M. R., Uylings, H. B., Rakic, P., & Kostović, I. (2011). Extraordinary neoteny of synaptic spines in the human prefrontal cortex. *Proceedings of the National Academy of Sciences*, *108*(32), 13281-13286.

Peters, A., Palay, S., & Webster, H. (1991). *The fine structure of the nervous system. Third edition.* Oxford University Press. 532

Peters, A. (2009). The effects of normal aging on myelinated nerve fibers in monkey central nervous system. *Front. Neuroanat*, *3*(11).

Petersen, S. C., & Monk, K. R. (2015). Neurobiology: myelin goes where the action is. *Current Biology*, *25*(13), R562-R565.

Philpot, B. D., Foster, T. C., & Brunjes, P. C. (1995). The effects of unilateral naris occlusion on spontaneous and odor-driven unit activity in the rat olfactory bulb. In *Chemical Senses 20*(6):226-226.

Pourabdolhossein, F., Mozafari, S., Morvan-Dubois, G., Mirnajafi-Zadeh, J.,

Lopez-Juarez, A., Pierre-Simons, J., ... & Javan, M. (2014). Nogo receptor inhibition enhances functional recovery following lysolecithin-induced demyelination in mouse optic chiasm. *PloS one*, *9*(9), e106378.

Rakic, P., Bourgeois, J. P., Eckenhoff, M. F., Zecevic, N., & Goldman-Rakic, P. S. (1986). Concurrent overproduction of synapses in diverse regions of the primate cerebral cortex. *Science*, *232*, 232-236.

Salami, M., Itami, C., Tsumoto, T., & Kimura, F. (2003). Change of conduction velocity by regional myelination yields constant latency irrespective of distance between thalamus and cortex. *Proceedings of the National Academy of Sciences*,*100*(10), 6174-6179.

Salzer, J. L. (2003). Polarized domains of myelinated axons. *Neuron*, *40*(2), 297-318.

Sampaio, R. C., & Truwit, C. L. (2001). Myelination in the developing human brain. *Handbook of developmental cognitive neuroscience*, 35-44.

Schikorski, T., & Stevens, C. F. (1999). Quantitative fine-structural analysis of olfactory cortical synapses. *Proceedings of the National Academy of Sciences*, *96*(7), 4107-4112.

Schwob, J. E., & Price, J. L. (1984). The development of axonal connections in the central olfactory system of rats. *Journal of Comparative Neurology*, *223*(2), 177-202.

Sengpiel, F., & Kind, P. C. (2002). The role of activity in development of the visual system. *Current Biology*, *12*(23), R818-R826.

Shepherd, G. M. (Ed.). (2003). *The synaptic organization of the brain*. Oxford University Press.

Shepherd, G., Chen, W., Willhite, D., Migliore, M., & Greer, C. (2007). The olfactory granule cell: From classical enigma to central role in olfactory processing. *Brain Research Reviews. 55*(2):373-382.

Shu, T., Butz, K. G., Plachez, C., Gronostajski, R. M., & Richards, L. J. (2003). Abnormal development of forebrain midline glia and commissural projections in Nfia knock-out mice. *The journal of Neuroscience*, *23*(1), 203-212.

Silbereis, J., Huang, E., Back, S., & Rowitch, D. (2010). Toward improved animal models of neonatal white matter injury associated with cerebral palsy. *Disease Models and Mechanisms. 3*:676-688.

Silver, J., Lorenz, S. E., Wahlsten, D., & Coughlin, J. (1982). Axonal guidance during development of the great cerebral commissures: descriptive and experimental studies, in vivo, on the role of preformed glial pathways. *Journal of Comparative Neurology*, *210*(1), 10-29.

Simons, M. & Trotter, J. (2007). Wrapping it up: the cell biology of myelination. *Current Opinion in Neurobiology. 17*(5):533-540.

Sturrock, R. (1975). A quantitative electron microscopic study of myelination in the anterior limb of the anterior commissure of the mouse brain. *Journal of Anatomy. 119*(1):67-75

Sur, M., & Leamey, C. A. (2001). Development and plasticity of cortical areas and networks. *Nature reviews. Neuroscience*, *2*(4), 251.

Takahashi, N., & Sakurai, T. (2013). Roles of glial cells in schizophrenia: possible targets for therapeutic approaches. *Neurobiology of disease*, *53*, 49-60.

Tomioka, N., Osumi, N., Sato, Y., Inuoe, T., Nakamura, S., Fujisawa, H., Hirata, T.

(2000). Neocortical origin and tangential migration of guidepost neurons in the lateral olfactory tract. *The Journal of Neuroscience. 20*(15:5802-5812.

Tullman, M. J. (2013). Overview of the epidemiology, diagnosis, and disease progression associated with multiple sclerosis. *Am J Manag Care*, *19*(2 Suppl), S15-20.

Urban, N. (2002). Lateral inhibition in the olfactory bulb and in olfaction. *Physiology & Behavior. 77*(4-5):607-612.

Vassar, R., Chao, S., Sitcheran, R., Nunez, J., Vosshall, L., & Axel, R. (1994). Topographic organization of sensory projections to the olfactory bulb. *Cell. 79*(6):981-991.

Vogel, M. (1978). Postnatal development of the cat's retina: a concept of maturation obtained by qualitative and quantitative examinations. *Graefe's Archive for Clinical and Experimental Ophthalmology*, *208*(1), 93-107.

Vora, P., Pillai, P., Zhu, W., Mustapha, J., Namaka, M., Frost, E. (2011). Differential effects of growth factors on oligodendrocyte progenitor migration. *European Journal of Cell Biology. 90*(8):649-656.

Walz, A., Omura, M., & Mombaerts, P. (2006). Development and topography of the lateral olfactory tract in the mouse: Imaging by genetically encoded and injected fluorescent markers. *Developmental Neurobiology. 6*(8): 835-846.

Westrum, L. E. (1975). Electron microscopy of synaptic structures in olfactory cortex of early postnatal rats. *Journal of neurocytology*, *4*(6), 713-732.

Wong, R. O. (1999). Retinal waves and visual system development. *Annual review of neuroscience*, *22*(1), 29-47.

Woodruff, R. H., & Franklin, R. J. (1999). Demyelination and remyelination of the caudal cerebellar peduncle of adult rats following stereotaxic injections of lysolecithin, ethidium bromide, and complement/anti-galactocerebroside: a comparative study. *Glia*, *25*(3), 216-228.

Xu, F., Greer, C. A., & Shepherd, G. M. (2000). Odor maps in the olfactory bulb. *Journal of Comparative Neurology*, *422*(4), 489-495.

Zoupi, L., Savvaki, M., & Karagogeos, D. (2011). Axons and myelinating glia: An intimate contact. *IUBMB life*, *63*(9), 730-735.

Chapter II

Developmental Myelination of the Lateral Olfactory Tract and Anterior Commissure

Abstract

Both the lateral olfactory tract (LOT) and anterior limb of the anterior commissure (AC) carry olfactory information. Axons of the LOT originate in the olfactory bulb and project to olfactory cortices, while the AC carries information across the midline to the contralateral olfactory cortex and bulb. The LOT and AC differ on a number of dimensions, including early development and functional onset. The present work examining developmental myelination in mice reveals additional important differences between the two tracts. For example, the LOT initiates myelination 3-4 days earlier than the AC, evidenced by both an earlier increase in myelin basic protein staining using immunohistochemistry and an earlier appearance of myelinated fibers using electron microscopy. Progression of myelination also differed between the two tracts, with a period of rapid myelination observed 4-6 days earlier in the LOT than the AC. The tracts also responded differently to early sensory deprivation. Mice that underwent unilateral naris occlusion the day after birth and reared to postnatal day 30 were compared to age-matched controls. The procedure did not affect the AC, but the LOT of naris-occluded animals had significantly thinner myelin sheaths relative to axon caliber. Structural differences were also observed: the LOT contains larger, more densely packed axons with significantly thicker myelin sheaths. The findings indicate that these two large, accessible tracts provide an important means for studying brain maturation due to basic differences in both the timing of maturation and general organization.

The onset of myelination is a significant milestone in the development of neural circuits in humans (Jakovcevski et al., 2009) and rodents (Downes and Mullins, 2014) as myelin provides trophic and structural support for axons and substantially increases conduction velocity (Aggarwal et al., 2011). Disrupted myelinogenesis, occurring naturally in developmental forms of leukodystrophy, results in a broad array of symptoms similar to those observed in demyelinating disorders such as multiple sclerosis (Medina, 1993; Padiath et al., 2006). The timing of myelination differs between functional systems and brain regions (Foran and Petersen, 1992; Sampaio and Truwit, 2010), and continues well into postnatal life (Baumann & Pham-Dinn, 2011; Gottleib et al., 1977; Watson et al., 2006).

The olfactory system is crucially important for mammals at birth as odors provide information essential for mammalian pups to locate sustenance and recognize caregivers (Logan et al., 2012). Two large myelinated tracts exclusively carry olfactory information: the lateral olfactory tract (LOT) and anterior limb of the anterior commissure (AC). The two tracts are functionally and geographically distinct (Fig. 1). The LOT, found on the ventrolateral surface of the telencephalon, consists of axons carrying sensory information from the olfactory bulb (OB) to olfactory cortices. Axons from OB mitral cells project into the LOT very early during development, beginning around embryonic day (E)13 in mice and continuing until E16. By two weeks after birth collateral projections are well established (Blanchart et al., 2006; Brunjes et al., 2014; Walz et al., 2006).

Axons from two regions of the olfactory cortex, the anterior olfactory nucleus (AON) and anterior piriform cortex, project across the midline via the AC to homologous structures on the contralateral side (Mori, 2014). The AC is well separated from

olfactory processing regions, about 4mm caudal to the OB in mice, and runs deep in the olfactory cortex, well away from the LOT (Fig. 1C). While the AC is composed of three divisions, only the anterior limb carries olfactory information (Brunjes, 2013). There has been little work on the postnatal development of the anterior limb of the AC (Sturrock, 1976) though our previous results indicate that a rapid increase in myelin basic protein (MBP) expression occurs from postnatal day (P)11-P14 (Brunjes et al., 2014).

In the present work the onset and progression of myelination in the LOT and AC was examined in several ways. First, the maturation of oligodendrocytes was assessed based on expression of several molecular indices including an early precursor marker (platelet derived growth factor receptor alpha, PDGF; Calver et al., 1998; Fruttiger et al., 1999; Pringle et al., 1992), a later precursor marker (neural-glial antigen 2, NG2; Nishiyama et al., 1996; Nishiyama et al., 2002; Rivers et al., 2008), a marker for mature oligodendrocytes (CC1; Bhat et al., 1996; Ness et al., 2005), a marker for compact myelin sheaths (myelin basic protein; MBP; Asou et al., 1995; Shiota et al., 1989), and one oligodendrocyte transcription factor expressed at all stages of development (Olig2; Takebayashi et al., 2002). Second, electron microscopy (EM) was used to quantify the ultrastructural development of axons within the LOT and AC. Finally, the effects of sensory deprivation on LOT and AC myelination were assessed. Substantial evidence indicates that early experience plays a critical role in developing and maintaining proper CNS myelination. For instance, early social isolation results in oligodendrocytes with shorter myelinating processes, fewer branch points and fewer internodes in the prefrontal cortex as well as impaired performance on social interaction and working memory tasks (Makinodan et al. 2012). Light deprivation alters myelin formation as well

as conduction velocity within the optic nerve (Etxeberria et al. 2016). Functional deprivation is easily accomplished in the olfactory system by surgically closing one naris, reducing airflow and odorant availability in one half of the nasal cavity (Brunjes, 1994; Coppola, 2012). Naris occlusion has been demonstrated to cause many changes in the OB including a 25% reduction in volume by P30. Deprivation of primary sensory information might not have the same effect on the myelination of the LOT and AC due to their different roles in olfactory processing. To test this hypothesis, a separate group of animals underwent unilateral naris occlusion on P1, were reared until P30, and were analyzed with EM.

Materials and Methods

Animals

C57BL/6J mice (Jackson Labs; Bar Harbor, ME, USA) were housed in standard polypropylene cages with food (8604, Harlan, Frederick, MD) and water *ad libitum* in a temperature-controlled room on a 12:12 light:dark cycle. Data were collected from 3-8 pups for each measure on P7, 9, 10, 11, 13, 15, 17, 20, 25, and 30 (the day of birth = P0). A separate group of animals underwent unilateral naris occlusion, accomplished by anesthetizing P1 mouse pups via hypothermia and briefly applying a cautery to the right external naris on P1, and then rearing the pups to P30 (Coppola, 2012). All procedures were performed according to NIH guidelines and protocols approved by the University of Virginia IACUC.

Analysis of oligodendrocyte maturation

Mice were deeply anesthetized with sodium pentobarbital (Euthasol; 0.39 mg drug/gm body weight; 150mg/kg; APP Pharmaceuticals; Schaumburg, IL) and perfused

intracardially with 0.01M phosphate buffered saline (PBS; pH 7.4) followed by 4% buffered formaldehyde. Brains were post-fixed for at least 2 hrs. Sixty µm coronal vibratome sections were rinsed four times for five minutes in PBS, and then incubated in 0.01 M citrate buffer (pH 8.5) at 80°C for 25 minutes (Jiao et al., 1999). Tissue was cooled to room temperature, washed twice in PBS for three minutes, and permeabilized in triton wash (TW; 0.03% Triton in PBS). Sections were then placed into a blocking solution (0.5% normal donkey serum in TW; Jackson ImmunoResearch, West Grove, PA) for one hr, followed by overnight incubation in primary antibody (Table 1) at 4°C.

Sections were then rinsed four times in PBS, and placed in a secondary antibody solution (1/250 to 1/500 in TW: Jackson ImmunoResearch, donkey anti-rabbit: Catalog number, 711-165- 152 or 711-545-152; donkey anti-goat: 705-165- 147 or 705-545-147; donkey anti-mouse: 715-485- 150 or 715-545- 151) for 2 hrs. Tissue went through a final 4x5min PBS rinse before being mounted on slides with SlowFade mounting media (Invitrogen: S36937)

Antibody Characterization

Cells within the oligodendrocyte lineage were identified using a rabbit polyclonal antibody against the protein encoded by the Olig2 gene, which is specific to the basic helix-loop-helix transcription factor expressed in oligodendrocytes (Millipore, Cat# AB9610, RRID:AB_10141047). This antibody recognizes the ~32kDa Olig2 protein by western blotting on mouse brain lysate (manufacturer's product insert, Table 1) and has been verified for use in labeling both immature as well as mature oligodendrocytes (Mateo et al., 2015; Wahl et al., 2014). Specificity of staining to oligodendrocytes in our

samples was confirmed by an absence of labeling in neurons and dense labeling in white matter tracts.

Oligodendrocyte precursors were identified using a rabbit polyclonal antibody against the NG2 integral membrane chondroitin sulfate proteoglycan (Millipore, Cat# AB5320, RRID: AB_11213678) and a goat polyclonal antibody against the PDGF receptor α (R&D Systems, Cat# AF1062, RRID:AB_2236897). Specificity of the antibody to the ~320kDa NG2 protein has been confirmed by western blot (Shearer et al., 2003). The NG2 protein is found on the surface of a group of cells which demonstrate properties of O-2A (oligodendrocyte-type 2 astrocyte) progenitor cells. The NG2 proteoglycan has been found on non-oligodendroglial cells such as pericytes (Stanton et al. 2015) and tumor cells (Al-Mayhani et al., 2011) but within white matter tracts is largely restricted the surface of oligodendroglia prior to terminal differentiation (Dawson et al., 2003). While NG2 is not expressed in all oligodendrocyte progenitor cells, of NG2+ cells represent a significant proportion of precursor cells within the oligodendrocyte lineage (Nishiyama et al., 2002). Specificity to the 160-200kDa PDGFRa protein has been confirmed through western blot (manufacturer's product insert, Table 1) and a lack of staining in conditional PDGFRa knockout mice (Matoba et al., 2017). PDGFRa is found on many types of proliferating cells, including immature oligodendrocytes (Bergsten et al. 2001; Gilbertson et al., 2001).

Mature oligodendrocytes were identified using a mouse monoclonal antibody against the tumor suppressor adenomatous polyposis coli (APC; Millipore, Cat# OP80, RRID:AB_2057371). Specificity to the ~321 kDa APC protein has been confirmed

through western blot (Smith et al., 1993). APC is a genetic clone of CC1, which has been shown to be specific to oligodendrocytes in the rodent CNS (Bhat et al., 1996).

Myelin sheaths were identified using a mouse monoclonal antibody against the ~21kDa form of MBP (Millipore, Cat# NE1019, RRID:AB_2140491). Specificity to myelin sheaths has been confirmed in both developing and mature myelin sheaths through co-expression with proteolipid protein, a known component of myelin sheaths (Grishchuk et al., 2015). Labeling in our samples was consistent with known patterns of myelination in the CNS.

Imaging and Analysis

Images were taken with a 20x objective using a Nikon 80i confocal microscope (Nikon Instruments, Inc., Melville, NY). Three optical sections separated by 3μm were imaged and collapsed. In order to facilitate comparisons across ages and subjects, standardized locations were used to gather data. For the LOT, sections were chosen in which the AON forms a complete ring around the subventricular zone (Fig. 1 B,C). For the AC, sections were chosen in which the AC crosses the midline (Fig. 1 E). Analysis of the AC was restricted to the area approximately 1 mm to each side of the midline in order to assure that the anterior limb was sampled. Image montages were constructed and minimally adjusted for brightness and contrast with Adobe Photoshop (San Jose, CA). Within the area of analysis, total numbers of labeled cell bodies were counted. Even though the markers we used are known to target different stages in the lineage of one population of cells, we were careful to confirm that there were no differences in the size of the labeled figures that might bias cell counts. Mean cell diameter was calculated using ImageJ (Rasband et al., 1997-2009) for 50 cells for each marker and compared

(Guillery and Herrup, 1997). No difference was found, so it was determined that there was an equal probability of encountering any labeled cell type in a given sample and no correction was applied. Cell density was calculated for Olig2, PDGF, NG2, and CC1 by dividing the number of labeled cells by the area of the LOT or AC. For MBP, which does not label somata, images were converted to 8-bit black and white images, Image J's white default thresholding setting was applied, and the area fraction measurement (A/A: proportion of labeled to total pixels) obtained and used to estimate the developmental changes in labeling. One-way analyses of variance with Bonferroni's multiple comparison post-hoc tests were used to determine differences between groups.

Analysis of Myelin Development

A separate group of animals (3 animals/age group: P7, 9, 11, 13, 15, 17, 20, 25, 30) was perfused with 2% paraformaldehyde, 2% glutaraldehyde, their brains removed and post-fixed for at least 2 hrs, and then sectioned in the coronal plane at 60µm on a vibratome and the specimens prepared for electron microscopy. Tissue was rinsed with 0.1% phosphate buffer (PB) and post-fixed with OsO_4 for one hr. Following post-fixing, tissue was sequentially dehydrated, counterstained with 4% uranyl acetate in 70% ethanol for at least one hr, and embedded in EPON resin. Tissue was then sectioned using an ultramicrotome (Leica UC7).

Images were taken at either 2500X or 6000X magnification with a JEOL 1010 transmission electron microscope. Counts of unmyelinated, pro-myelinated, and myelinated axons per unit area were made. Axons were considered to be pro-myelinated if an oligodendrocytic process had begun wrapping the axon and myelinated if multiple layers of myelin sheath could be observed. Myelin thickness was measured

as the distance between the innermost and outermost point of compacted segments. Axon caliber was estimated by calculating the diameter of a circle with the same circumference as the perimeter of myelinated axons. For naris occlusion studies, G-ratios (Rushton, 1951; Chomiak and Hu, 2009) were calculated by dividing the axon caliber by the diameter of the entire fiber (axons and myelin sheath). ImageJ was used for all measurements. Means were calculated for each animal on each measure. Kruskal-Wallis tests were used to assess changes over time and Mann-Whitney tests used to determine differences between groups.

Results

Survey of postnatal development: light microscopy

For an overview of myelination in the LOT and AC three ages were examined: P10 (an immature stage before eye or ear opening), P20 (around the time of weaning), and P30 (once OB growth has reached asymptote; Hinds and Hinds, 1976; Roselli-Austin and Altman, 1979). All measurements were made at the standardized locations described above.

Lateral Olfactory Tract Development

As a first step in the analysis, the total density of all cells in the oligodendrocyte lineage was determined using the pan-oligodendroglial marker Olig2. In the LOT, Olig2+ cell density was higher at P10 (Mean=6.48 +/- 2.46 cells/100μm^2) than at P20 (M=3.80 +/- 0.61 cells/100μm^2) or P30 (M=4.90 +/- 1.22 cells/100μm^2; Fig. 2a-d). To determine whether the high density of Olig2+ cells seen in early ages could be attributed to a high precursor population, two glial precursor cell markers that are co-expressed in early progenitor cells (Nishiyama et al., 1996) were used. While both PDGF and NG2 label a

significant proportion of oligodendrocyte progenitor cells, neither antigen alone labels the entire population (Nishiyama et al., 1996, 2009). PDGF+ precursor cell density significantly decreased in labeling from P10 to P30 ($F=21.87$, $p<0.01$; Fig. 2i-l). Density was highest at P10 (M=7.09 +/- 1.29 cells/100μm^2) followed by a significant decrease by P20 (M=3.93 +/- 0.32 cells/100μm^2; $t=4.374$, $p<0.05$) and a further decrease by P30 (M=2.41 +/- 0.77 cells/100μm^2). NG2 showed a different developmental pattern, with little change over time ($F=1.636$, *n.s.*; Fig. 2l). NG2+ precursor cell density at P10 (M=5.67 +/- 2.19 cells/100μm^2) was statistically similar to that seen at both P20 (M=7.38 +/- 2.60 cells/100μm^2) and P30 (M=4.38 +/- 0.97 cells/100μm^2).

Terminally differentiated oligodendrocyte density was determined by expression of CC1 and the presence of myelinating sheaths by the expression of MBP. CC1 staining significantly changed over time ($F=5.24$, $p<0.05$) with more than a three-fold increase between P10 (M=4.01 +/- 1.06 cells/100μm^2) and P20 (M=12.75 +/- 3.11 cells/100μm^2) and a 65% decrease by P30 (M=8.32 +/- 4.69; Fig. 2t). At P20 and 30 CC1+ cells were found at a similar density as Olig2+ cells, indicating that by P20 most Olig2+ cells in the LOT are mature oligodendrocytes. Indeed, substantial myelination was already exhibited by P10 in the LOT as evidenced by the density of MBP staining (A/A = 33.85 +/- 5.33; Fig. 2q, o). The amount of MBP labeling significantly increased across the period observed ($F=47.78$, $p<0.001$). Between P10 and P20 MBP labeling almost doubled (A/A=64.66 +/- 7.6; $t=6.90$, $p<0.01$) and slightly rose by P30 (A/A=76.04 +/- 1.73; $t=2.55$, *n.s.*; Fig. 2q-t).

Anterior Commissure Development

In the AC, Olig2+ cell density was similar to that of the LOT at P10 (M=12.78 +/- 1.51 cells/100μm^2). Density peaked at P20 (M=18.96 +/- 1.82 cells/100μm^2) and slightly decreased by P30 (M=14.01 +/- 4.55 cells/100μm^2; Fig. 2e-h). As seen in the LOT, PDGF+ precursor cell populations in the AC dropped significantly over time (F=10.03, *p<0.05*), but the decrease occurred later, between P20 (M=5.66 +/- 0.24 cells/100μm^2) and P30 (M=3.25 +/- 0.66 cells/100μm^2; t=4.39, *p<0.05*; Fig. 2m-p). NG2 labeling followed a different pattern, with no significant changes over time (F=0.651, *n.s.*; Fig. 2p). At P10 the AC showed little evidence of myelination, with low CC1 staining (M=4.06 +/- 1.14 cells/100μm^2) and few nascent MBP+ sheaths present (A/A= 13.92; Fig. 2u, x). CC1 staining increased between P10 (M=4.03 +/- 1.14 cells/100μm^2) and P20 (M=5.78 +/- 0.87 cells/100μm^2) and slightly increased by P30 (M=6.56 +/- 1.02 cells/100μm^2; Fig. 2x). MBP staining rapidly increased across time (F=66.07, *p<0.0001*). The largest increase in MBP labeling was observed between P10 (A/A=8.01 +/- 1.32) and P20 (A/A=31.39 +/-4.05; t=5.11, *p<0.01*) and an additional increase occurred between P20 and P30 (A/A=60.51 +/- 8.72; t=6.36, *p<0.01*; Fig. 2u-x).

Period of rapid myelination: light microscopy

The data above indicate that the LOT and AC have different times of rapid myelination. Therefore, a second study more closely defined the time course of these changes. Three early ages (P7, 9, and 11) were chosen for a closer examination of the LOT because mature myelinating cells were already present by P10. Later ages (P11, 13, and 15) were chosen for AC analyses based on data presented above as well as previously reported results (Brunjes et al., 2014). Tissue was stained for expression of

Olig2, PDGF, and MBP as these markers showed the largest changes across P10 to 30 and allow for distinguishing between all oligodendrocytes (Olig2+), oligodendrocyte precursor cells (PDGF+), and mature myelin sheaths (MBP+).

Lateral Olfactory Tract

The total density of Olig2+ cells in the LOT significantly changed over time (F=14.29, *p<0.01*), almost doubling between P7 (M=10.44 +/- 3.39 cells/100μm^2) and P9 (19.31 +/- 1.28 cells/100μm^2; t=4.01, *p<0.05*) and decreasing by P11 (M=9.03 +/- 1.25 cells/100μm^2; t=5.69, *p<0.01*; Fig. 3a-d). PDGF+ cell density at all ages was similar to that observed at P10, with no significant change over time (F=0.23, *n.s.* Fig. 3a-d). As early as P7 MBP labeling was detected (A/A=15.94 +/- 2.43). MBP staining increased significantly during the period (F=11.65, *p<0.01*), with the largest increase observed between P9 (A/A=25.53 +/- 4.91) and P11 (A/A=36.51 +/- 6.98; t=3.39, *p<0.05*; Fig. 3a-d).

Anterior Commissure

A different pattern was observed during the onset of rapid myelination in the AC (Fig. 3e-h). Unlike in the LOT, Olig2+ oligodendrocyte density did not change over the period observed (F=1.7, *n.s.*). However, PDGF staining increased steadily from P11 to P15 with a 60% increase observed between P11 (M=3.69 +/- 0.77 cells/100μm^2) to P13 (M=6.16 +/- 1.90 cells/100μm^2) and an additional 61% increase by P15 (M=10.13 +/- 2.50 cells/100μm^2; F=9.09, *p<0.05*). Myelination as measured by MBP staining followed a similar pattern. Labeling stayed stable between P11 (A/A=14.61 +/- 4.20) and P13 (A/A=16.83 +/- 0.65; t=0.97, *n.s.*) but significantly increased by P15 (A/A=31.59 +/- 2.31; t=6.47, *p<0.01*). At all ages examined MBP staining was lower than the corresponding

P30 value, indicating that significant myelination occurs after the period of rapid myelination in the AC (Fig. 3h).

Electron microscopy

An analysis of LOT and AC tissue at P5, 7, 9, 11, 13, 15, 17, 20, 25, and 30 was made in both tracts. The presence and density of unmyelinated, pro-myelinated, and myelinated axons was quantified to complement the developmental time courses established by immunological markers. EM analysis also allowed for measurement of axon caliber and thickness of the myelin sheath.

Lateral Olfactory Tract

The first evidence of myelination in the LOT was the presence of pro-myelinating oligodendrocytes at P7 (Fig. 4a). The number of pro-myelinated fibers peaked in the LOT at P15, followed by a steady decline (Fig. 4k). The first myelinated fibers appeared at P9, and mirroring the results described above, a sharp increase in number of myelinated axons occurred between P9 and 11 (36.61 +/- 15.26 to 226.26 +/- 16.9 myelinated axons/mm^2; Fig. 4b,m).

Average myelinated axon caliber increased with age, from 1.15 +/- 0.36μm at P9 to 1.46 +/- 0.21μm at P30 (Fig. 4l). Myelin thickness slightly increased across time, but was restricted to a range of only 0.5nm (Fig. 4n). By P30 the average myelin thickness was 0.14μm.

Anterior Commissure

Little evidence of myelination was present in the AC at P11, with only 15.5 pro-myelinated axons/mm^2 on average and only one myelinated axon per approximately 20μm^2 (Fig.4f,k,m). Number of pro-myelinated axons in the AC peaked at 45.6/mm^2 at

P13, followed by a decrease until P30 (M =13.38/mm^2; Fig. 4k). Mean number of myelinated axons/μm^2 increased by a factor of 100 (from 0.03 to 3.55) between P11 and P30, with the sharpest increase occurring between P17 and P20 (Fig. 4m).

At P30, there was substantial variation in density of myelinated fibers in different areas of the AC (from 58.39 to 908.76 myelinated fibers/mm^2), although no consistent patterns were found (Brunjes, 2013). Mean axon caliber of myelinated axons varied widely and did not significantly change with age (H=3.5, p=0.74; Fig. 4l). Mean myelin thickness was also stable over time, with a range of 0.18μm; Fig. 4n).

Unilateral Naris Occlusion

Given the findings described in the introduction showing that function affects myelination, it was important to determine if activity also affects development of these two olfactory system tracts. As the bundles carry different aspects of the same information (the LOT carries primary information from the OB to the cortices, while the AC carries processed information between hemispheres), unilateral naris occlusion might differentially affect the two tracts. Deprivation has been shown to have large effects on the developing OB, and to induce changes in the AON and PC (Brunjes, 1994; Coppola, 2012).

Lateral Olfactory Tract

The LOT ipsilateral to occlusion in experimental animals was compared to both the contralateral LOT as well as to the LOT of normal controls at P30. To confirm that samples represented similar populations, myelinated axon caliber was compared. Mean caliber was consistent in the LOT ipsilateral to occlusion (M =1.50 ± 0.58μm), the contralateral LOT (M =1.55 ± 1.01μm), and that of control animals (M=1.46 ± 0.67μm;

H=5.4, *p=0.07*). Occlusion had two large effects. First, myelin thickness was significantly smaller in both the LOT ipsilateral (0.11 ± 0.06nm) and contralateral to occlusion (0.10 ± 0.04) compared to age-matched controls (0.14 ± 0.06nm; H=7.2, *p=0.02*). In order to determine if the difference in myelin thickness could be explained by a sampling of smaller axons, g-ratios were calculated for 150 axons in occluded and control samples. The difference in myelin thickness was reflected in a significantly larger mean g-ratio of axons from the ipsilateral LOT (M=0.853 +/- 0.047) compared to the contralateral LOT of the same animals (M=0.810 +/- 0.048; *p<0.0001*) and to normal controls (M=0.813 +/- 0.048; *p<0.001*). Second, a large decrease in the number of pro-myelinated axons/μm^2 was observed in both the LOT ipsilateral (5.88 ± 3.2) and contralateral (5.80 ± 2.59) to occlusion compared to P30 controls (11.62 ± 10.26). No difference in the number of myelinated axons per area (H=3.4, *p=0.18*), density of Olig2+ oligodendrocytes, or density of PDGF+ precursor cells were observed between groups.

Anterior Commissure

Similar to the LOT, myelin thickness was significantly smaller in the AC of occluded animals (0.060 ± 0.02nm) compared to age-matched controls (0.067 ± 0.03nm; *p<0.001*). However, unlike the findings in the LOT, mean myelinated axon caliber was significantly smaller in experimental animals (M=0.68 ± 0.21μm) compared to controls (M=0.91 ± 0.27μm; H=10.29, *p=0.001*). Mean g-ratios of myelinated axons in occluded animals (0.811 +/- 0.057) was higher but did not significantly differ from controls (0.803 +/- 0.048; t=1.262; *p=0.21*). Unlike the LOT, no differences in the number of pro-myelinated axons was found between experimental and control animals.

The density of axons myelinated did not significantly differ (H=12, $p<0.05$) between groups and Olig2+ and PDGF+ cell densities was consistent between naris occluded and control samples.

Discussion

Very few studies have examined myelination in the LOT and AC despite the fact that they are major forebrain white matter tracts that are conserved across the vertebrate lineage (Eisthen, 1997; Suarez et al., 2014). Each tract processes different aspects of the olfactory data stream. Odors are detected by sensory neurons in the nose and the information is translated into a topographic code in the OB. The LOT then transmits the information to the olfactory cortices where the odors are identified and assigned into behavioral categories (Schwob and Price, 1984; Gire et al., 2013; Kadohisa and Wilson, 2006; Gottfried, 2010; Mori, 2014). The AC is involved in coordinating activity between the left and right cortices, allowing for localization of odor sources (Esquivelzeta-Rabell et al., 2017) and facilitating the interhemispheric transfer of stored memories (Kucharski and Hall, 1987 and 1988; Kucharski et al., 1990; Fontaine et al., 2013).

The results presented above provide the opportunity to directly compare the two tracts on a number of dimensions (Table 2). The findings add substantial confirmation that the tracts differ in their patterns of development. It has been well established that the LOT begins to develop very early compared to the rest of the forebrain (Lopez-Mascaraque et al., 1996; Sato et al., 1998). Mitral cell axons exit the OB as early as E11.5 and begin to form the LOT by E13 (Walz et al., 2006), around the time that retinal ganglion cell axons begin forming the optic tract (Diener et al., 1997), and before olfactory sensory neurons form synapses in the olfactory bulb (Hinds and Hinds, 1976).

Mitral cell projections separate into dorsal and ventral components of the LOT, and this rough topography can be seen as early as the day after birth (Walz et al., 2006). Prenatal development of the LOT allows for odor information to reach the ipsilateral bulb and cortex by birth, as it is crucial that olfactory pathways be established before birth to initiate suckling behavior (Logan et al., 2012). Axons first enter the AC much later (E16), around the same time as the corpus callosum forms (Silver et al., 1982). As the AC is involved in higher-order processing of olfactory information it appears to not be necessary for survival in neonates. In fact, AC transection does not affect performance on olfactory memory tasks until P12 in mice (Kucharski and Hall, 1987).

The work presented here focused on examining patterns of postnatal development in the two tracts. Several approaches were used to demonstrate conclusively that the time of myelination onset differs between the LOT and AC. Evidence for this difference was found in two ways. First, quantitative confocal analysis of expression of a number of markers for early-to-late stages of oligodendrocyte development demonstrated that precursor (PDGF+ and NG2+) populations decline earlier in the LOT than AC and markers for mature oligodendrocytes (CC1) and myelin sheaths (MBP) appeared later in the AC. Second, EM was used to quantify the number of pro-myelinated and myelinated axons as well as myelin thickness. Pro-myelinated axons were first encountered in the LOT at P7, but not until P11 in the AC. A large increase in the density of myelinated fibers occurred in the LOT between P9 and P11, while a similar increase did not occur in the AC until between P17 and P20.

The present findings also demonstrate that there are notable organizational and morphological differences between the LOT and AC that can be seen across many

ages (Table 2). For example, myelinated axon caliber was approximately 50% larger in the LOT than AC. A difference in axon size has been noted before (Brunjes, 2013) and suggests that the olfactory system has two processing streams: one for immediate odor processing (LOT) and one for slower subsequent processing (AC). The LOT also includes a much higher percentage of myelinated axons by P30 (~80%) than the AC (~20%). Myelin sheaths of LOT fibers are 2x thicker than that of the AC, which doubtlessly contributes to previously observed differences in conduction velocity: the AC is 2.8m/s at the midline and 1.6 m/s in the anterior limb (Mori et al., 1978) while conduction velocity in the LOT is 9.8 m/s (Schwob et al., 1984).

The proper formation of myelin sheaths is linked to efficient neuronal activity *in vivo* and *in vitro* (Demerens et al., 1996), and it has been repeatedly demonstrated that early experience affects the rate and extent of myelination. For example, sensory deprivation decreases myelin thickness in the barrel cortex (Barrera et al., 2012) and social isolation has large effects on the development of myelin in the prefrontal cortex (Makinodan et al., 2012). It was important, therefore, to see if activity affects the development of these two tracts. Many studies have demonstrated that blocking air flow through one half of the nasal cavity causes profound changes in the development of the OB and olfactory cortices (Brunjes, 1994; Coppola, 2012). The LOT and AC differed in response to naris occlusion. In the LOT, thinner myelin sheaths and an increased density of pro-myelinating cells were observed at P30 in comparison to age-matched controls. In the AC, no significant effects were detected. There are a few potential explanations for this difference between tracts. First, it is possible that the LOT is more affected by sensory deprivation because the LOT is closer to primary sensory receptors.

Second, differences could have been more difficult to assess because the AC contains axons from both the manipulated and unmanipulated hemisphere, while the LOT only contains ipsilateral projections. Furthermore, subtle differences in myelin thickness might be more difficult to detect in the AC as myelin sheaths are thinner than the LOT. Interestingly, changes in myelin thickness and pro-myelination were observed on both the LOT ipsilateral and contralateral to occlusion, suggesting that unilateral naris occlusion does not only affect the occluded hemisphere (Coppola, 2012). No difference in the number of myelinated axons or oligodendrocytes was found in either tract, supporting findings from other sensory systems that neuronal activity is important for initiation of myelination as well as regulation of sheath thickness and internodal length, but not for maintaining oligodendrocyte cell density or density of myelinated fibers (Barrera et al., 2012; Makinodan et al., 2012; Bercury and Macklin, 2015).

Taken together, the findings presented above indicate that the LOT and AC are particularly interesting and unique regions for studying myelination. Both tracts are compact, easily defined, and geographically separated yet are both contained in the small olfactory peduncle. Both exhibit considerable developmental differences, including the time of initial formation, functional state at birth, and rates of postnatal maturation. The two tracts have different spectrums of axons, including caliber and percentage myelinated. Furthermore, as both tracts carry sensory information, activity levels are relatively easy to manipulate. Interestingly, they carry different aspects of the olfactory data stream, and, as shown above, are differently affected by early changes in function. The present work substantially adds to previous findings of developmental and structural differences between the LOT and AC by providing the first direct comparison

of myelination of these two olfactory system tracts (Table 2). The outlined differences between the LOT and the AC make the olfactory system a uniquely appropriate subject for studying the development of and factors affecting myelination.

Literature Cited

Aggarwal, S., Yurlova, L., Simons, M. (2011). Central nervous system myelin: structure, synthesis, and assembly. *Trends in Cell Biology. 21*(10)585-593.

Al-Mayhani, M. T. F., Grenfell, R., Narita, M., Piccirillo, S., Kenney-Herbert, E., Fawcett, J. W., & Watts, C. (2011). NG2 expression in glioblastoma identifies an actively proliferating population with an aggressive molecular signature. *Neuro-oncology*, *13*(8), 830-845.

Asou, H., Hamada, K., Miyazaki, T., Sakota, T., Hayashi, K., Takeda, Y., ... & Uyemura, K. (1995). CNS myelinogenesis in vitro: time course and pattern of rat oligodendrocyte development. *Journal of neuroscience research,* 40(4), 519-534.

Barrera, K., Chu, P., Abramowitz, J., Steger, R., Ramos, R. L., & Brumberg, J. C. (2013). Organization of myelin in the mouse somatosensory barrel cortex and the effects of sensory deprivation. *Developmental neurobiology*, *73*(4), 297-314.

Baumann, N. & Pham-Dinh, D. (2001). Biology of oligodendrocyte and myelin in the mammalian central nervous system. *Physiological Reviews. 81*(2):871-927.

Bercury, K. K., & Macklin, W. B. (2015). Dynamics and mechanisms of CNS myelination. *Developmental cell*, 32(4), 447-458.

Bergsten, E., Uutela, M., Li, X., Pietras, K., Östman, A., Heldin, C. H., ... & Eriksson, U. (2001). PDGF-D is a specific, protease-activated ligand for the PDGF [beta]-receptor. *Nature cell biology*, *3*(5), 512.

Bhat, R. V., Axt, K. J., Fosnaugh, J. S., Smith, K. J., Johnson, K. A., Hill, D. E., ... & Baraban, J. M. (1996). Expression of the APC tumor suppressor protein in oligodendroglia*. Glia,* 17(2), 169-174.

Blanchart, A., De Carlos, J., & Lopez-Mascaraque, L. (2006). Time frame of mitral cell development in the mice olfactory bulb. *Journal of Comparative Neurology. 496*(4)529-543.

Brunjes, P. (1994). Unilateral naris closure and olfactory system development. *Brain*

Research Reviews. 19(1): 146-160.

Brunjes, P. (2013). The mouse olfactory peduncle. 2. The anterior limb of the anterior commissure. *Frontiers in neuroanatomy*, *6*, 51.

Brunjes, P., Collins, L., Osterberg, S., Phillips, A. (2014). The mouse olfactory peduncle. 3. Development of neurons, glia, and centrifugal afferents. *Frontiers in Neuroanatomy. 8*(4).

Calver, A. R., Hall, A. C., Yu, W. P., Walsh, F. S., Heath, J. K., Betsholtz, C., & Richardson, W. D. (1998). Oligodendrocyte population dynamics and the role of PDGF in vivo. *Neuron,* 20(5), 869-882.

Chomiak, T., & Hu, B. (2009). What is the optimal value of the g-ratio for myelinated fibers in the rat CNS? A theoretical approach. *PloS one*, *4*(11), e7754.

Collins, L. & Brunjes, P. *(*In prep) Experimental demyelination of the lateral olfactory tract and anterior commissure.

Coppola, D. (2012). Studies of olfactory system neural plasticity: the contribution of the unilateral naris occlusion technique. *Neural Plasticity. 2012.*

Dawson, M. R., Polito, A., Levine, J. M., & Reynolds, R. (2003). NG2-expressing glial progenitor cells: an abundant and widespread population of cycling cells in the adult rat CNS. *Molecular and Cellular Neuroscience*, *24*(2), 476-488.

Deiner, M. S., Kennedy, T. E., Fazeli, A., Serafini, T., Tessier-Lavigne, M., & Sretavan, D. W. (1997). Netrin-1 and DCC mediate axon guidance locally at the optic disc: loss of function leads to optic nerve hypoplasia. *Neuron*, *19*(3), 575-589.

Demerens, C., Stankoff, B., Logak, M., Anglade, P., Allinquant, B., Couraud, F., ... & Lubetzki, C. (1996). Induction of myelination in the central nervous system by electrical activity. *Proceedings of the National Academy of Sciences*, *93*(18), 9887-9892.

Downes, N., & Mullins, P. (2014). The development of myelin in the brain of the juvenile rat. *Toxicologic pathology*, *42*(5), 913-922.

Eisthen, H. L. (1997). Evolution of vertebrate olfactory systems. *Brain, behavior and evolution*, *50*(4), 222-233.

Etxeberria, A., Mangin, J. M., Aguirre, A., & Gallo, V. (2010). Adult-born SVZ progenitors receive transient synapses during remyelination in corpus callosum. *Nature neuroscience*, *13*(3), 287-289.

Fontaine, C. J., Harley, C. W., & Yuan, Q. (2013). Lateralized odor preference training in rat pups reveals an enhanced network response in anterior piriform cortex to olfactory input that parallels extended memory. *Journal of Neuroscience,* 33(38), 15126-15131.

Foran, D. R., & Peterson, A. C. (1992). Myelin acquisition in the central nervous system of the mouse revealed by an MBP-Lac Z transgene. *Journal of Neuroscience*, *12*, 4890-4890.

Fruttiger, M., Karlsson, L., Hall, A. C., Abramsson, A., Calver, A. R., Bostrom, H., ... & Richardson, W. D. (1999). Defective oligodendrocyte development and severe hypomyelination in PDGF-A knockout mice. *Development*, 126(3), 457-467.

Gilbertson, D. G., Duff, M. E., West, J. W., Kelly, J. D., Sheppard, P. O., Hofstrand, P. D., ... & Feldhaus, A. L. (2001). Platelet-derived growth factor C (PDGF-C), a novel growth factor that binds to PDGF α and β receptor. *Journal of Biological Chemistry*, *276*(29), 27406-27414.

Gire, D. H., Restrepo, D., Sejnowski, T. J., Greer, C., De Carlos, J. A., & Lopez-Mascaraque, L. (2013). Temporal processing in the olfactory system: can we see a smell?. *Neuron,* 78(3), 416-432.

Gottfried, J. A. (2010). Central mechanisms of odour object perception. *Nature reviews*. *Neuroscience*, 11(9), 628.

Gottlieb, A., Keydar, I. K., & Epstein, H. T. (1977). Rodent brain growth stages: an analytical review. *Neonatology*, *32*(3-4), 166-176.

Grishchuk, Y., Peña, K. A., Coblentz, J., King, V. E., Humphrey, D. M., Wang, S. L., ... &

Slaugenhaupt, S. A. (2015). Impaired myelination and reduced brain ferric iron in the mouse model of mucolipidosis IV. *Disease models & mechanisms,* 8(12), 1591-1601.

Guillery, R. W., & Herrup, K. (1997). Quantification without pontification: choosing a method for counting objects in sectioned tissues. *Journal of comparative neurology*, *386*(1), 2-7.

Hinds, J. W., & Hinds, P. L. (1976). Synapse formation in the mouse olfactory bulb. Quantitative studies. *Journal of Comparative Neurology*, *169*(1), 15-40.

Jakovcevski, I., Filipovic, R., Mo, Z., Rakic, S., & Zecevic, N. (2009). Oligodendrocyte development and the onset of myelination in the human fetal brain. *Frontiers in neuroanatomy*, *3*.

Jiao, Y., Sun, Z., Lee, T., Fusco, F. R., Kimble, T. D., Meade, C. A., ... & Reiner, A. (1999). A simple and sensitive antigen retrieval method for free-floating and slide-mounted tissue sections. *Journal of neuroscience methods*, *93*(2), 149-162.

Kadohisa, M., & Wilson, D. A. (2006). Separate encoding of identity and similarity of complex familiar odors in piriform cortex. *Proceedings of the National Academy of Sciences*, *103*(41), 15206-15211.

Kucharski, D., & Hall, W. G. (1987). New routes to early memories. *Science*, *238*(4828), 786-788.

Kucharski, D. & Hall, W. (1988). Developmental change in the access to olfactory memories. *Behavioral Neuroscience. 102*(3):340-348.

Kucharski, D., Burka, N., & Hall, W. G. (1990). The anterior limb of the anterior commissure is an access route to contralateral stored olfactory preference memories. *Psychobiology*, *18*(2), 195-204.

Kukley, M., Nishiyama, A., & Dietrich, D. (2010). The fate of synaptic input to NG2 glial cells: neurons specifically downregulate transmitter release onto differentiating oligodendroglial cells. *Journal of Neuroscience*, *30*(24), 8320-8331.

Logan, D., Brunet, L., Webb, W., Cutforth, T., Ngai, J., Stowers, L. (2012). Learned

recognition of maternal signature odors mediates the first suckling episode in mice. *Current Biology. 22*(21)1998-2007.

López-Mascaraque L., De Carlos J.A., Valverde F. Early onset of the rat olfactory bulb projections. *Neuroscience*. 1996;70:255–66

Makinodan, M., Rosen, K., Ito, S., & Corfas, G. (2012). A critical period for social experience-dependent oligodendrocyte maturation and myelination. *Science. 337*:1357-1360.

Mateo, J. L., van den Berg, D. L., Haeussler, M., Drechsel, D., Gaber, Z. B., Castro, D. S., ... & Ettwiller, L. (2015). Characterization of the neural stem cell gene regulatory network identifies OLIG2 as a multifunctional regulator of self-renewal. *Genome research*, *25*(1), 41-56.

Matoba, K., Muramatsu, R., & Yamashita, T. (2017). Leptin sustains spontaneous remyelination in the adult central nervous system. *Scientific reports*, 7, 40397.

Medina, E. (1993). Demyelinating and Dysmyelinating Diseases. *Rivista di Neuroradiologia,* 6(2_suppl), 33-38.

Mori, K., & Takagi, S. F. (1978). An intracellular study of dendrodendritic inhibitory synapses on mitral cells in the rabbit olfactory bulb. *The Journal of physiology*, *279*, 569.

Mori, K. (Ed.). (2014). The olfactory system: from odor molecules to motivational behaviors. *Springer.*

Ness, J. K., Valentino, M., McIver, S. R., & Goldberg, M. P. (2005). Identification of oligodendrocytes in experimental disease models. *Glia,* 50(4), 321-328.

Nishiyama, A. L. X. G. H. H., Lin, X. H., Giese, N., Heldin, C. H., & Stallcup, W. B. (1996). Co- localization of NG2 proteoglycan and PDGF α- receptor on O2A progenitor cells in the developing rat brain. *Journal of neuroscience research,* 43(3), 299-314.

Nishiyama, A., Watanabe, M., Yang, Z., & Bu, J. (2002). Identity, distribution, and development

of polydendrocytes: NG2-expressing glial cells. *Journal of neurocytology*, 31(6-7), 437-ppl.

Nishiyama, A., Komitova, M., Suzuki, R., & Zhu, X. (2009). Polydendrocytes (NG2 cells): multifunctional cells with lineage plasticity. *Nature reviews. Neuroscience,* 10(1), 9.

Padiath, Q. S., Saigoh, K., Schiffmann, R., Asahara, H., Yamada, T., Koeppen, A., ... & Ying-Hui, F. (2006). Lamin B1 duplications cause autosomal dominant leukodystrophy. *Nature genetics,* 38(10), 1114.

Polito, A., & Reynolds, R. (2005). NG2-expressing cells as oligodendrocyte progenitors in the normal and demyelinated adult central nervous system. *Journal of Anatomy*, *207*(6), 707–716. http://doi.org/10.1111/j.1469-7580.2005.00454.

Pringle, N. P., Mudhar, H. S., Collarini, E. J., & Richardson, W. D. (1992). PDGF receptors in the rat CNS: during late neurogenesis, PDGF alpha-receptor expression appears to be restricted to glial cells of the oligodendrocyte lineage. *Development,* 115(2), 535-551.

Rabell, J. E., Mutlu, K., Noutel, J., del Olmo, P. M., & Haesler, S. (2017). Spontaneous Rapid Odor Source Localization Behavior Requires Interhemispheric Communication. *Current Biology*, *27*(10), 1542-1548.

Rasband, W. 1. (1997). ImageJ. Bethesda, MD: US National Institutes of Health. *Available on http://rsb. info. nih. gov/ij*, *2009*.

Rivers, L. E., Young, K. M., Rizzi, M., Jamen, F., Psachoulia, K., Wade, A., ... & Richardson, W. D. (2008). PDGFRA/NG2 glia generate myelinating oligodendrocytes and piriform projection neurons in adult mice. *Nature neuroscience*, 11(12), 1392-1401.

Rosselli-Austin, L., & Altman, J. (1979). The postnatal development of the main olfactory bulb of the rat. *Journal of developmental physiology*, *1*(4), 295-313.

Rushton, W. A. H. (1951). A theory of the effects of fibre size in medullated nerve. *The Journal of physiology*, *115*(1), 101-122.

Sampaio, R. C., & Truwit, C. L. (2001). Myelination in the developing human brain.

Handbook of developmental cognitive neuroscience, 35-44.

Sato Y., Hirata T., Ogawa M., Fujisawa H. Requirement for early-generated neurons recognized by monoclonal antibody lot1 in the formation of lateral olfactory tract. *J Neurosci.* 1998;18:7800–10.

Schwob, J. E., Haberly, L. B., & Price, J. L. (1984). The development of physiological responses of the piriform cortex in rats to stimulation of the lateral olfactory tract. *Journal of Comparative Neurology*, *223*(2), 223-237.

Schwob, J. E., & Price, J. L. (1984). The development of axonal connections in the central olfactory system of rats. *Journal of Comparative Neurology*, *223*(2), 177-202.

Shearer, M. C., Niclou, S. P., Brown, D., Asher, R. A., Holtmaat, A. J., Levine, J. M., ... & Fawcett, J. W. (2003). The astrocyte/meningeal cell interface is a barrier to neurite outgrowth which can be overcome by manipulation of inhibitory molecules or axonal signalling pathways. *Molecular and Cellular Neuroscience,* 24(4), 913-925.

Shiota, C., Miura, M., & Mikoshiba, K. (1989). Developmental profile and differential localization of mRNAs of myelin proteins (MBP and PLP) in oligodendrocytes in the brain and in culture. *Developmental Brain Research,* 45(1), 83-94.

Silver, J., Lorenz, S. E., Wahlsten, D., & Coughlin, J. (1982). Axonal guidance during development of the great cerebral commissures: descriptive and experimental studies, in vivo, on the role of preformed glial pathways. *Journal of Comparative Neurology*, *210*(1), 10-29.

Smith, K. J., Johnson, K. A., Bryan, T. M., Hill, D. E., Markowitz, S., Willson, J. K., ... & Vogelstein, B. (1993). The APC gene product in normal and tumor cells. *Proceedings of the National Academy of Sciences,* 90(7), 2846-2850.

Stanton, G. B., Kohler, S. J., Boklweski, J., Cameron, J. L., & Greenough, W. T. (2015). Cytogenesis in the adult monkey motor cortex: Perivascular NG2 cells are the major adult born cell type. *Journal of Comparative Neurology*, *523*(6), 849-868.

Sturrock, R. (1976). Development of the mouse anterior commissure. Part I. A comparison of myelination in the anterior and posterior limbs of the anterior commissure of the mouse brain. *Zbl. Vet. Med. 5*:54-67.

Suárez, R., Gobius, I., & Richards, L. J. (2014). Evolution and development of interhemispheric connections in the vertebrate forebrain. *Frontiers in human neuroscience*, *8*.

Takebayashi, H., Nabeshima, Y., Yoshida, S., Chisaka, O., Ikenaka, K., & Nabeshima, Y. I. (2002). The basic helix-loop-helix factor olig2 is essential for the development of motoneuron and oligodendrocyte lineages. *Current biology*, 12(13), 1157-1163.

Wahl, S. E., McLane, L. E., Bercury, K. K., Macklin, W. B., & Wood, T. L. (2014). Mammalian target of rapamycin promotes oligodendrocyte differentiation, initiation and extent of CNS myelination. *Journal of Neuroscience*, *34*(13), 4453-4465.

Walz, A., Omura, M., & Mombaerts, P. (2006). Development and topography of the lateral olfactory tract in the mouse: Imaging by genetically encoded and injected fluorescent markers. *Developmental Neurobiology. 6*(8): 835-846.

Watson, R. E., DeSesso, J. M., Hurtt, M. E., & Cappon, G. D. (2006). Postnatal growth and morphological development of the brain: a species comparison. *Birth Defects Research Part B: Developmental and Reproductive Toxicology*, *77*(5), 471-484.

Table 1 Antibodies

Antigen	Immunogen	Manufacturer	Cat./lot #	Species	Dilution
Olig2	Recombinant mouse Olig2	Millipore (Temecula, CA)	AB9610 2728398	Rabbit polyclonal	1/500
PDGF-Rα	Mouse myeloma cell line NS0-derived recombinant mouse PDGF-Rα	R&D Systems (Minneapolis, MN)	AF1062 HMQ0215111	Goat polyclonal	1/200
NG2	NG2 chondroitin sulfate proteoglycan from rat	Millipore (Temecula, CA)	AB5320 2517782	Rabbit polyclonal	1/200
CC1/APC	Recombinant protein consisting of amino acids 1-226 of APC	Millipore (Temecula, CA)	OP80 D00172565	Mouse monoclonal	1/500
MBP	Human myelin basic protein	Millipore (Temecula, CA)	NE1019 D00174372	Mouse monoclonal	1/500

Table 2 Comparisons between the Lateral Olfactory Tract and Anterior Commissure

	LOT	**AC**
Developmental Differences		
Initial tract formation	E13[1]	E16[2]
First appearance of myelinated fibers	P7	P11
Onset of function	Birth[3]	P12[4]
Period of rapid myelination	P9-11	P13-15
Effects of unilateral naris occlusion	Thinner myelin sheaths, fewer pro-myelinated axons	No observed effects
Structural Differences		
Axon caliber	0.768μm[5]	0.553μm[5]
Myelinated axon caliber	1.5μm	1μm
Percent myelinated at maturity	~80%	~20%
Myelin thickness	0.14μm	0.07μm
G-ratio	0.84[6]	0.79[6]
Conduction velocity	9.8m/s[7]	1.6 - 2.8m/s[8]

E = embryonic day; P = postnatal day; [1] Walz et al., 2006; [2] Silver et al., 1982; [3] Logan et al., 2012; [4] Kucharski and Hall, 1987; [5] Brunjes, 2012; [6] Collins and Brunjes, in prep; [7]Schwob et al., 1984; [8] Mori et al., 1978

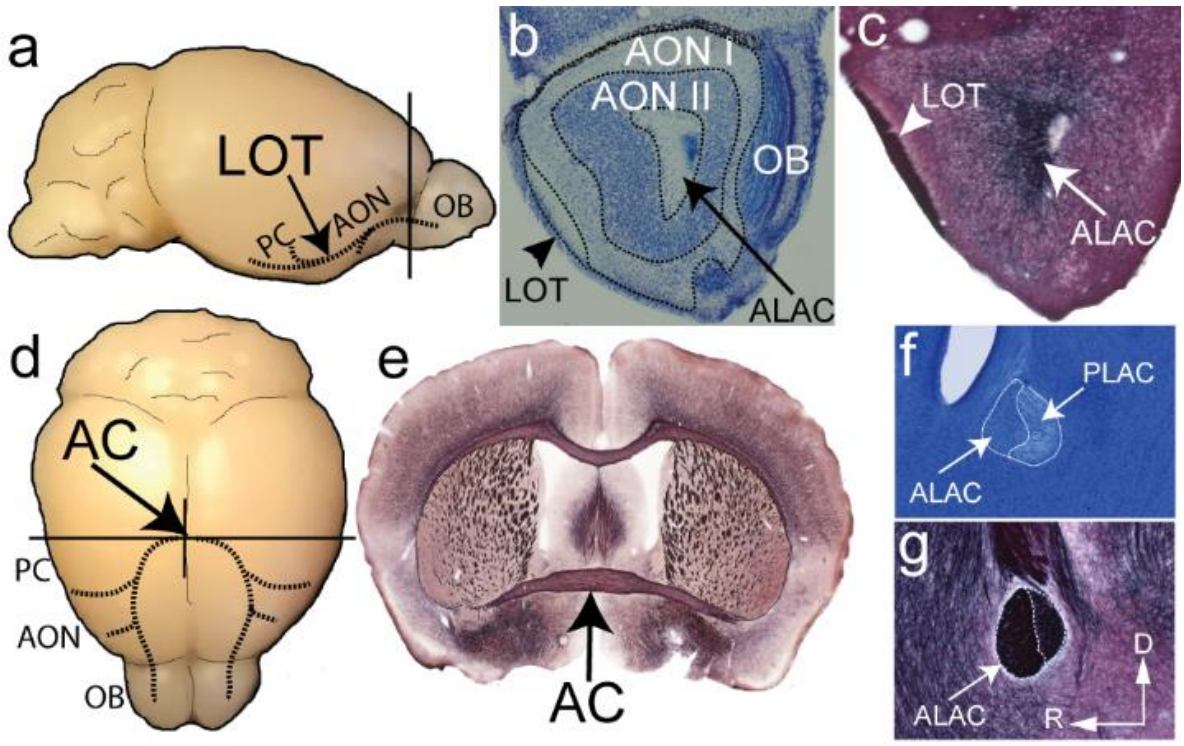

Fig. 1 General organization of the LOT and AC. A. Lateral view of the mouse brain. The LOT (dotted line) originates in the OB and projects ipsilaterally to the anterior olfactory nucleus (AON) and piriform cortex (PC). Solid vertical black line indicates the approximate level of coronal Nissl (B) and myelin (C) stained sections. B. The LOT (arrowhead) is adjacent to layer I of the AON pars lateralis. The AON is comprised of two layers, an outer plexiform layer AON I) and an inner cellular layer (AON II). The anterior (olfactory) limb of the AC (ALAC, arrow) courses lateral to the rostral migratory stream in the center of the olfactory peduncle, surrounded by AON II. C. Myelin stained section through similar region demonstrating the location of the LOT and AC. D. Dorsal view of the mouse brain. The AC (dotted line) contains axons arising in the AON and PC that innervate the contralateral PC, AON, and OB. Solid black lines indicate the approximate level of coronal section in E and midsagittal sections in F and G. E. Myelin

stained coronal section at the level where the AC crosses the midline. F-G. Sagittal sections taken near the midline show a clear difference between the anterior (olfactory, ALAC) and posterior (PLAC) limbs of the AC in both cell body density (F, Nissl stain) and extent of myelination (G, myelin stain). D = dorsal; R = rostral.

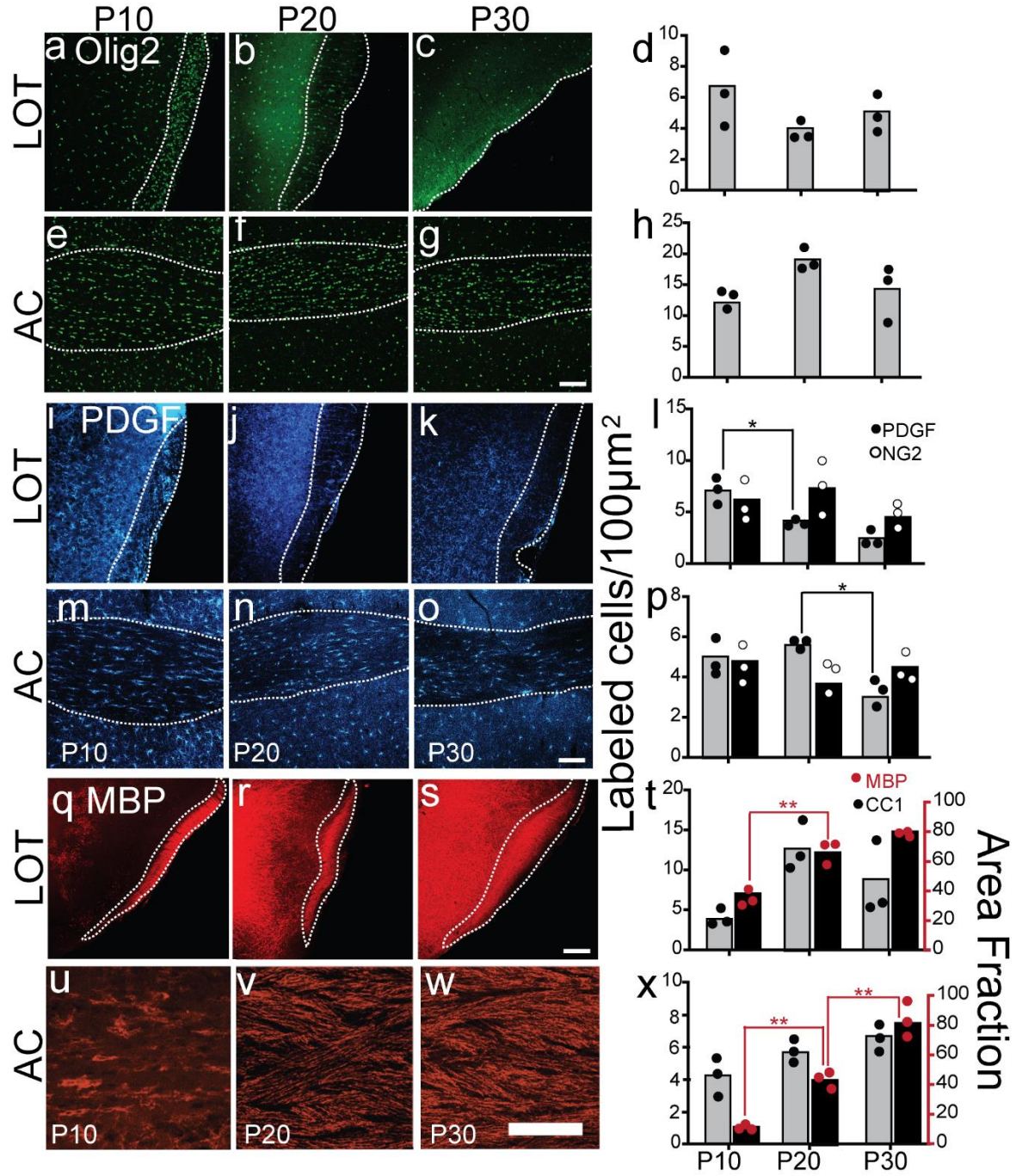

Fig. 2 Oligodendrocyte maturation in the developing LOT and AC. Left panels: Representative sections immunostained for oligodendrocyte developmental markers (Olig2, PDGF, and MBP) at P10, 20, and 30 in the LOT and AC. Right panels:

Quantification of cell density of Olig2 (d,h), PDGF (l,p) NG2 (l,p), CC1 (t,x) and MBP (t,x). Circles represent mean recorded density for each animal and bars represent average density of three animals. A-H. Olig2 labeling (a marker for all cells in the oligodendrocyte lineage) was much higher in the LOT (a-d) than the AC (e-h), but did not change over time in either tract. I-P. Developmental changes in oligodendrocyte precursor populations differed between the LOT and AC. A significant decrease in PDGF labeling (l-k, m-o) was observed in the LOT between P10 and P20 (I, gray bars) and in the AC between P20 and P30 (p). NG2 labeling (black bars) remained consistent over time in both tracts. Q-X. MBP staining for myelin sheaths and quantification of the presence of mature oligodendrocytes with MBP staining (black bars, red circles) and CC1+ oligodendrocyte density (gray bars, black circles). Note the large increase in both MBP and CC1 labeling between P10 and P20 in the LOT and a similar increase in staining between P20 and P30 in the AC. Scale bar = 100μm.

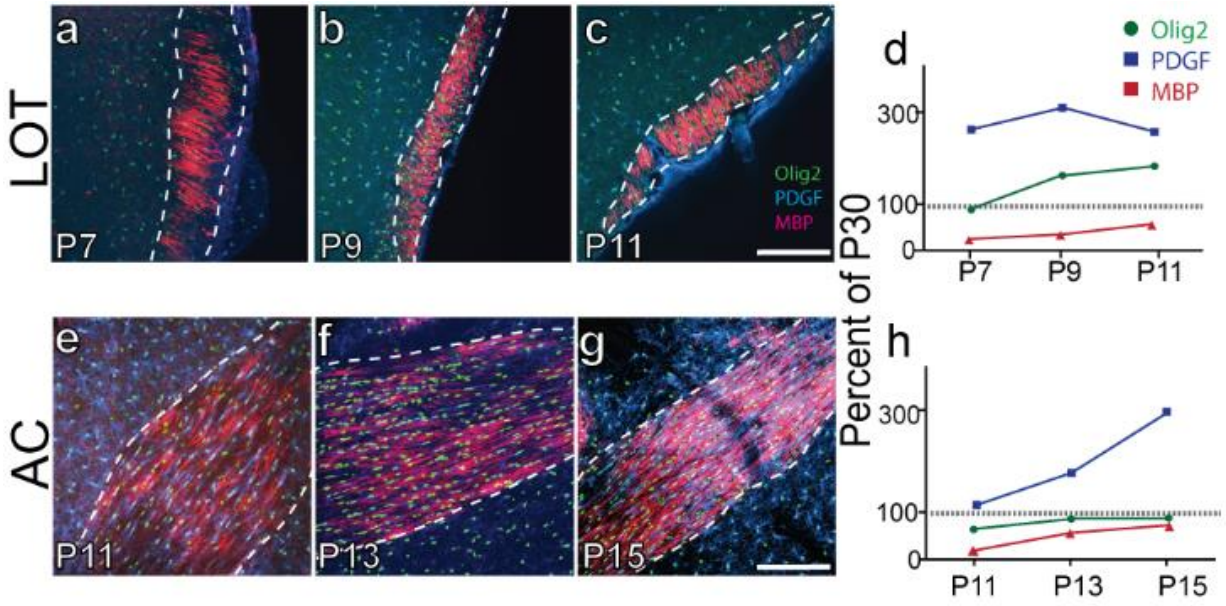

Fig. 3. Comparison of the period of rapid myelination in both the LOT (top row) and AC (bottom row). Tissue was immunostained for Olig2 (green), PDGF (blue), and MBP (red). A-C. Representative LOT sections from mice aged P7, 9, and 11; E-G depict AC sections from P11, 13, and 15. D,H. Quantification of developmental changes in immunostaining for each of the antigens (MBP,red; Olig2, green; and PDGF,blue) with data presented as the percentage of staining observed at P30 (dotted lines). Grey dotted lines represent 100%, or amount of labeling recorded at P30. Note that PDGF staining for precursor cells was high while MBP staining was low throughout the period examined, indicating that substantial myelination occurs after the period of rapid myelination in both tracts. Scale bar = 100μm.

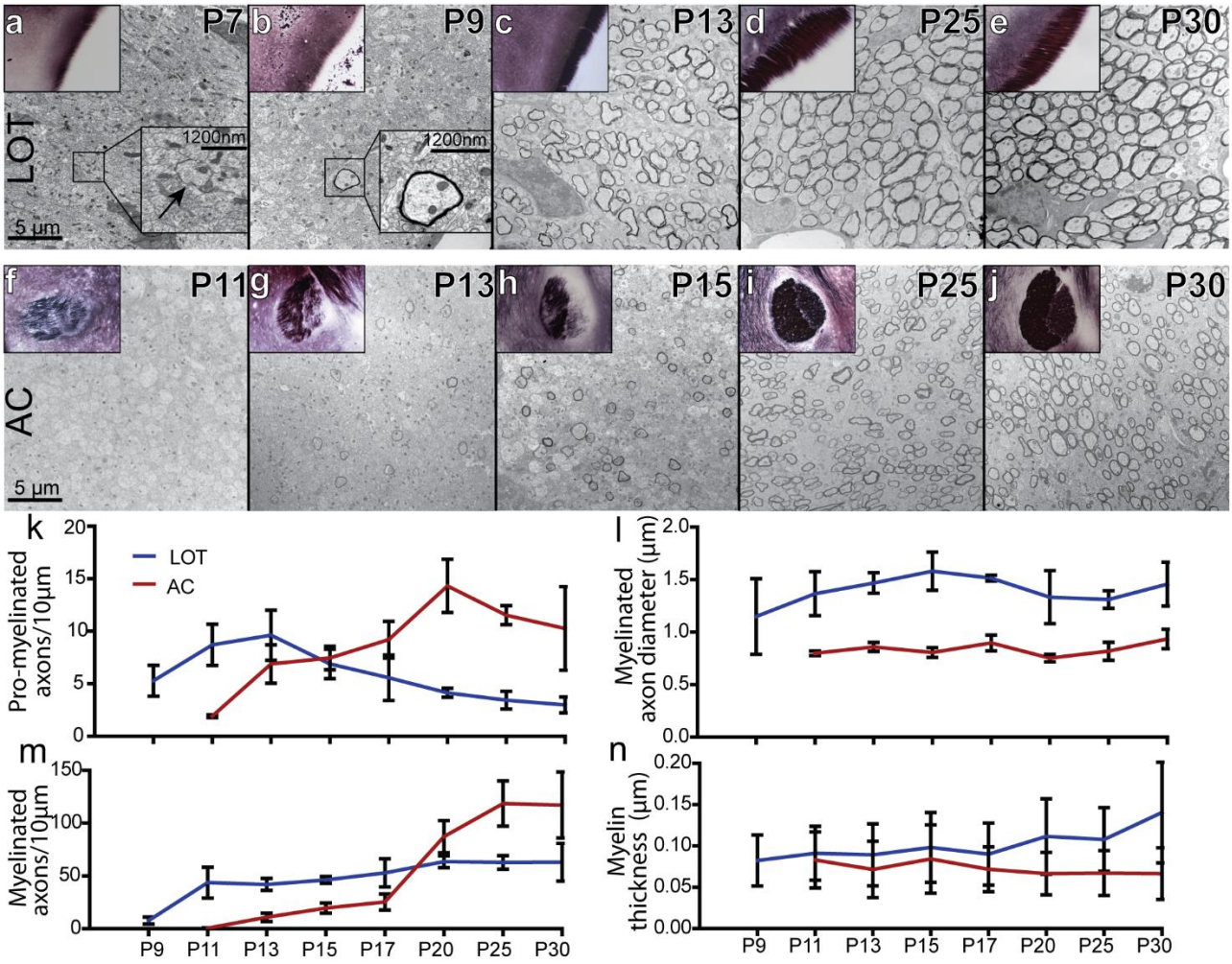

Fig. 4 Ultrastructural development of the LOT and AC. Top: Myelin-stained sections (insets) and EM micrographs of the developing LOT (A-E) and AC (F-J). With age the area of the LOT as well as the density of myelin staining increases dramatically, especially between P9 and P13. A. At P7 no myelinated axons are present, but pre-myelinating oligodendrocyte processes can be seen in between axons (boxed inset). B. Early myelination was observed at P9, evidenced by few wrappings and oligodendrocyte cytoplasm surrounding the axon (inset). C. Myelinated fibers were more apparent by P13, often clustered nearby glial cells or glial precursor cells. D,E. Average

myelinated cell density greatly increased by P25 (D), and continued to increase through P30 (E). Myelin stains demonstrated that with age the AC (F-J, inset) enlarges and the difference between the heavily myelinated anterior limb (left) and the posterior limb (right) becomes more apparent. No myelinated fibers were observed in the AC at P11 (F) with only sporadic por-myelinated fibers. By P13 (G) the AC has begun myelinating large-caliber fibers. At the same time the LOT contained many myelinated figures (C). A large increase in myelinated fiber density caliber occurs between P13 and P15 (H) that continues through the period observed (I, J). Bottom panels: quantification of ultrastructural development of the LOT and AC. K. Number of pro-myelinated axons per $10\mu m^2$ in the LOT (blue line) and AC (red line) with age. Pro-myelinated fibers decreased in density earlier in the LOT (after P13) than in the AC (after P20). L. Mean axon caliber of myelinated fibers was substantially greater in the LOT than in the AC at every age examined. M. Myelinated cell counts (number of myelinated axons per $10\mu m^2$) increased much earlier in the LOT (between P9 and P11) than the AC (between P17 and 25). N. Mean myelin thickness was similar throughout the development of both the LOT the AC, but was consistently higher in the LOT compared to the AC.

Chapter III

Lysolecithin-Induced Demyelination and Remyelination of the Lateral Olfactory Tract and Anterior Commissure

Abstract

Demyelination significantly affects brain function. In order to understand the process of myelin loss and to find new therapies promoting remyelination several experimental methods have been employed, each with varying levels of myelin and neuronal damage. Lysolecithin is one demyelinating agent commonly used to assess demyelination and strategies for remyelination. The present work investigates whether the olfactory system's white matter tracts are affected by lysolecithin administration. The olfactory system has two distinct tracts with differing developmental histories, axonal composition, and function: the lateral olfactory tract (LOT), which carries ipsilateral olfactory information from the olfactory bulb to the olfactory cortex, and the anterior commissure (AC), which contains fibers connecting olfactory regions across hemispheres. The effects of lysolecithin injections was assessed in two ways: the expression of myelin basic protein, a component of compacted myelin sheaths, was quantified using immunohistochemistry and electron microscopy was used to obtain measurements of myelin thickness of individual axons. Data were collected at 7, 14, 21, and 30 days post-injection (dpi). While both the LOT and AC exhibited significant demyelination at 7 dpi and had returned to control levels by 30 dpi, the recovery process differed between the two tracts. Remyelination occurred more rapidly in the LOT: substantial remyelination was observed in the LOT by 14 dpi, but not in the AC until 21 dpi. The findings indicate that a) the LOT and AC are indeed suitable tracts for studying lysolecithin-induced de- and remyelination and b) experimental demyelination proceeds differentially between the two tracts.

Myelin enhances neural circuit function by increasing axonal conduction velocity. Proper myelination is therefore essential for efficient brain function. Consequently, demyelinating disorders such as multiple sclerosis or developmental leukodystrophies are a significant public health concern. Several animal models of demyelinating disorders have been developed to both examine the candidate cellular changes underlying demyelination and to investigate ways of promoting faster and more complete remyelination (Podbielska et al., 2013; Denic et al., 2011).

Lysolecithin is among a small group of compounds used to experimentally produce demyelination (Blakemore and Franklin, 2008). It is a detergent that selectively degrades myelin sheaths at low concentrations, presumably by activating phospholipase A2 (Gregson, 1989). Lysolecithin-induced demyelination is a particularly useful model as it a) initiates demyelination rapidly, b) allows for remyelination, and c) induces damage that is selective to myelin sheaths (Woodruff and Franklin, 1999). Low concentrations of lysolecithin selectively damage myelin sheaths due to their high lipid content, leaving myelinated axons and oligodendrocytes largely intact (Fressinaud et al., 1996; Caren and Mitchell, 1982), and inducing demyelination independent of the immune system (Beiber et al., 2002). Demyelination begins within 1hr following application (Hall, 1988); but the subsequent time course varies considerably based on injection location, species, and vicinity to progenitor cells (Blakemore and Franklin, 2008). For example, remyelination can begin as early as 7 days post-injection (dpi) in the rodent spinal cord (Jeffrey and Blakemore, 1995), takes 3-4 weeks in the optic tract, (Mozafari et al., 2010, Woodruff and Franklin, 1999). CNS remyelination is complete by 5-6 weeks after injection in rodents (Bieber et al., 2002; Denic, et al., 2011), but the

process can last much longer in other species (e.g. rabbit corpus callosum; Ousman and David, 2000).

Recent work in our lab has characterized and compared the development of myelin in the two white matter tracts that interconnect the olfactory forebrain (Collins and Brunjes, in prep). The lateral olfactory tract (LOT) transfers primary olfactory information from the olfactory bulb to the ipsilateral olfactory cortices. The anterior commissure (AC) is involved in higher order sensory processing; it interconnects the left and right olfactory cortices (Brunjes, 2013). Both the architecture and timing of myelination in these two tracts is notably different. For instance, the LOT myelinates 3-4 days earlier than the AC, has a much higher percentage of myelinated fibers, and has thicker sheaths surrounding larger axons than in the AC. These differences have functional significance: large, heavily myelinated axons in the LOT carry sensory information quickly to ipsilateral olfactory processing centers while slower projections in the AC course contralaterally for subsequent processing (Collins and Brunjes, in prep; Mori et al., 1978; Schwob et al., 1984).

No work exists detailing the susceptibility to demyelination or capacity for remyelination in either of these tracts. The LOT and AC are particularly interesting in this regard since 1) they are within one functional system yet have different developmental histories and functions, 2) as a portion of a sensory system their function is readily manipulatable, 3) both are large, discrete bundles that are easily accessible, and 4) the proximity of both tracts to the to the subventricular zone (SVZ) of the lateral ventricle suggests that remyelination could progress quickly due to the presence of SVZ-derived oligodendrocyte precursor cells (Menn et al., 2006; Nait-Oumesmar et al.,

1999). The following study is an examination of lysolecithin-induced demyelination and remyelination in the LOT and AC, contributing to the growing literature on myelination development, loss, and repair in the CNS.

Methods

Animals

C57BL/6J mice (Jackson Labs; Bar Harbor, ME, USA) were housed in standard polypropylene cages with food (8604, Harlan, Frederick, MD) and water *ad libitum* in a temperature-controlled room on a 12:12 light:dark cycle. Data were collected from at least 6 mice for each post-injection time point. All procedures were performed according to NIH guidelines and protocols approved by the University of Virginia IACUC.

Procedures

Surgeries

Mice were anesthetized with isoflurane and placed on a stereotaxic apparatus supplied with isoflurane and kept warm on a heating pad circulating water at 42℃. Approximately 1.5µl of a 1% lysolecithin (Millipore Sigma, Temecula, CA) solution in phosphate buffered saline (PBS) was injected into either the LOT or AC with a Picospritzer (General Valve Corporation, Fairfield, NJ). The LOT was targeted at the point in the olfactory peduncle where the anterior olfactory nucleus (AON) forms a complete ring around the SVZ, approximately 2mm lateral and 2mm anterior to bregma and 3mm from the surface of the brain (Fig. 1A,B) . The anterior (olfactory) limb of the AC was experimentally manipulated with injections 1mm lateral and 1mm anterior to bregma lowered 3mm beneath the pia (Fig. 1A,C). Sham injections with vehicle only

were made into the contralateral LOT or AC of the same animals to minimize individual variability within our samples. All animals were monitored closely during recovery.

At least six mice in each group received injections at P30 and were sacrificed at 7, 14, 21 or 30 days post-injection (dpi; Fig. 1D) and examined with either electron microscopy and/or immunohistochemistry. Survival times were chosen based on evidence from the rodent optic tract and corpus callosum indicating that peak lysolecithin-induced demyelination occurs 7-10 days post-injection and is followed by a period of remyelination beginning approximately three weeks after injection (Blakemore and Franklin, 2008). Mice were deeply anesthetized with sodium pentobarbital (Euthasol; 0.39 mg drug/gm body weight; 150mg/kg; APP Pharmaceuticals, Schaumburg, IL) and perfused with 2% paraformaldehyde, 2% glutaraldehyde. Brains were post-fixed for several days, and sectioned at 60μm on a vibratome. Every other section was processed for either immunohistochemistry or electron microscopy.

Immunohistochemistry

Tissue collected from at least three animals at each post-injection day was stained for myelin basic protein (MBP), to visualize myelin membranes (Grischuk et al., 2015). Tissue was rinsed four times for five minutes in PBS (pH 7.4), incubated in 0.01 M citrate buffer (pH 8.5) at 80°C twice for 15 minutes. Tissue was cooled to room temperature, washed twice in PBS for three minutes, and permeabilized with triton wash (TW; 0.03% Triton in PBS). Sections were then placed into a blocking solution (0.5% normal donkey serum in TW; Jackson ImmunoResearch, West Grove, PA) for one hour, followed by overnight incubation in primary antibody (1:500 mouse monoclonal human myelin basic protein, Cat #: NE1019, lot #: D00174372, Millipore, Temecula, CA;

RRID:AB_2140491) at room temperature. Sections were then rinsed four times in PBS, and placed in a secondary antibody solution (1/250 to 1/500 in TW: Jackson ImmunoResearch, donkey anti-mouse: 715-485-150 or 715-545-151) for 2 hours. Tissue went through a final 4x5min PBS rinse before being mounted on slides with SlowFade mounting media (Invitrogen: S36937).

Electron Microscopy

Tissue from 3 animals at each post-injection time point was processed for electron microscopy. Following at least 12 hrs of post-fixation, tissue was rinsed three times with 0.1% phosphate buffer (PB) and post-fixed with 1% OsO_4 for one hr. Tissue was then sequentially dehydrated and counterstained with 4% uranyl acetate in 70% EtOH overnight. Sections were sequentially dehydrated, embedded in EPON resin, and sectioned at 80nm using an ultramicrotome (Leica UC7).

Imaging and Analysis

Immunostained tissue was used to assess experimentally-induced changes in MBP staining. Sections were imaged with 20x objective with a Nikon 80i confocal microscope (Nikon Instruments, Inc., Melville, NY). Images were minimally adjusted for brightness and contrast using Adobe Photoshop (San Jose, CA). In order to assess experimentally induced changes in MBP staining, ImageJ (Rasband et al., 1999-2007) was used to determine the ratio of labeled to total pixels (the area fraction: A/A) in each image. To standardize the analyses, measurements were only made within a circle with a radius of 100μm around the center of the injection.

After identifying injection sites with MBP staining, adjacent sections were chosen for imaging on a Jeol 1010 transmission electron microscope (EM) at 2,500 and 5,000x

magnification. At least 5 images were examined from three experimental animals at each survival time, yielding a sample of at least 500 axons per group for g-ratio, axon caliber, and myelin thickness measurements. Percentages of myelinated and unmyelinated axons were determined for at least 1000 axons from three experimental animals and three controls. Means were calculated for each sample and compared using non-parametric statistics. G-ratios were calculated by dividing the axon caliber (determined by computing the diameter of a circle with the same circumference as the perimeter of myelinated axons) by the diameter of the entire fiber (axons and myelin sheath; Rushton, 1951; Chomiak and Hu, 2009). G-ratios were calculated for 50 axons adjacent to the injection site for each of three experimental and two control animals at each postinjection time point. Myelin thickness was estimated by subtracting the inner diameter from the outer diameter. G-ratios and myelin thickness measures were compared using unpaired t-tests.

Results

Immunohistochemistry

In order to confirm lysolecithin-induced demyelination, MBP staining was quantified at each postinjection time point. In the LOT, labeling in the area surrounding the injection site was nearly absent at 7dpi (mean A/A = 9.57 +/- 1.02; Fig. 2A,E,I) and significantly increased over time (H=10.38, $p<0.05$). By 14dpi substantial recovery was observed (A/A = 30.78+/- 4.39; Fig. 2B,F,I) and at 21dpi MBP staining had doubled that of 14dpi (A/A=61.11 +/- 6.71; Fig. 2C,G,I). By 30dpi, MBP staining had returned to control levels (30dpi A/A=81.80 +/- 13.34, 30dpi control A/A =78.97+/-0.72, U= 4, *n.s.;* Fig. 2D,H,I).

MBP staining in the AC followed a different pattern to that of the LOT. Once again, very little staining was observed at 7dpi (A/A=18.77 +/- 3.08; Fig. 3A,E) and a significant increase occurred over time (H=12.12, *p<0.01;* Fig. 3I). However, the largest increase in MBP labeling in the AC occurred between 14 and 21dpi (compared to between 7 and 14dpi in the LOT). MBP labeling remained stable through 14dpi (A/A=21.37 +/- 12.44; Fig. 3B-C) but underwent a large increase by 21dpi (A/A = 67.24 +/- 9.84; Fig. 3C,G). As observed in the LOT, MBP labeling returned to control levels by 30dpi (A/A=82.65 +/- 3.20; control A/A =78.36 +/-11.72, U= 2; *n.s.;* Fig. 2D,H,I).

Electron Microscopy

To examine the effects of lysolecithin administration in more detail, electron microscopy was used to visualize changes in myelin at the individual axon level. In the LOT, the percentage of axons exhibiting myelination was significantly lower at 7dpi (M=27.91 +/- 12.47%; Fig. 4A) compared to controls (M=83.79 +/- 4.5%, U=0.0, *p<0.01*) and myelin sheaths were markedly thinner compared to controls (experimental M = 0.17 +/- 0.15nm, control M = 0.28 +/- 0.12, t=5.514, *p<0.0001*; Fig. 4C). By 14 dpi increases in both the percentage of myelinated axons (M=52.84 +/- 17.33%; U=8, *p<0.05*) and myelin thickness (M=0.23 +/- 0.09nm; t=3.21; *p=<0.01)* were observed. Nevertheless, myelin thickness of 14 dpi controls (M=0.25 +/- 0.09nm) was still significantly higher than in experimental animals (t=2.625, *p<0.01)*. Little change occurred between 14 and 21 dpi: neither the percentage of axons myelinated (M=64.1 +/- 19.47%; *n.s.*) nor myelin thickness (M=0.21nm +/- 0.16; *n.s.*) significantly changed. By 30dpi the percentage of axons myelinated (M=83.23 +/-7.89%) had significantly increased from 21dpi (U=1, *p<0.05)* and achieved levels similar to that of a control (M=82 +/- 4.85%, *n.s.*) Myelin

was also significantly thicker after 30 days (M=0.28nm +/- 0.11nm) than 21 dpi *(*t=5.596, *p<0.0001*) or controls (M=0.25 +/- 0.09nm, t=2.17, *p<0.05).*

G-ratios were calculated to ensure that thinner myelin sheaths were not observed as a result of sampling smaller-caliber axons. One week following injection in the LOT the g-ratios of the few axons that remained myelinated in experimental animals (M=0.845 +/- 0.08) were statistically similar to controls (M=0.839 +/- 0.05; *n.s*; Fig.5E). G-ratios increased by 14dpi (M=0.855 +/- 0.05; Fig. 5F) and were significantly higher than controls (M=0.838 +/- 0.05; t=3.-076, *p=<0.01*), indicating thinner myelin sheaths in experimental animals. Between 14 and 21dpi, no change in g-ratio was observed (21dpi M = 0.854 +/- 0.07; *n.s.*; Fig. 5G) and g-ratios of experimental animals remained significantly higher than controls (M=0.790 +/- 0.07; t=7.715; *p<0.0001*). After 30 days, mean g-ratio of experimental animals (M=0.831 +/- 0.05) was statistically similar to controls (M=0.850 +/- 0.05; t=1.843; *n.s.*; Fig. 5H).

Once again, patterns observed in the AC were different than those found in the LOT. The percentage of myelinated axons remained low three weeks after injection (7dpi M = 14.13 +/- 12.99%; 14 dpi M = 15.78 +/- 3.49%, 21 dpi M = 14.12 +/- 4.20%; F=0.068; *n.s.*). A large increase was observed between 21 and 30dpi (24.26 +/- 8.72%) and by 30dpi the percentage of myelinated axons was similar in experimental and control groups (control = 22.05 +/- .366%; *n.s*; Fig. 4B). Myelin thickness remained low two weeks following injection (7 dpi M = 0.17 +/- 0.13nm, 14 dpi M = 0.17 +/- 0.06nm) with an increase at 21 dpi (M = 0.21 +/- 0.13nm; t=3.156; *p<0.001*) and a further increase by 30 dpi (M=0.25 +/- 0.17nm; *n.s.*; Fig. 4D). Compared to controls, myelin was significantly thinner at 7dpi (t=3.211, *p<0.01*) and 21dpi (t=2.980, *p<0.01*).

G-ratios of myelinated axons did not differ between experimental and control groups at 7dpi (experimental M=0.831 +/- 0.16, control M =0.839 +/- 0.05; t=0.205, *n.s*; Fig. 6E) or 14dpi (experimental M = 0.824 +/- 0.06nm, control M= 0.816 +/- 0.07nm, t= 0.872, *n.s.*; Fig. 6F). By 21dpi, g-ratios of shams were significantly lower (experimental=0.845 +/- 0.07, control=0.783 +/- 0.06; t-7.406, *p<0.0001*; Fig. 6G). At 30 dpi, g-ratios of control (M=0.79 +/- 0.08) and experimental (M=0.78 +/- 0.06) did not differ (t=0.637, *n.s.*; Fig. 6H).

Discussion

The present experiments were designed to test whether lysolecithin-induced demyelination and remyelination occurs in two relatively unstudied large forebrain white matter tracts: the LOT and the AC. These tracts serve distinct functions within olfactory system circuitry, the LOT transmitting information from the olfactory bulb to the ipsilateral olfactory cortex and the AC mediating interhemispheric processing. The two tracts differ in many other ways as well. For example, axons comprising the the LOT first emerge embryonically three days earlier than the AC (E13 vs. E16; Walz et al., 2006, Silver et al., 1982). While there is evidence that the LOT is functional at birth (Logan et al., 2012), evidence suggests that the AC is not functional until around P12 (Kucharski and Hall, 1987). Recent work from our lab demonstrates that LOT myelination is initiated 3-4 days earlier (LOT: P7, AC: P11; Collins and Brunjes, in prep). Furthermore, significant structural differences also exist: the LOT consists of larger, more heavily myelinated axons, and a much larger percentage of axons are myelinated than in the AC (~80% and ~20%, respectively; Collins and Brunjes, in prep; Sturrock 1976; Brunjes, 2013). Moreover, LOT myelination is more vulnerable to effects of

sensory deprivation (Collins and Brunjes, in prep). Numerous differences between the two tracts suggested that the LOT and AC might also differ in susceptibility to and recovery from a demyelinating insult.

Evidence presented above indicates that both tracts are indeed significantly affected by lysolecithin administration. Immunostaining for MBP revealed extensive demyelination one week following injection in both regions. An electron microscopic analysis of the area surrounding the injection site demonstrated a significant reduction in the percentage of axons myelinated, and those remaining had significantly thinner myelin sheaths. Furthermore, both tracts exhibited substantial recovery. Thirty days after injection MBP labeling returned to normal and the percentage of axons displaying myelination was similar to controls in both tracts. This time course is similar to previous reports of lysolecithin-induced demyelination and remyelination in the mouse caudal cerebellar peduncle (Woodruff and Franklin, 1999) and corpus callosum (Woodruff et al., 2004).

However, recovery rates differed substantially between the LOT and AC. Numbers of myelinated axons remained low from 7 to 14 days after lysolecithin injection. Between 14 and 21dpi substantial remyelination occurred in the LOT, with continued increases in numbers to control levels by 30dpi. The process was delayed in the AC. Numbers of myelinated axons remained low three weeks after injections, with only ~15% of total fibers myelinated at that time. Rapid remyelination ensued thereafter, with control levels attained by 30dpi. What might be responsible for the observation that the LOT begins to recover from a lysolecithin insult earlier than the AC? One possibility is that clearance of myelin debris (critical for remyelination to occur; Lampron, 2015;

Miron et al., 2013; Neumann et al., 2008) occurs more readily in the LOT. Alternatively, oligodendrocyte precursor cells (OPCs) in the LOT might be more likely to differentiate into mature, myelinating cells. Indeed, recent work has demonstrated that the percentage of cells in the oligodendrocyte lineage (Olig2+) classifiable as precursor cells (expressing platelet-derived growth factor receptor α, a marker for OPCs) is approximately twice as high in the LOT than the AC (Collins and Brunjes, in prep). Such a high proportion of OPCs present in the LOT could contribute to more efficient recovery after lysolecithin administration, as OPC proliferation is necessary for remyelination (Gensert and Goldman, 1997; Pohl et al., 2011; Paez et al., 2012; Zawadzka et al., 2010).

The LOT and AC have a number of characteristics that make them attractive for studies of myelination and early development. They are compact, well defined, and are found across the vertebrate lineage. While they transmit information related to the same sensory modality, each carries different portions of the data stream. Nevertheless, the two tracts differ in several interesting and fundamental ways, including the timing of early myelination, extent of myelination, caliber of axons within the tracts, and susceptibility to functional restriction. The present results demonstrate that both tracts are easily manipulated with lysolecithin and thus can be used to study both the process of myelin de-and regeneration. Furthermore, by demonstrating that rates of remyelination differ substantially, the findings add to the growing list of fundamental differences between the LOT and AC, and thus strengthens the impact of using these tracts as tools for examining nervous system development.

Literature Cited

Bieber, A. J., Warrington, A., Asakura, K., Ciric, B., Kaveri, S. V., Pease, L. R., & Rodriguez, M. (2002). Human antibodies accelerate the rate of remyelination following lysolecithin-induced demyelination in mice. *Glia*, 37(3), 241-249.

Bieber, A. J., Kerr, S., & Rodriguez, M. (2003). Efficient central nervous system remyelination requires T cells. *Annals of neurology*, *53*(5), 680-684.

Blakemore, W. F., & Franklin, R. J. M. (2008). Remyelination in experimental models of toxin-induced demyelination. In *Advances in Multiple Sclerosis and Experimental Demyelinating Diseases* (pp. 193-212). Springer Berlin Heidelberg.

Brunjes, P. (2013). The mouse olfactory peduncle. 2. The anterior limb of the anterior commissure. *Frontiers in neuroanatomy,* 6, 51.

Brunjes, P., Collins, L., Osterberg, S., Phillips, A. (2014). The mouse olfactory peduncle. 3. Development of neurons, glia, and centrifugal afferents. *Frontiers in Neuroanatomy*. 8(4).

Caren, C.A., & Mitchell, J. (1982). Degeneration of non-myelinated axons in the rat sciatic nerve following lysolecithin injection. *Acta Neuropathologica*, 56, 187-193.

Chomiak, T., & Hu, B. (2009). What is the optimal value of the g-ratio for myelinated fibers in the rat CNS? A theoretical approach. *PloS one,* 4(11), e7754.

Collins, L. & Brunjes, P. (in prep). Myelination of the developing lateral olfactory tract and anterior commissure.

Denic, A., Johnson, A. J., Bieber, A. J., Warrington, A. E., Rodriguez, M., & Pirko, I. (2011). The relevance of animal models in multiple sclerosis research. *Pathophysiology,* 18(1), 21-29.

Fressinaud C, Vallat JM, Pouplard-Barthelaix A. (1996). Platelet-derived growth factor partly prevents chemically induced oligodendrocyte death and improves myelin-like membranes repair in vitro. *Glia* 16: 40–50.

Gensert, JoAnn M., and James E. Goldman. (1997) Endogenous progenitors remyelinate demyelinated axons in the adult CNS. *Neuron* 19.1: 197-203.

Gregson, N. A. (1989). Lysolipids and membrane damage: lysolecithin and its interaction with myelin.

Grishchuk, Y., Peña, K. A., Coblentz, J., King, V. E., Humphrey, D. M., Wang, S. L., ... & Slaugenhaupt, S. A. (2015). Impaired myelination and reduced brain ferric iron in the mouse model of mucolipidosis IV. *Disease models & mechanisms,* 8(12), 1591-1601.

Hall, Susan M. (1988). Neurotoxic effects of lysolecithin, mouse, rat. *Nervous System*. Springer Berlin Heidelberg. 63-73.

Jeffery, N. D., & Blakemore, W. F. (1995). Remyelination of mouse spinal cord axons demyelinated by local injection of lysolecithin. *Journal of neurocytology*, *24*(10), 775-781.

Kucharski, D., & Hall, W. G. (1987). New routes to early memories. *Science*, 238(4828), 786-788.

Lampron, Antoine, et al. "Inefficient clearance of myelin debris by microglia impairs remyelinating processes." *Journal of Experimental Medicine* 212.4 (2015): 481-495.

Lein, E.S. et al. (2007) Genome-wide atlas of gene expression in the adult mouse brain, *Nature* 445: 168-176. doi: 10.1038/nature05453

Logan, D., Brunet, L., Webb, W., Cutforth, T., Ngai, J., Stowers, L. (2012). Learned recognition of maternal signature odors mediates the first suckling episode in mice. *Current Biology*. 22(21)1998-2007.

Menn, B., Garcia-Verdugo, J. M., Yaschine, C., Gonzalez-Perez, O., Rowitch, D., & Alvarez-Buylla, A. (2006). Origin of oligodendrocytes in the subventricular zone of the adult brain. *Journal of Neuroscience*, *26*(30), 7907-7918.

Miron, V. E., Boyd, A., Zhao, J. W., Yuen, T. J., Ruckh, J. M., Shadrach, J. L., ... & Franklin, R. J. (2013). M2 microglia and macrophages drive oligodendrocyte differentiation during CNS remyelination. *Nature neuroscience*, 16(9), 1211-1218.

Mori, K., & Takagi, S. F. (1978). An intracellular study of dendrodendritic inhibitory synapses on mitral cells in the rabbit olfactory bulb. *The Journal of physiology,* 279, 569.

Mozafari, S., Sherafat, M. A., Javan, M., Mirnajafi-Zadeh, J., & Tiraihi, T. (2010). Visual evoked potentials and MBP gene expression imply endogenous myelin repair in adult rat optic nerve and chiasm following local lysolecithin induced demyelination. *Brain research*, *1351*, 50-56.

Nait-Oumesmar, B., Decker, L., Lachapelle, F., Avellana-Adalid, V., Bachelin, C., Evercooren, V., & Baron, A. (1999). Progenitor cells of the adult mouse subventricular zone proliferate, migrate and differentiate into oligodendrocytes after demyelination. *European Journal of Neuroscience*, 11(12), 4357-4366.

Neumann, H., M. R. Kotter, and R. J. M. Franklin. "Debris clearance by microglia: an essential link between degeneration and regeneration." *Brain.* 132.2 (2008): 288-295.

Ousman, S. S., & David, S. (2000). Lysophosphatidylcholine induces rapid recruitment and activation of macrophages in the adult mouse spinal cord. *Glia*, *30*(1), 92-104.

Paez, Pablo M., et al. "Golli myelin basic proteins stimulate oligodendrocyte progenitor cell proliferation and differentiation in remyelinating adult mouse brain." *Glia* 60.7 (2012): 1078-1093.

Podbielska, M., Banik, N. L., Kurowska, E., & Hogan, E. L. (2013). Myelin recovery in multiple sclerosis: the challenge of remyelination. *Brain sciences*, 3(3), 1282-1324.

Pohl, Hartmut BF, et al. "Genetically induced adult oligodendrocyte cell death is associated with poor myelin clearance, reduced remyelination, and axonal damage." *Journal of Neuroscience* 31.3 (2011): 1069-1080.

Rasband, W. 1. (1997). ImageJ. Bethesda, MD: US National Institutes of Health. *Available on http://rsb. info. nih. gov/ij*, *2009*.

Rushton, W. A. H. (1951). A theory of the effects of fibre size in medullated nerve. *The Journal of physiology*, 115(1), 101-122.

Schwob, J. E., & Price, J. L. (1984). The development of axonal connections in the central olfactory system of rats. *Journal of Comparative Neurology,* 223(2), 177-202.

Silver, J., Lorenz, S. E., Wahlsten, D., & Coughlin, J. (1982). Axonal guidance during development of the great cerebral commissures: descriptive and experimental studies, in vivo, on the role of preformed glial pathways. *Journal of Comparative Neurology*, 210(1), 10-29.

Sturrock, R. (1976). Development of the mouse anterior commissure. Part I. A comparison of myelination in the anterior and posterior limbs of the anterior commissure of the mouse brain. *Zbl. Vet. Med.* 5:54-67.

Walz, A., Omura, M., & Mombaerts, P. (2006). Development and topography of the lateral olfactory tract in the mouse: Imaging by genetically encoded and injected fluorescent markers. *Developmental Neurobiology.* 6(8): 835-846.

Woodruff, R. H., & Franklin, R. J. (1999). Demyelination and remyelination of the caudal cerebellar peduncle of adult rats following stereotaxic injections of lysolecithin, ethidium bromide, and complement/anti-galactocerebroside: a comparative study. *Glia*, *25*(3), 216-228.

Woodruff, R. H., Fruttiger, M., Richardson, W. D., & Franklin, R. J. (2004). Platelet-derived growth factor regulates oligodendrocyte progenitor numbers in adult CNS and their response following CNS demyelination. *Molecular and Cellular Neuroscience*, 25(2), 252-262.

Zawadzka, M., Rivers, L. E., Fancy, S. P., Zhao, C., Tripathi, R., Jamen, F., ... & Rowitch, D. H. (2010). CNS-resident glial progenitor/stem cells produce Schwann cells as well as oligodendrocytes during repair of CNS demyelination. *Cell stem cell,* 6(6), 578-590.

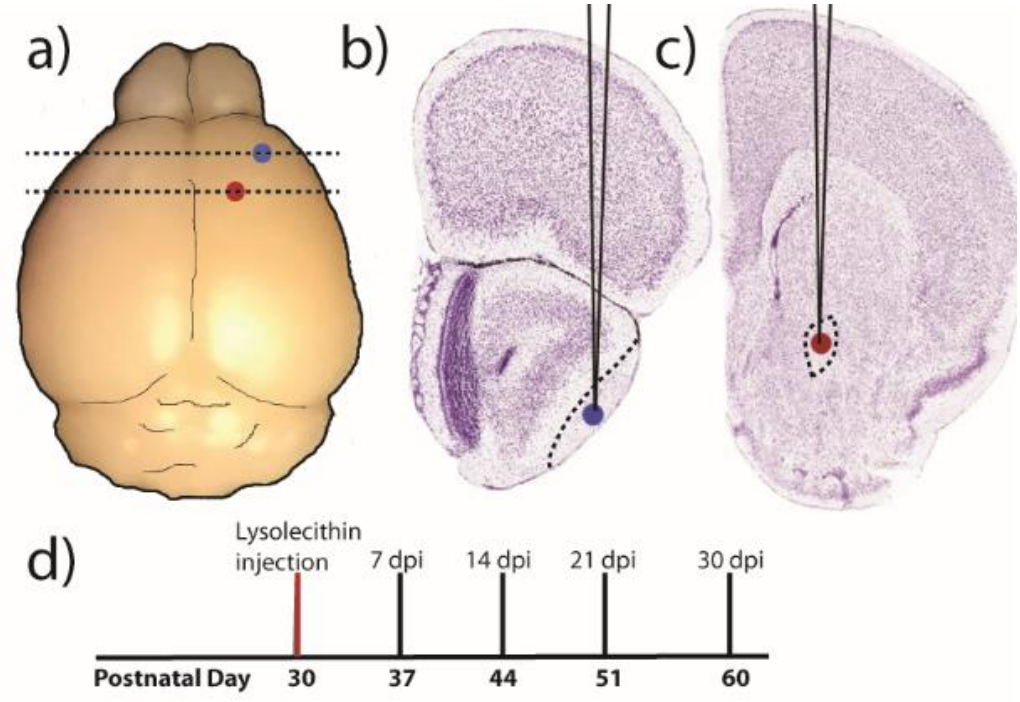

Fig. 1 Lysolecithin injection methods. (A) Dorsal view of the brain showing location of craniotomy for injections into the LOT (blue) and AC (red). Dotted lines represent planes of sectioning for Nissl images in B and C. (B,C) Placements of pipettes for lysolecithin injections in the lateral olfactory tract (B) and anterior limb of the anterior commissure (C). Nissl image credit: Allen Institute (Lein et al., 2007). (D) Lysolecithin injections were performed on postnatal day 30. Animals were sacrificed at 7, 14, 21, or 30 days post-injection (dpi).

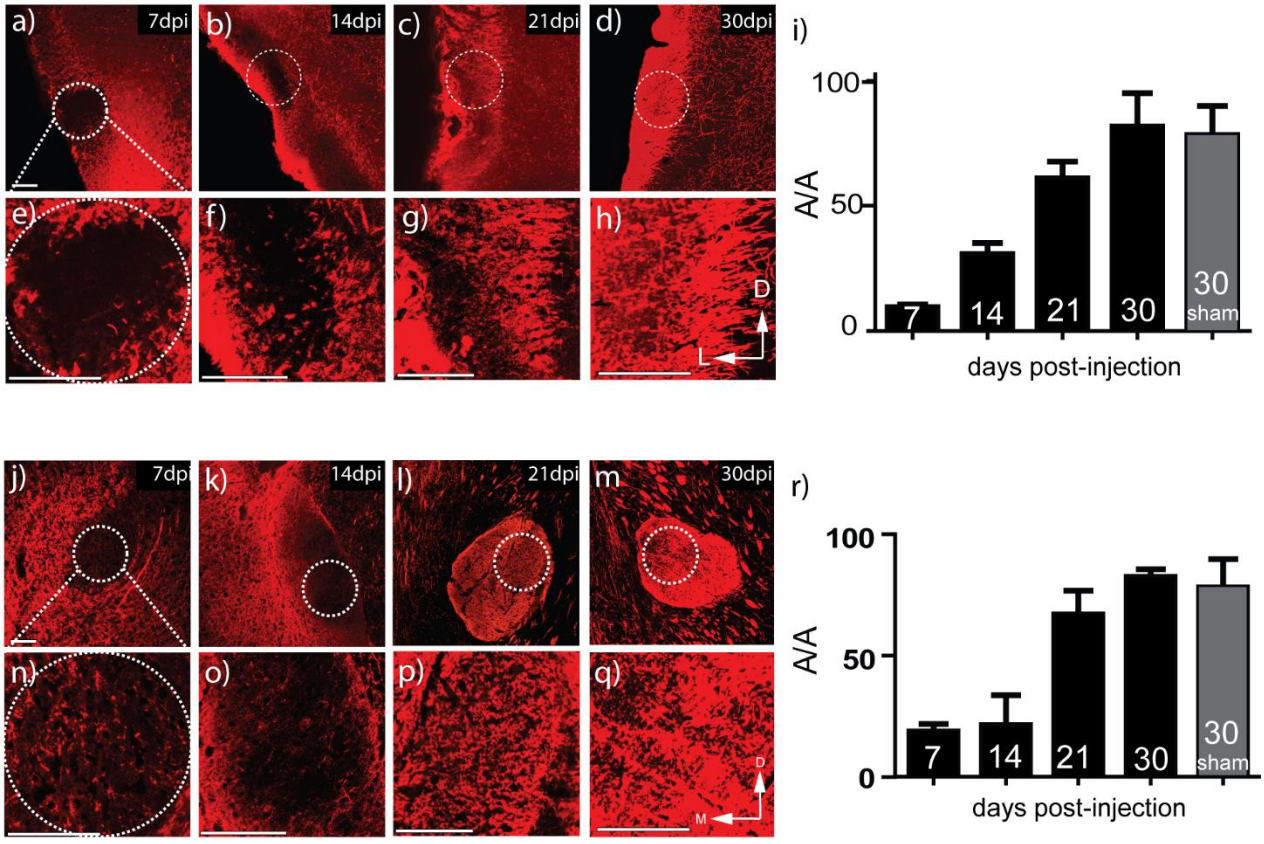

Fig. 2 Changes in MBP staining after lysolecithin administration in the LOT (top panels) and AC (bottom panels). (A-D, J-M) Lower power images of MBP labeling (red) in the 7, 14, 21, and 30 dpi lysolecithin administration in the LOT and AC, respectively. Dotted circle represents 200μm-diameter region used in quantification. (E-H, N-P) Higher power view of test region. Scale bars = 100μm. (I,Q) Changes in MBP labeling after injection. A/A = area fraction (ratio of labeled to total pixels).

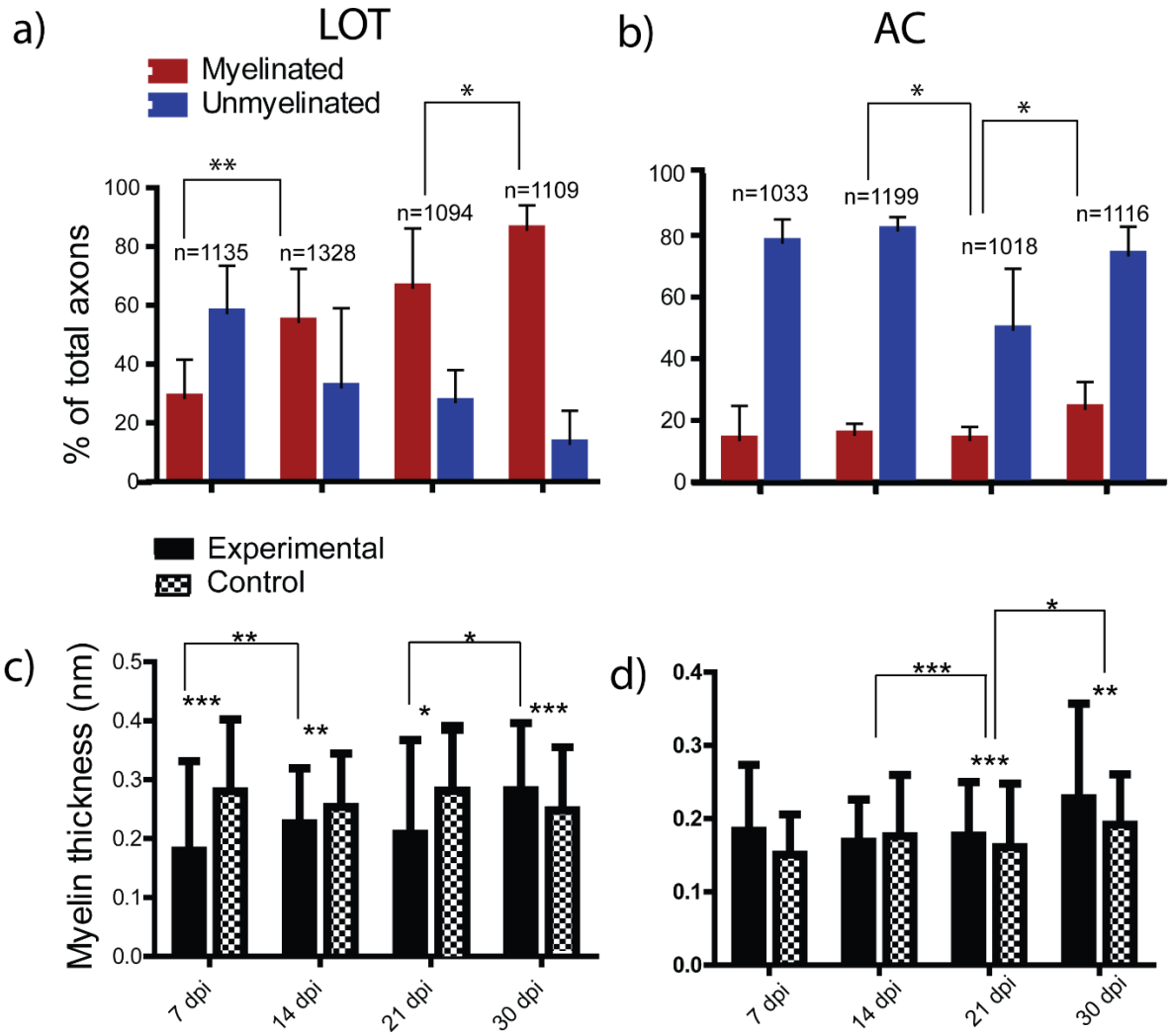

Fig. 3 Quantification of demyelination in the LOT and AC. (A) Percent of myelinated (red) and unmyelinated (blue) axons in the LOT. 7 days following lysolecithin administration the percentage of axons myelinated (red bars) within the LOT had substantially decreased. Percentage of myelinated axons increased largely between 7 and 14 dpi and again between 21 and 30 dpi. (B) In the AC, a slightly altered pattern was observed. After 7 days there was a significant reduction in the percentage of axons myelinated. Myelination remained low through 21 dpi and increased significantly by 30 dpi. (C) Myelin sheaths were significantly thinner in experimental animals (solid bars)

than sham-injected controls (checkered bars) at all time points examined. An increase in myelin thickness was observed between 7 and 14 dpi and again between 21 and 30 dpi. (D) In the AC, myelin thickness did not significantly differ from controls at 7 or 14 dpi, but was significantly lower at 21 dpi and higher at 30 dpi. Myelin sheath thickness in experimental animals rose between 14 and 30 dpi. Error bars represent standard deviation. *$p<0.05$, **$p<0.01$, ***$p<0.001$

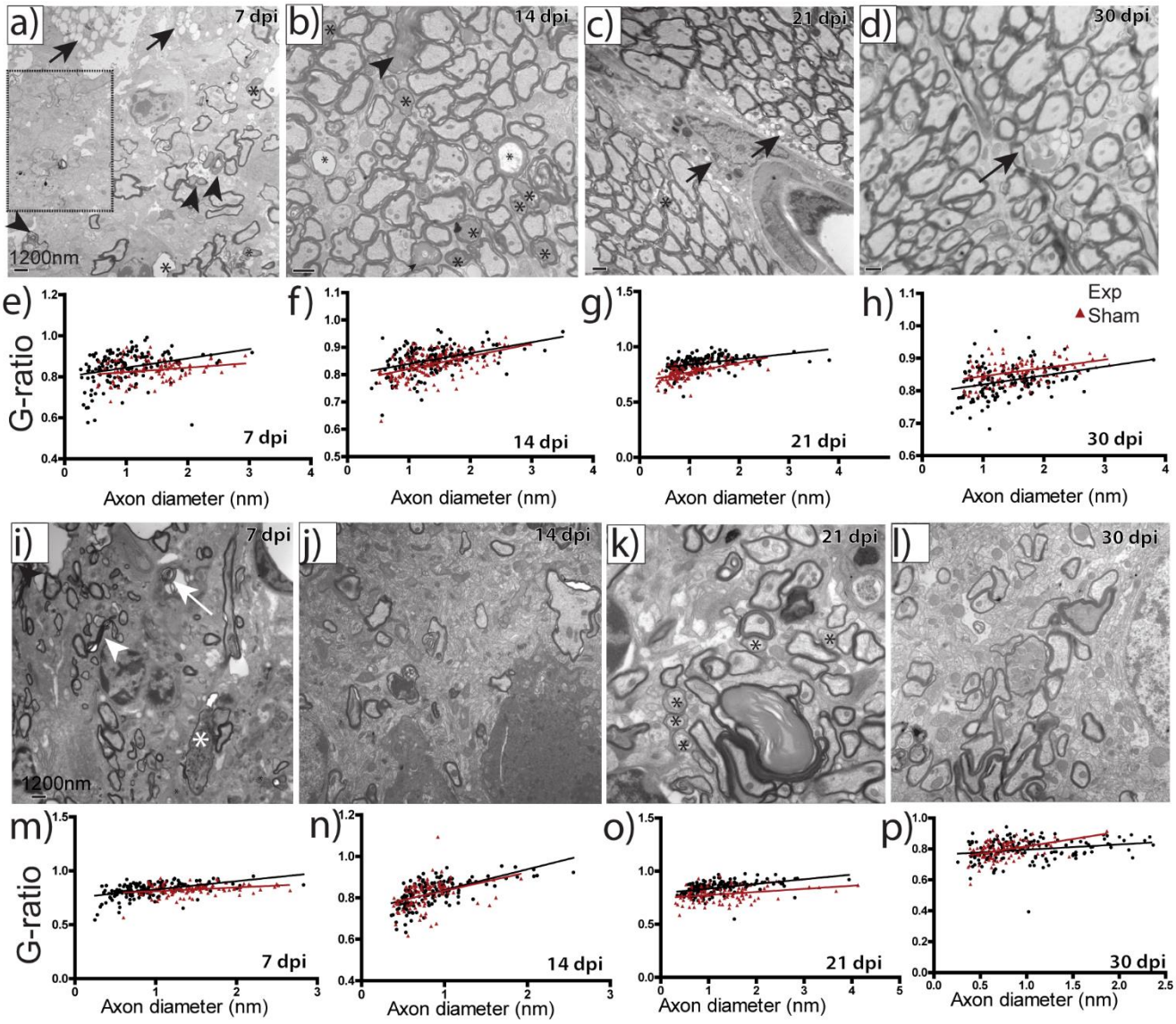

Fig. 4 Visualization of myelinated axons the LOT (top) and AC (bottom) following lysolecithin administration. A) In the LOT at 7 days post-injection (dpi) large patches of demyelinated fibers (dotted box) and lipid deposits (arrows) are present, along with some evidence of degenerating axons (asterisks) and degenerating myelin sheaths (arrowheads). B) At 14dpi several damaged axons are observed along with a substantial increase in the density of myelinated axons. C) By 21dpi, most debris have been cleared and by 30dpi (D) little evidence of damage remains. E-H) G-ratios for

experimental (black circles) and sham (red triangles) animals with corresponding linear regression lines. Higher caliber axons were more significantly affected at 7dpi, while lower-caliber axons show the greatest effect later in recovery, suggesting that larger axons are affected by lysolecithin first. (I) In the AC at 7dpi, extensive damage was observed, including ovoid bodies (asterisk) and myelin out-foldings (arrowhead), along with damaged myelin sheaths and myelin whorls (arrows). (J) A similar extent of myelination disruption was observed at 14 days post-injection (dpi). (K) At 21 dpi, aberrant myelination was still present and evidence of myelinating axons was observed (asterisks). (L) Some damage was still present at 30 dpi, but myelination had largely returned to normal. (M-P) G-ratios for experimental (black circles) and sham (red triangles) animals with corresponding linear regression lines. Similar to the LOT, higher-caliber axons were consistently more affected than lower-caliber axons.

Chapter IV

Synaptic Development of Contralaterally-Projecting Axons Terminating in the Anterior Olfactory Nucleus

Abstract

The present work examines postnatal synaptogenesis in the anterior olfactory nucleus (AON). This analysis is accomplished in three ways. First, a developmental analysis of synapse formation and maturation in the AON was conducted using electron microscopy (EM) in order to a) determine whether synaptogenesis proceeds uniformly across the AON and b) clarify the relationship between myelination and synaptogenesis in the olfactory system. Results demonstrate that overall, synapses within the plexiform layer of the AON (layer I) reach maturity earlier than those of layer II, a deeper layer which consists of tightly packed cell bodies. This finding indicates that considerable postnatal circuit refinement occurs in layer II. Moreover, synapse development in layers receiving input from the two large white matter tracts of the olfactory system was found to occur very early in development, preceding myelination of those tracts. These findings point to a role of synaptic activity in initiation of myelination of olfactory tracts. Next, a fluorescent anterograde tracer was used to specifically investigate where AON projection neurons innervate the contralateral hemisphere. Labeling was tightly restricted to the border between the superficial molecular layer (I) and the deeper cell body layer (II), indicating that synapses are formed onto dendrites close to the cell body. Interestingly, labeling in younger animals was confined to pars lateralis of the AON, supporting the idea that AON subregions are functionally distinct. Last, EM analysis of anterogradely-labeled terminals revealed that these terminals are larger than the population and indeed form axodendritic synapses deep within layer I, presumably on apical dendrites extending from layer II, which suggests a large role of contralateral input in driving activity of the AON.

The olfactory system has long been considered a useful model for examining processes of early neural development because olfactory regions exhibit strict laminar structure and sensory input is easily manipulated. Furthermore, olfaction is crucially important from birth for recognition of food and caregivers (Logan et al., 2012). Therefore, an understanding of early development is vital to an understanding of olfactory processing.

Organization of olfactory pathways has been well studied (Mori, 2014; Haberly, 1985; Brunjes et al., 2005). Axons exiting the olfactory bulb (OB), which receives input from primary sensory neurons, project ipsilaterally via the lateral olfactory tract (LOT) to the anterior olfactory nucleus (AON) and piriform cortex (PC). The AON is a two-layered cortical structure with strict lamination. The most superficial layer (layer I) is a plexiform, or molecular, layer often subdivided into layer Ia, immediately adjacent to the LOT containing axon collaterals from the OB, and a deeper layer Ib, containing association fibers from the PC and contralateral AON (Brunjes et al., 2005; Friedman and Price, 1984). Layer II is a cell-dense zone containing pyramidal cells that extend spiny apical dendrites into layer I. Based on evidence of different neurochemical phenotypes and cell density, layer II has been further divided into superficial layer IIa and deeper IIb zones (Meyer et al., 2006). The AON has also been divided based on functionally segregated subregions: pars lateralis, pars dorsalis, pars medialis, pars ventroposterior, and pars externa. The PC is a three-layered cortical structure that lies caudal to the AON. Decussating fibers arising in the AON and PC cross the midline via the anterior (or olfactory) limb of the anterior commissure (AC), and project to the contralateral AON, PC, and OB (Haberly and Price, 1978a; Haberly and Price, 1978b; Schwob and Price,

1984). Axons arising from different AON subregions form different connections with the contralateral side. For example, contralateral projections from all subregions of the AON are found in pars dorsalis, but pars medialis does not receive contralateral input (Haberly and Price, 1978b). Additionally, injections into pars lateralis and pars ventroposterior in rats selectively label deep layer I and superficial layer II of the contralateral AON (Illig and Eudy, 2009). These contralaterally-projecting axons have been implicated in left-right localization of odors (Kikuta et al., 2010) and the transfer of olfactory memories and preferences to the opposite hemisphere (Kucharski et al., 1990).

Early development of the olfactory system proceeds in a generally anterior-posterior fashion: the olfactory epithelium develops earlier than the OB, which develops earlier than olfactory cortices (Schwob and Price, 1984). However, the PC undergoes extensive neurogenesis around the same time as the OB, while neurogenesis in the AON is delayed by several days (Lopez-Mascaraque and Castro, 2002). Moreover, within the AON and PC, cells are added in a caudal-rostral, superficial-deep pattern (Schwob and Price, 1984; Brunjes et el., 2005). These findings suggest that maturation of the system mirrors olfactory circuitry. Indeed, innervation patterns in adulthood parallel developmental patterns such that regions that receive less extensive innervation from the OB (e.g. pars medialis of the AON) develop slower than regions with heavy bulbar input, like the piriform cortex (Schwob and Price, 1984).

The study of synaptic development within olfactory cortical regions is in its infancy. Primary sensory neurons form synapses in the OB very early. Synaptogenesis begins around E14, continues more than a month into postnatal development, and the

most rapid synaptogenesis is observed before P10 (Hinds and Hinds, 1976). In other sensory systems, synapses made by primary sensory neurons appear earlier than cortical synapses (Rakic et al., 1986; Blankenship and Feller; 2010) and several reports indicate that the AON develops later than the OB on other parameters such as neurogenesis (Lopez-Mascaraque and Castro, 2002) and volumetric growth (Brunjes et al, 2005; Frazier and Brunjes, 1988). Therefore, it is likely that a sharp increase in synaptic density within the AON occurs later than in the OB and extends beyond P10.

No present work exists characterizing synaptology in the developing or adult AON; however, synaptic density and morphology within the PC have been previously examined (Haberly and Feig, 1983; Haberly and Behan, 1983; Westrum, 1975; Schikorski and Stevens, 1999; Derer et al., 1977). Differences in cellular morphology and synaptic distribution between layers suggest functional segregation of olfactory processing within the PC. Similar functional segregation likely also exists in the AON, evidenced by distinct morphology and innervation patterns between layers (Brunjes et al., 2005; Illig and Eudy, 2009).

The present work examines postnatal synaptogenesis in the AON in order to clarify the relationship between synapse development, axonal development, and functional onset in the olfactory system. Previous work has demonstrated that the AC undergoes a period of rapid myelination between P11 and P15 (Brunjes et al., 2014; Collins and Brunjes, in prep), pointing to this period as a critical time for formation of contralateral olfactory connections (Downes and Mullins, 2014). Additionally, synaptogenesis and myelinogenesis have been shown to occur alongside each other in other brain regions (Huttenlocher & Dabholkar, 1997). Therefore, it was hypothesized

that timing of synaptogenesis of contralateral terminals would correspond with myelination of the AC. A developmental time course of synapse formation in the AON is established by determining the distribution and maturity of AON synapses through early postnatal development using EM. In addition, the distribution of contralaterally-projecting terminals in the AON is examined developmentally using a viral fluorescent tracer.

Methods

Development of synapses in the AON

To establish a trajectory of synapse development in the AON, an analysis of synapse distribution was conducted in a developmental series. Electron microscopy was used to allow for a detailed investigation of synapse density, synapse length, and terminal bouton area. Data were collected from layer Ia, Ib, IIa, and IIb of pars lateralis.

Animals

Groups of 3 C57BL/6J mice aged P5 (early in olfactory system development), P13 (at the beginning of the period of rapid myelination of the AC; Collins and Brunjes, in prep), P17 (immediately following rapid myelination of the AC), and P30 (when olfactory system growth plateaus; Hinds and Hinds 1976) were used in this study.

Tissue Preparation

Mice were anesthetized with sodium pentobarbital (Euthasol; 0.39 mg drug/gm body weight; 150mg/kg) and perfused with 0.01M phosphate buffered saline (PBS; pH 7.4) followed by a 2% glutaraldehyde, 2% paraformaldehyde solution. Brains were dissected, post-fixed at least 12 hours, and sectioned at 60µm on a vibratome. Tissue was rinsed in 0.1M phosphate buffer (PB) three times followed by an hour incubation in

a 1% osmium tetroxide solution in PB. Tissue was then rinsed two more times with PB, once with 50% EtOH, once with 70% EtOH, and finally placed in 4% uranyl acetate in 70% EtOH overnight. Tissue was then serially dehydrated with ethanol, placed in a 1:1 solution of acetone and EPON resin and kept overnight. The acetone-EPON solution was exchanged for full EPON and let sit for at least 2 hours. Sections were flat-embedded on aclar and heated in an oven at 60℃ overnight. Flat-embedded tissue was then transferred to EPON-filled capsules and again placed in an oven overnight to allow for the EPON to polymerize. After polymerization, the tissue was sectioned on an ultramicrotome (Leica UC7) at 80µm.

Imaging and Analysis

To examine synapse development 10,000x magnification images were taken on a JEOL 1010 electron microscope with a 16MB camera. This yielded a pixel size of 0.73nm, allowing for discrimination of synaptic membranes. Four locations were selected at increasing depth in the AON, corresponding to layer Ia (plexiform layer immediately adjacent to the lateral olfactory tract, receiving primary afferent projections from the OB; Price, 1973), layer Ib (deeper plexiform zone that receives input from associational fibers; Heimer, 1968), layer IIa (superficial portion of the cell-dense region of the AON), and layer IIb (deep portion of the cellular layer; Fig. 1A,B). Between 8 and 15 images were taken in each layer.

Image ProPlus 5.1 (Media Cybernetics, Silver Spring, MD) was used for collecting measurements. The total area of neuropil examined was measured excluding any space taken by cell somas, myelinated axons, or blood vessels. To estimate synapse density, synapse counts were divided by area. Because synapse terminal size

is larger than the thickness of the examined ultrathin section, correction for synapse size bias was applied (Defelipe et al., 1999; Erisir and Harris, 2003; Wang et al., 2013). In this correction, the number of synapses is divided by the product of the area of the region examined and the average synapse length in that region. This method afforded a close estimation of synapse distribution between layers. Averages were calculated for each animal in each layer and a one-way ANOVA with Bonferroni post-hoc tests was used to determine difference between groups.

In addition to synapse density, synapse length was measured and synaptic terminals were traced (Fig. 1C-E). Non-parametric statistics (Kruskal-Wallis with Dunn's multiple comparisons post-hoc tests) were used to compare data across layers and ages because distributions of synapse length and terminal area were not normally distributed.

Visualizing contralateral projections

To visualize the location and distribution of AC fiber terminals in the AON, an anterograde fluorescent viral tracer (AAV9.hSyn.TurboRFP.WPRE.rBG) was used. The tracer was injected into pars lateralis of the right AON and the entire left AON was imaged using confocal microscopy.

Animals

Injections were made in C57BL/6J mice aged P1, 5, 20, and 40. Animals were perfused, respectively, at P5, P12, P30, and P50, allowing ample time for the viral tracer to travel to the contralateral hemisphere. These ages were chosen to correspond closely with ages used in EM analyses.

Procedure

Mice were anesthetized with isoflurane and placed on a stereotaxic apparatus. Approximately 1nl of adeno-associated virus (AAV9, $2x10^{4}$ particles/µl; Penn Vector Core) in PBS was injected into the right AON with a picospritzer. A hole was drilled 2mm lateral and 1mm anterior to bregma and a pipette lowered 3mm from the surface of the brain to hit pars lateralis of the AON (Fig. 2A, B). Pars lateralis has been established as a source of contralateral AON input (Illig and Eudy, 2009); therefore, injections in pars lateralis ensured that contralateral terminals would be labeled. Animals were monitored during recovery and once a day after surgery.

Four to 10 days after injection, mice were deeply anesthetized with sodium pentobarbital (Euthasol; 0.39 mg drug/gm body weight; 150mg/kg) and perfused intracardially with 0.01M phosphate buffered saline (PBS; pH 7.4) followed by 2% buffered formaldehyde. Brains were post-fixed for at least 12 hours. Tissue was sectioned at 60µm using a vibratome. Sections were mounted on slides with SlowFade mounting media (Invitrogen: S36937).

The left AON was imaged at 20x and 40x magnification using a Nikon 80i confocal microscope fitted with a Nikon C2 scanning system (Nikon Instruments, Inc., Melville, NY). Images were combined using Photoshop to visualize the distribution of labeled fibers through the AON.

Synaptology of AC fibers terminating in the AON

To specifically analyze terminals from contralaterally-projecting axons in P30 mice, biotinylated dextran amine (BDA)-labeled sections from the left AON were prepared for EM.

Procedure

Approximately 1nl of 10,000 molecular weight BDA (Invitrogen Molecular Probes, cat #: D1956) in PBS was injected into the right AON with a picospritzer as described above for AAV injections. Seven to 10 days after injection, animals were perfused intracardially with Tyrode's solution followed by a 2% paraformaldehyde, 1% glutaraldehyde solution. Brains were dissected and postfixed for at least 2 hrs. Sixty μm vibratome sections were collected and rinsed in 0.1M PBS 4 times for 5 minutes. Tissue was then placed in 1% sodium borohydride in PBS for 30 minutes and then incubated in an ABC solution (Vector Elite) for 1-2 hours while gently agitated on a shaker. Tissue was then placed in a 0.05% DAB, 3% hydrogen peroxide solution for 15-20 minutes. Tissue was rinsed in PBS four more times before being prepared for EM.

Stained AON sections were selected and prepared for EM. Tissue was rinsed three times with 0.1% phosphate buffer (PB) and post-fixed with osmium tetroxide for one hour. Following post-fixing, tissue was sequentially dehydrated, counterstained with 4% uranyl acetate in 70% EtOH overnight, and embedded in EPON resin. Tissue was then sectioned at the interface between the tissue and EPON using an ultramicrotome (Leica UC7).

Imaging and Analysis

Images were taken at 10,000x magnification using a JEOL 1010 electron microscope, yielding a resolution of 0.73nm/pixel to allow for visualization of synapses. Sampling was biased to labeled synapses. BDA injections produced both anterograde and retrograde labeling (Fig. 5). In instances of anterogradely-labeled terminals, synapse length as well as terminal area were measured for 20 synapses and 14

terminals. For retrogradely-labeled synapses, labeled synapse length was measured for 15 synapses. Measures from labeled synapses were compared to population data using a Mann-Whitney nonparametric test.

Results

Development of synapses in the AON

In order to address whether there are differences in developmental trajectory or mature synapse distribution within layers receiving different types of input (afferent vs. association), the AON of 3 mice aged P5, 13, 17, and 30 was examined using EM. Analysis of at least 8 10,000x magnification images yielded a minimum analyzed area of 177μm^2 per layer in each animal. Images were analyzed for synapse density, length, and terminal area.

Synapse density

In this study, we used synapse density as a measure of maturation of the AON. Rapid synaptogenesis in early development leads to increased synapse density while later increases in dendrite branching or developmental synapse pruning can lead to a subsequent reduction. In mature (P30) mice, no significant differences were observed in synapse density between layers (Fig. 1F); however, different developmental patterns were observed between layers. In layers Ia and b, no notable changes in synapse density occurred across time (Fig. 2A,B), confirmed with a one-way ANOVA ($F=1.15$, *n.s.*). Conversely, synapse density in layers IIa and b increased through P17 (IIa: $F=4.57$, $p<0.05$; IIb: $F=6.42$, $p<0.05$) and slightly declined by P30 (Fig. 2A). In both IIa and IIb, Bonferroni's post-hoc tests revealed that the developmental change observed

can be accounted for by large increases between P5 and P17 (IIa: t=3.62, *p<0.05*; IIb: t=4.09, *p<0.05*).

Synapse length

Synapse length (a measure of the diameter of the synapse active zone) did not significantly differ between layers at the most mature age examined (P30; H=5.04, *n.s.*; Fig. 1G). Developmental increases in synapse length were observed in layer II but not layer I. In both layer Ia and b, little change in synaptic length occured over time (Ia: H=0.53, *n.s.*; Ib: H=3.323, *n.s.*; Fig. 2B,C). Conversely, in both layer IIa and b developmental changes were observed across the examined period with large increases between P13 and P30 (IIa: H=25.2, *p<0.0001*; IIb: H=16.94, *p<0.001*; Fig. 2D,E).

Terminal Area

Terminal bouton size can be used as both a measure of synapse development as well as an indicator of subpopulations receiving different input within a given region. For instance, developmental increases in terminal area have been previously reported in the visual cortex (Erisir and Dreusicke, 2005) and within the visual thalamus inputs from different areas (i.e. cortex and brainstem) form terminals that differ in size (Erisir et al, 1997). At P30, all layers of the AON exhibited statistically similar terminal area distributions (H=2.58, *n.s.*; Fig. 1H). In layer Ia and b no significant changes occurred across time (Ia: H=2.20, *n.s.*; Ib: H=2.03, *n.s.*; Fig. 2F,G). Layer IIa increased in synapse density across time (H=20.67, *p<0.0001*) with the largest change observed between P17 and 30 (difference in rank sum = -46.02, *p<0.0001*). Interestingly, distribution of terminal areas at P5 resembled that of P30 (difference in rank sum =

17.27, *n.s.*; Fig. 2H). In layer IIb no significant changes in terminal area distribution were observed (H-0.87, *n.s.*; Fig. 2I).

Visualizing contralateral projections

In order to determine the precise location of axon terminals within the AON that originate from the contralateral hemisphere, an anterograde tracer was injected into the right AON and the left AON was visualized with confocal microscopy (Fig. 3A,B). Large tracer injections resulted in contralateral labeling restricted to a tight band deep within layer I. An analysis of terminal distribution in a developmental series was also conducted in order to clarify the pattern by which AC fibers first innervate the AON.

Location of contralateral terminals

In adults, AAV injections into the right AON pars lateralis led to robust labeling in the contralateral pars lateralis and dorsalis. Relatively less robust labeling was encountered in pars ventroposterior, and little to no label traveled to pars medialis (Fig.3G,H). The pattern of axon projections are similar to those reported by Illig and Eudy (2009) and Haberly and Price (1978) in the rat. Fibers can be seen coursing out of the ALAC and distributing through the lateral and dorsal AON in layer II with few fibers continuing into superficial layer I (Fig. 3F-H).

Development of contralateral projections

At P5 many labeled fibers could be seen extending across the midline in the AC (Fig. 3C), although very few labeled axons were present in the contralateral AON (Fig. 3D,E). The density of labeled axons terminating in the AON sharply increased by P12 and again by P30 (Fig. 2F,G). During this time the band of labeled fibers present in layer Ib/IIa became substantially thicker. Labeling at P50 was stronger than that

observed at P30, suggesting that contralateral connections continue to be added long after development of the rest of the olfactory system has plateaued (Fig. 2H).

Synaptology of AC fibers terminating in the AON

Anterogradely filled axon terminals were found deep in layer Ib (Fig. 4A) and labeled axons could be seen coursing through layer II. Terminals were seen contacting both dendritic shafts and spines (Fig. 4 B,C). Synapse length did not significantly differ from population data (U=1362, *n.s.*; Fig. 4D), but labeled terminals were significantly larger (U=342, $p<0.01$; Fig. 4E), indicating that contralateral projections provide a distinct subpopulation of terminals within layer I.

Injection of BDA also produced retrograde labeling, evidenced by labeling of cell bodies and postsynaptic fibers in the contralateral hemisphere (Fig. 5). In the AON contralateral to injection retrogradely labeled fibers were found in pars lateralis and dorsalis. Cell body labeling was encountered in layer II with an even superficial-to-deep distribution (Fig. 5C-D). Labeled postsynaptic fibers were largely restricted to layer I so synapse length distribution was compared to combined population data from layer Ia and b. The distribution of labeled synapse length was not different than the population data (U=848.5, *n.s.*; Fig. 5F).

Discussion

The present work was designed to test whether there are substantial differences in synaptogenesis across regions within the AON, a relatively understudied component of olfactory circuitry. It was hypothesized that areas receiving input from the LOT, which develops very early in postnatal life, would undergo extensive synaptogenesis earlier than areas receiving input from the AC, which has been shown to myelinate significantly

later (Collins and Brunjes, in prep). Additionally, it was hypothesized that terminals of contralaterally-projecting axons terminating in the AON would be restricted to layer Ib of the AON and would demonstrate a distinct synapse morphology, either in length or terminal bouton area, from other synapses in the region. Results presented above advance our understanding of olfactory system development and circuitry in several fundamental ways.

First, findings indicate that synapse maturation in the plexiform layer of the AON occurs earlier than the cellular layer. Changes in synapse density or morphology (length and terminal bouton size) are indicative of synapse formation or circuit refinement. Within the plexiform layer of the AON, these parameters did not change over the developmental period examined, indicating that synapse maturity is achieved earlier than P5. Such early synaptic maturation within layer I of the AON has implications for the importance of neural activity in other developmental processes. For example, axons forming terminals in layer Ia and b in the AON initiate myelination at P7 and P11, respectively (Collins and Brunjes, in prep). The present work suggests that synaptic activity is a prerequisite for myelination onset because mature synaptic distribution was achieved well before myelination begins.

Second, it was confirmed that the commissural projections contained within the AC are added even beyond P30, long after the LOT establishes adult-like innervation patterns around P14 (Walz et al., 2006). These data support the claim that commissural and association fibers reach their final postsynaptic targets later than primary afferents. A similar developmental pattern is observed in other sensory systems. For example, within the visual cortex establishment of thalamocortical synapses occurs well before

that of intracortical association connections (Sur and Leamey, 2001). In the olfactory system, early development of primary afferents is particularly important because neonatal mice require olfactory cues for survival (Logan et al., 2012). Commissural fibers carried in the AC allow for interhemispheric refinement of olfactory information. The later development of the AC could indicate that postnatal olfactory experience is required to shape these olfactory associational connections.

Third, differences in development and connectivity between AON subregions (pars lateralis, dorsalis, medialis, and ventroposterior) suggest that these areas serve distinct roles in olfactory processing. Pars lateralis and dorsalis were most heavily innervated by the contralateral pars lateralis, similar to reports from the rat (Illig and Eudy, 2009). Interestingly, innervation of pars lateralis preceded that of pars dorsalis, indicating that pars lateralis processes the majority of contralateral input in early postnatal life. Pars ventroposterior and medialis received little to no contralateral input. These data support claims that the two subregions are organized differently than pars lateralis and dorsalis and may contribute differently to processing of olfactory information (Brunjes et al., 2005; Brunjes et al., 2014).

Finally, anterograde tracing revealed that contralateral projections carried in the AC terminate in a thin band deep within layer I. Furthermore, EM studies revealed that these terminals synapse onto dendrites, presumably apical dendrites extending from layer II, and form large terminal boutons. The tight regulation of terminal location at the proximal end of these apical dendrites and large terminal size suggests an important role for contralateral projections in driving activity of the AON.

The present findings bring to light new questions. For instance, why does synaptic development in the cellular layer of the AON trail that of the plexiform layer? Layer II consists of a wide variety of excitatory and inhibitory cells with diverse morphologies, subsets of which do not achieve mature neurochemical phenotypes until P30 (Brunjes et al., 2014). It is possible that the later development of certain subtypes of cells could account for differences observed in the present study, although it is unclear what implications this might have for olfactory processing in early life. Future studies should clarify the relationship between delayed maturation of the AON and early postnatal olfactory-guided behavior. Additionally, our results demonstrate that synaptogenesis precedes myelin formation of the LOT and AC, suggesting a role for activity in myelination onset within these tracts. However, the existence of a causal relationship between synaptic activity and myelination was not examined in the present study. In order to more clearly define the relationship between synaptic activity and myelinogenesis in olfactory white matter tracts, neural activity could be manipulated pharmacologically or via sensory deprivation and myelination examined developmentally. Together, the present results provide important insight into olfactory system development and circuitry that have strong implications for the role of the AON in processing complex olfactory information.

Literature Cited

Blankenship, A. G., & Feller, M. B. (2010). Mechanisms underlying spontaneous patterned activity in developing neural circuits. *Nature reviews. Neuroscience*, *11*(1), 18.

Brunjes, P. C., Illig, K. R., & Meyer, E. A. (2005). A field guide to the anterior olfactory nucleus (cortex). *Brain research reviews*, *50*(2), 305-335.

Brunjes, P., Collins, L., Osterberg, S., Phillips, A. (2014). The mouse olfactory peduncle. 3. Development of neurons, glia, and centrifugal afferents. *Frontiers in Neuroanatomy. 8*(4).

Collins, L. & Brunjes, P. (in prep). Myelination of the developing lateral olfactory tract and anterior commissure.

Derer, P., Caviness, V. S., & Sidman, R. L. (1977). Early cortical histogenesis in the primary olfactory cortex of the mouse. *Brain research*, *123*(1), 27-40.

Downes, N., & Mullins, P. (2014). The development of myelin in the brain of the juvenile rat. *Toxicologic pathology*, *42*(5), 913-922.

Erisir, A., & Dreusicke, M. (2005). Quantitative morphology and postsynaptic targets of thalamocortical axons in critical period and adult ferret visual cortex. *Journal of Comparative Neurology*, *485*(1), 11-31.

Erişir, A., Van Horn, S. C., & Sherman, S. M. (1997). Relative numbers of cortical and brainstem inputs to the lateral geniculate nucleus. *Proceedings of the National Academy of Sciences*, *94*(4), 1517-1520.

Frazier, L. L., & Brunjes, P. C. (1988). Unilateral odor deprivation: early postnatal changes in olfactory bulb cell density and number. *Journal of Comparative*

Neurology, *269*(3), 355-370.

Friedman, B., & Price, J. L. (1984). Fiber systems in the olfactory bulb and cortex: a study in adult and developing rats, using the Timm method with the light and electron microscope. *Journal of Comparative Neurology*, *223*(1), 88-109.

Haberly, L. B. (1985). Neuronal circuitry in olfactory cortex: Anatomy and functional implications. *Chemical Senses*.

Haberly, L., & Behan, M. (1983). Structure of the piriform cortex of the opossum. III. Ultrastructural characterization of synaptic terminals of association and olfactory bulb afferent fibers. *Journal of Comparative Neurology*, *219*(4), 448-460.

Haberly, L. B., & Feig, S. L. (1983). Structure of the piriform cortex of the opossum. II. Fine structure of cell bodies and neuropil. *Journal of Comparative Neurology*, *216*(1), 69-88.

Haberly, L. & Price, J. (1978). Association and commissural fiber systems of the olfactory cortex of the rat I. Systems originating in the piriform cortex and adjacent areas. *Journal of Comparative Neurology. 178 :* 711-740.

Haberly, L. & Price, J. (1978). Association and commissural fiber systems of the olfactory cortex of the rat II. Systems originating in the olfactory peduncle. *Journal of Comparative Neurology. 181:* 781-808.

Hinds, J. W., & Hinds, P. L. (1976). Synapse formation in the mouse olfactory bulb Quantitative studies. Journal of Comparative Neurology, 169(1), 15-40.

Huttenlocher, P. R., & Dabholkar, A. S. (1997). Regional differences in synaptogenesis in human cerebral cortex. *Journal of comparative Neurology*, *387*(2), 167-178.

Illig, K. R., & Eudy, J. D. (2009). Contralateral projections of the rat anterior olfactory

nucleus. *Journal of Comparative Neurology*, *512*(1), 115-123.

Kikuta, S., Sato, K., Kashiwadani, H., Tsunoda, K., Yamasoba, T., & Mori, K. (2010). Neurons in the anterior olfactory nucleus pars externa detect right or left localization of odor sources. *Proceedings of the National Academy of Sciences*, *107*(27), 12363-12368.

Kucharski, D., Burka, N., & Hall, W. G. (1990). The anterior limb of the anterior commissure is an access route to contralateral stored olfactory preference memories. *Psychobiology*, *18*(2), 195-204.

Logan, D., Brunet, L., Webb, W., Cutforth, T., Ngai, J., Stowers, L. (2012). Learned recognition of maternal signature odors mediates the first suckling episode in mice. *Current Biology. 22*(21)1998-2007.

Lopez-Mascaraque, L., & De Castro, F. (2002). The olfactory bulb as an independent developmental domain. *Cell death and differentiation*, *9*(12), 1279.

Meyer, E. A., Illig, K. R., & Brunjes, P. C. (2006). Differences in chemo-and cytoarchitectural features within pars principalis of the rat anterior olfactory nucleus suggest functional specialization. *Journal of Comparative Neurology*, *498*(6), 786-795.

Mori, K. (2014). Odor Maps in the Olfactory Bulb. In *The Olfactory System* (pp. 59-69). Springer Japan.

Rakic, P., Bourgeois, J. P., Eckenhoff, M. F., Zecevic, N., & Goldman-Rakic, P. S. (1986). Concurrent overproduction of synapses in diverse regions of the primate cerebral cortex. *Science*, *232*, 232-236

Schikorski, T., & Stevens, C. F. (1999). Quantitative fine-structural analysis of olfactory cortical synapses. *Proceedings of the National Academy of Sciences*, *96*(7), 4107-4112.

Schwob, J. E., & Price, J. L. (1984). The development of axonal connections in the central olfactory system of rats. *Journal of Comparative Neurology*, *223*(2), 177-202.

Sur, M., & Leamey, C. A. (2001). Development and plasticity of cortical areas and networks. *Nature reviews. Neuroscience*, *2*(4), 251.

Walz, A., Omura, M., & Mombaerts, P. (2006). Development and topography of the lateral olfactory tract in the mouse: Imaging by genetically encoded and injected fluorescent markers. *Developmental Neurobiology. 6*(8): 835-846.

Westrum, L. E. (1975). Electron microscopy of synaptic structures in olfactory cortex of early postnatal rats. *Journal of neurocytology*, *4*(6), 713-732.

Table 1

Synaptic Density (synapses/um²)

	Ia			*Ib*			*IIa*			*IIb*		
	Mean	*SD*	*Range*	*Mean*	*SD*	*Range*	*Mean*	*SD*	*Range*	*Mean*	*SD*	*Range*
P5	3.18E-10	1.14E-10	2.17E-10	3.71E-10	3.55E-11	6.30E-11	2.59E-10	9.62E-11	1.74E-10	3.06E-10	6.80E-11	1.32E-10
P13	5.72E-10	2.67E-10	5.03E-10	5.39E-10	1.47E-10	2.89E-10	4.95E-10	1.03E-10	1.85E-10	5.29E-10	1.03E-10	1.79E-10
P17	4.35E-10	3.90E-11	6.80E-11	4.33E-10	1.48E-10	2.93E-10	7.64E-10	2.78E-10	5.24E-10	6.13E-10	9.55E-11	1.90E-10
P30	6.42E-10	3.63E-10	6.42E-10	5.12E-10	1.02E-10	1.87E-10	5.95E-10	1.42E-10	2.82E-10	5.55E-10	9.66E-11	1.94E-10

Synapse Length (nm)

	Ia				*Ib*				*IIa*				*IIb*			
	n	*Mean*	*SD*	*Range*	*n*	*Mean*	*SD*	*Range*	*n*	*Mean*	*SD*	*Range*	*n*	*Mean*	*SD*	*Range*
P5	67	297.3	140.4	700.6	44	264.9	133.1	592.9	44	264.2	106.5	131.4	52	261.1	125.8	592.9
P13	85	278.2	113.7	502.5	98	272.0	111.1	631.5	87	246.6	89.52	382.4	95	263.4	139.6	804.6
P17	123	286.0	134.2	713.3	99	292.3	135.3	836.3	901	234.1	84.62	455.3	106	248.9	99.8	591.0
P30	168	282.8	131.1	888.2	148	285.8	135.5	916.5	150	310.0	136.5	801.8	140	297.8	120.5	649.5

Terminal Area (um²)

	Ia				*Ib*				*IIa*				*IIb*			
	n	*Mean*	*SD*	*Range*	*n*	*Mean*	*SD*	*Range*	*n*	*Mean*	*SD*	*Range*	*n*	*Mean*	*SD*	*Range*
P5	50	306.15	229.24	1343	33	347.85	224.08	1254	67	285.2	158.3	656.8	41	309.54	214.99	925
P13	54	286.81	298.06	1485	71	306.66	205.44	983	43	352.3	171.4	659.6	64	264.44	136.27	602
P17	102	341.18	242.71	1069	68	336.38	276.61	1249	75	344.0	221.7	872.5	58	274.45	191.19	976
P30	99	365.89	286.67	778	86	315.75	249.54	1284	59	213.0	158.2	675.7	70	310.43	231.08	1386

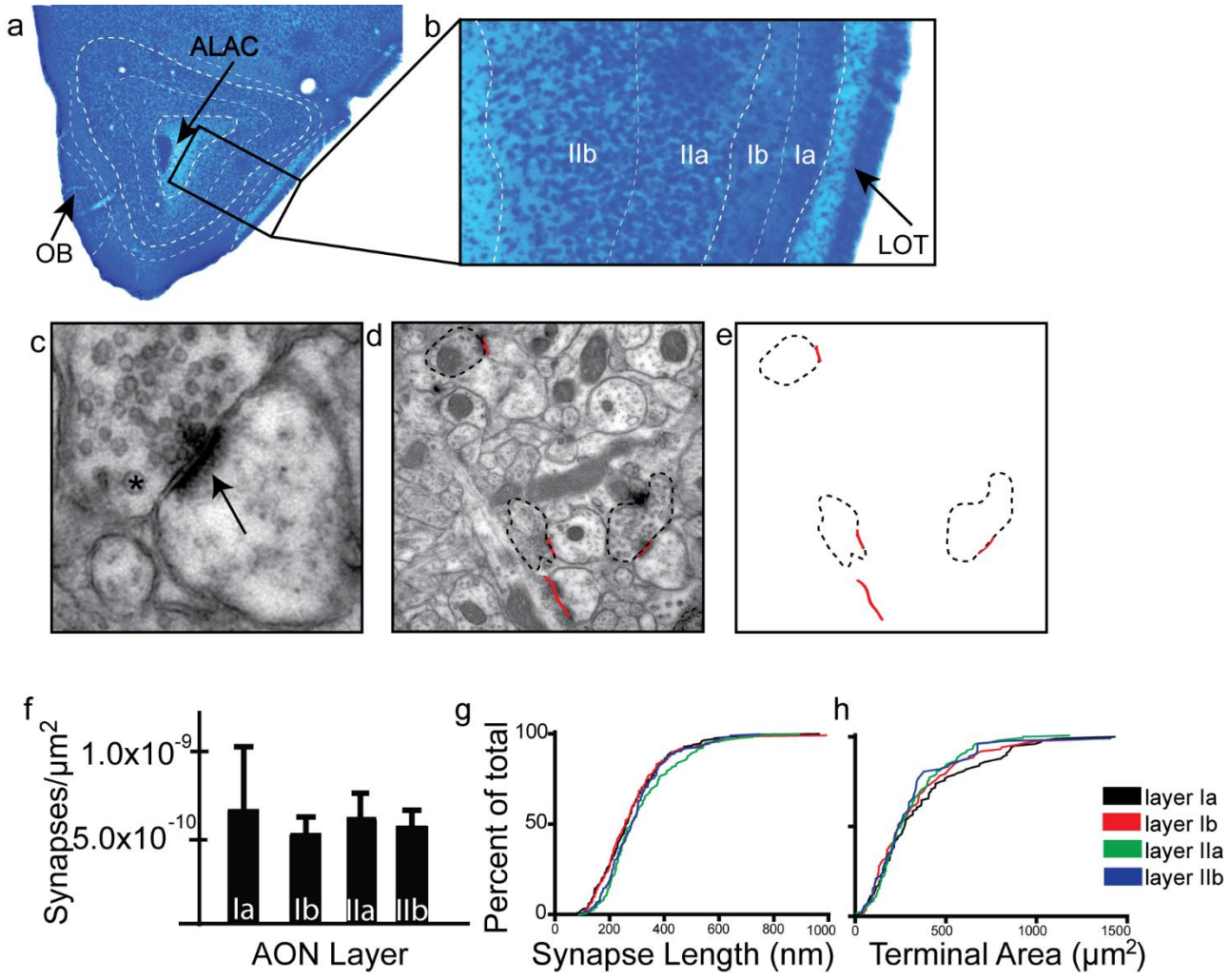

Figure 1 Synapse development in the anterior olfactory nucleus (AON) pars lateralis. A. The AON emerges caudal to the olfactory bulb (OB) as a laminated cortical structure wrapping around the anterior limb of the anterior commissure (ALAC). B. The AON has been divided into four layers: Ia, a superficial plexiform layer lying adjacent to the lateral olfactory tract (LOT); Ib, a deeper plexiform layer; IIa, a superficial, densely-packed cell layer; and IIb, a deeper cell layer. Synaptic development was compared across these four layers in pars lateralis. C.Existence of an asymmetric synapse was determined by the presence of presynaptic vesicles (asterisk), a synaptic cleft, and a postsynaptic

density (arrow). D-E. Synapses (red lines) and presynaptic terminals (dotted black lines) were traced for each electron micrograph for quantification of synaptic development. In P30 animals, no differences were observed in synapse density (F), length (G), or terminal area (H) between layers. Error bars represent standard deviation.

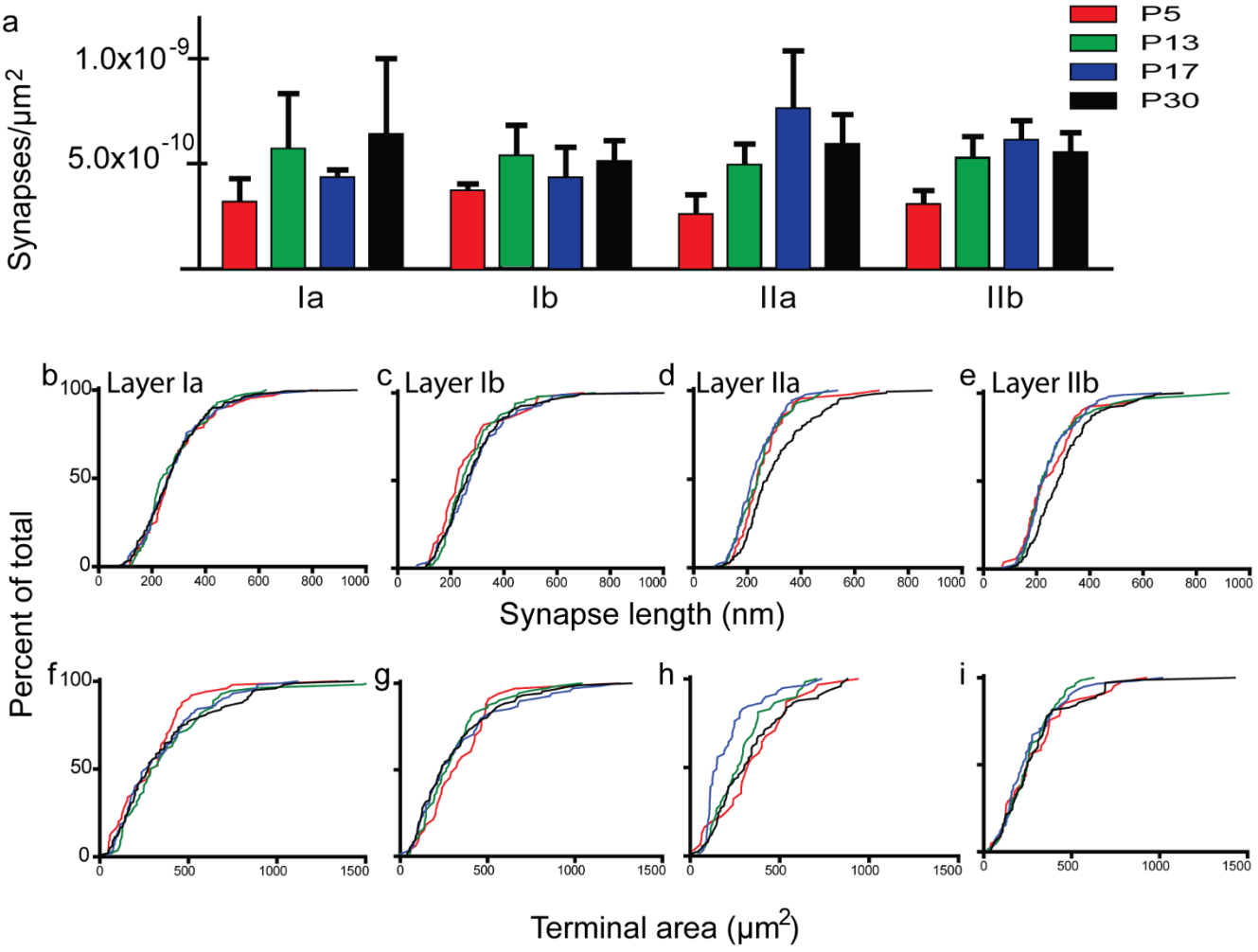

Figure 2 Developmental comparison of synapses in the AON. For all graphs, P5 data are presented in red, P13 in green, P17 in blue, and P30 in black. A. In layer Ia, synapse density considerably varied across samples and did not significantly change across the period examined. Similarly, in layer Ib, no significant changes occurred across time. In both layer IIa and b, synapse density increased through P17 before decreasing at P30. Error bars represent standard deviation. B-I. Cumulative frequency histograms for synapse length (B-E) and terminal area measurements (F-I) in each layer across time. Note that there is little difference in either measure between ages in

layer I. In layer IIa, both synapse length and terminal area measurements were significantly different at P30 compared to younger ages. Interestingly, at P5 terminal area in this layer resembles that of P30, indicating that the first synapses to be formed within layer IIa are large. In layer IIb, longer synapses were observed in P30 compared to younger ages.

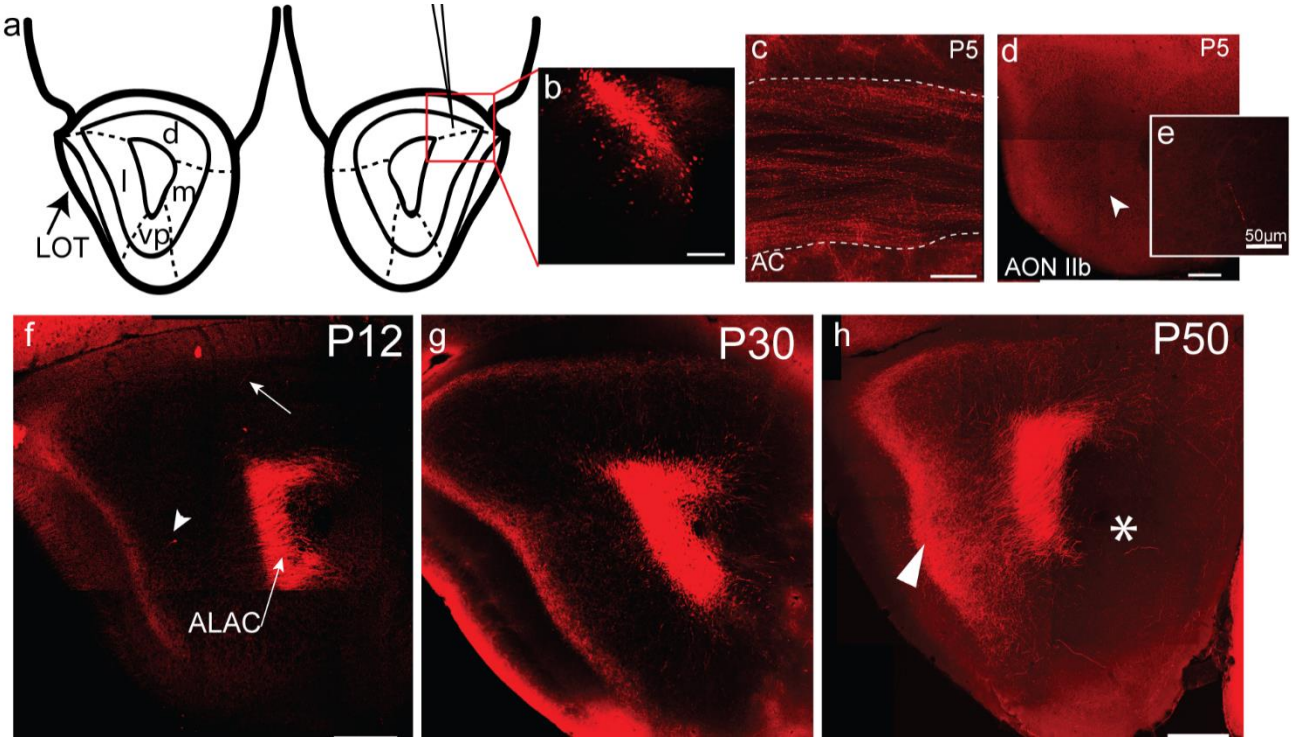

Figure 3 Visualization of contralateral projections in the anterior olfactory nucleus (AON). A. Injections of AAV were made into the right AON at the junction between pars lateralis and dorsalis, producing strong cell body labeling at the injection site (B) L=pars lateralis, d=pars dorsalis, m=pars medialis, vp=pars ventroposterior, LOT=lateral olfactory tract. C. As early as P5, several labeled fibers can be seen coursing across the midline via the anterior commissure (AC). Dotted lines represent borders of the AC. D. At this young age very few labeled fibers have reached the contralateral AON. Arrowhead represents approximate location of magnified fiber depicted in (E). F. By P12, fibers within the anterior limb of the AC are strongly labeled and a band of labeled fibers can be seen in the contralateral AON pars lateralis. At P12 very few instances of labeled fibers extend into pars dorsalis (arrow). Some retrograde labeling occurred with AAV injections, evidenced by labeled cell bodies (arrowhead). ALAC=anterior limb of the anterior commissure. G. At P30 labeled fibers are distributed throughout layer Ib/IIa

of both pars lateralis and dorsalis. H. Between P30 and P50 the band of labeled fibers in pars lateralis thickens (arrowhead), indicating that fibers from the contralateral AON continue to enter layer Ib and IIa. Labeling is still restricted to lateralis and dorsalis, with little labeling in ventroposterior and sparse labeling in medialis (asterisk). Scale bars = 100μm.

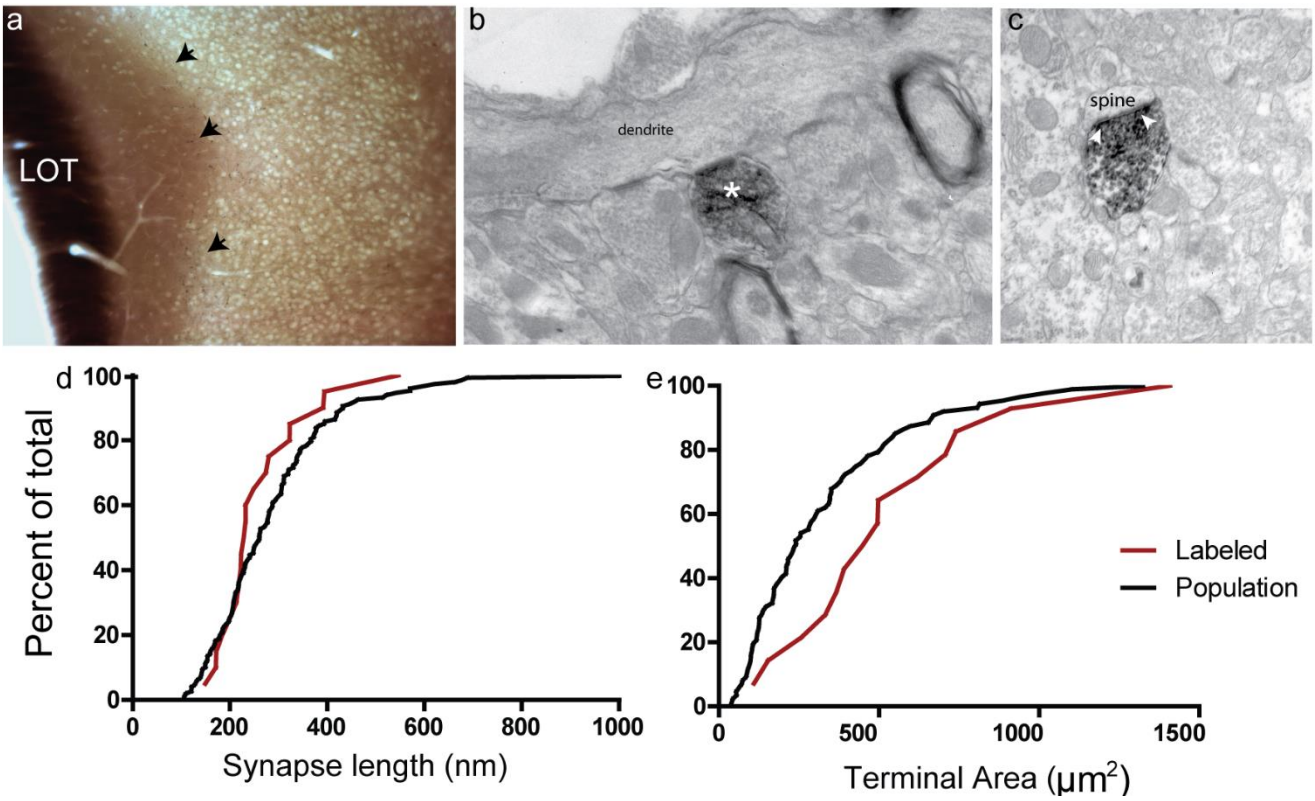

Figure 4 Anterograde labeling in the anterior olfactory nucleus (AON). A. BDA injections into the right AON produced some axonal and terminal labeling in the contralateral AON. Terminal labeling was restricted to the border between layer Ib and IIa (arrowheads). Labeled terminals were visualized using electron microscopy (B-C). B. Labeled axon terminals (asterisk) were found making contact with both dendritic shafts (B) and spines (C). D. Synapse length did not differ between labeled terminals and population data. E. Anterogradely labeled terminals were larger than the population, suggesting that these terminals might play a strong role in shaping olfactory signals within the AON.

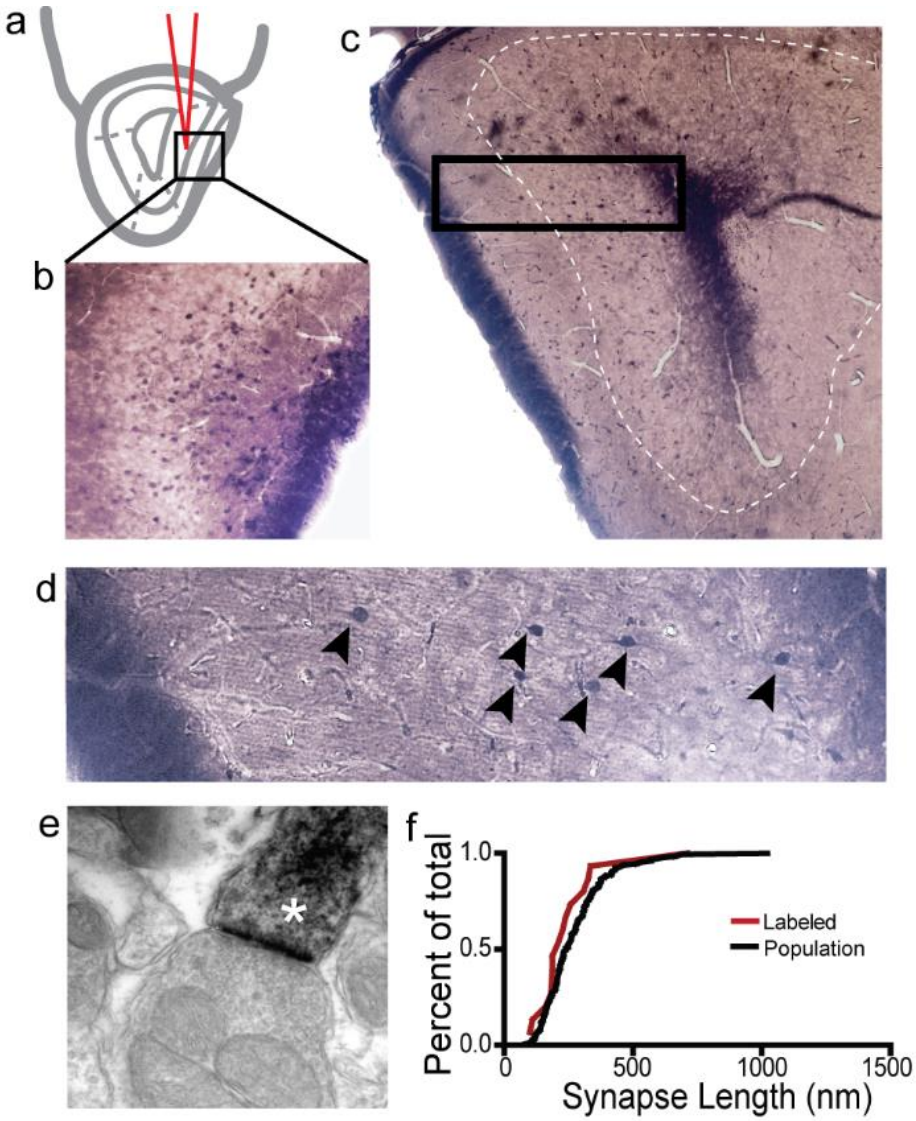

Figure 5 Retrograde tracing in the anterior olfactory nucleus (AON). A. BDA was injected into the right AON pars lateralis. B. Representative DAB-stained section of injection site. C. Retrograde labeling of AON fibers filled cell bodies in the contralateral AON. Dotted white line represents border between layer I and II. Area within black box is magnified in (D). D. Labeled cell bodies were found distributed throughout layer II. E. Example of BDA-labeled postsynaptic terminal (asterisk). F. Synapses of labeled postsynaptic terminals were found in layer I and synapse length did not differ between groups.

Chapter V

General Discussion

The work presented in the previous chapters represents the first comparison of the temporal relationship between myelination of the LOT and AC and synaptogenesis in the AON. Olfactory processing relies heavily on precise timing of information transfer (Schusterman et al., 2011) and myelination can change axonal conduction velocity as much as 50 fold (Aggarwal et al., 2010), making proper myelination essential for efficient olfactory processing. Synaptogenesis represents the onset of neural activity but it is unclear to what extent it is required for initiation of myelination. As such, this work offers insight into olfactory system circuitry and development as well as CNS myelination.

Olfactory system circuitry

The olfactory system is organized to allow animals to rapidly detect, localize, and discriminate between complex stimuli. Primary sensory neurons arranged topographically within the nasal mucosa allow for detection of olfactory stimuli and project to the OB in a rough topographic code. Projections out of the OB innervate olfactory cortical regions in a much less well-defined fashion. Terminal fields of axons in the AON, anterior PC, and posterior PC are progressively larger and overlap more. This organization suggests that the olfactory signals converge and are integrated in more caudal processing centers (Brunjes et al., 2005). The AON has been proposed to play a large role in odor localization based on evidence that cells within pars Externa, a subregion within the AON, are inhibited by odor presentation to the contralateral naris (Kituta et al., 2010). The larger component of the AON, pars Principalis, is likely also heavily involved in integration of olfactory information and thus vital for discrimination or localization of odors. The AON sends and receives both contralateral input as well as

associational connections between ipsilateral olfactory processing regions (Luskin and Price, 1983; Haberly and Price, 1978), setting it up for heavy involvement in refinement of olfactory information.

Mass information transfer within the olfactory system is accomplished via the LOT and AC. Chapter 2 highlighted structural differences between the two tracts that doubtlessly contribute to differences in speed of information transfer between olfactory processing areas. The LOT consists of large-caliber, heavily myelinated axons that provide fast information transfer and allow for immediate odor detection. The AC contains thinly myelinated, small-caliber axons. As such, the AC has a significantly slower conduction velocity (Mori et al., 1978; Schwob et al., 1984) and provides a pathway for refinement of olfactory signals through interhemispheric connections between the OB, AON, and PC.

Chapter 4 provided further insight into olfactory circuitry by confirming that ipsilateral and contralateral input into the AON are segregated into tight bands in layer Ia and b, respectively. Furthermore, reciprocal connections may exist between the AON in each hemisphere. After an injection into the AON, retrograde and anterograde labeling were both seen in layer Ib, indicating that the same region that sends contralateral projections also receives contralateral input. It is possible that reciprocal communication allows for refinement of olfactory signals or for odor localization.

Olfactory system development

Chapter 2 and 4 also demonstrated significant differences in developmental trajectory between the LOT and AC. The LOT carries olfactory information earlier in the sensory processing stream (from second-order neurons in the OB to olfactory cortices)

and develops earlier than the AC, which carries information across hemispheres for subsequent processing. Results presented in chapter 2 demonstrate that myelination onset in the LOT occurs 3-4 days earlier than in the AC. In the LOT MBP+ nascent myelin sheaths are present as early as P7 and fully myelinated fibers are observed by P9. In the AC MBP is not expressed until P11 and the first fully myelinated fibers do not appear until P13. Findings presented in chapter 4 confirm that development of afferent synapses precedes that of association synapses within the AON. Synapses in layer Ib, which receives primarily contralateral innervation, reached a mature state later than those in layer Ia, which contains terminals of afferent fibers from the OB. This pattern may indicate that commissural and associational connections are more heavily involved in processes important later in life, such as forming rich odor percepts and memories (Wilson et al., 2006).

Activity-dependent myelination

The results of Chapters 2 and 4 suggest that neural activity is required for myelination onset in the LOT and AC. Findings presented in chapter 4 demonstrate that adult-like distribution of synapses is achieved in layer Ib as early as P5. Interhemispheric communication via the AC is established by P12 (Kucharski and Hall, 1987). Rapid myelination is observed subsequently (~P13-17). Based on the temporal relationship of synaptogenesis and rapid myelination, it is likely that myelination of the AC is dependent upon synaptic activity originating in the contralateral AON. Further evidence for activity-dependent myelination of the LOT was reported in Chapter 2. Most strikingly, decreasing primary olfactory input via unilateral naris occlusion resulted in

thinner myelin sheaths within the LOT, indicating that development and/or maintenance of myelination is dependent upon sufficient amounts of neural activity.

Previous work has hinted that neural activity is required for white matter tract development in the olfactory system. For example, in genetically engineered mice lacking mitral cells (the main output cells of the OB) myelination of the LOT is dramatically reduced (Bartolomei and Greer, 1998) and the AC undergoes extensive degeneration (Recio et al, 2007). Synaptic activity has been shown to drive myelination onset *in vitro* (Demerens et al., 1996) and *in vivo* (Gibson et al., 2014). Our results suggest that synapse formation is required before myelination onset can occur within olfactory system white matter tracts.

Usefulness of LOT and AC in examining CNS myelination

Results from chapter 2 and 3 point to the LOT and AC as particularly useful regions for studying CNS myelination. Both tracts are large, accessible, and carry sensory information. As such, experimental manipulation is relatively easily accomplished. Importantly, the two tracts are contained within the same sensory system but differ in several ways. The LOT develops significantly earlier, is more susceptible to sensory deprivation, and recovers more quickly after a demyelinating insult. The olfactory system could be set up in such a way that allows the LOT to be more responsive to changes occurring as a result of damage as well as experiential changes in order to maintain tight regulation of signaling of primary olfactory information to the cortices.

Concluding Remarks

The work presented here provides novel findings on olfactory system development and circuitry as well as a groundwork for future studies. First, differences between the LOT and AC in response to sensory deprivation at adulthood could suggest that decreased sensory input either 1) differentially affects maturation of the tracts or 2) alters the mature state of the LOT due to a decreased demand for ipsilateral information transfer. Future studies should examine the maturation of the LOT and AC after naris occlusion to determine whether the effects observed in the present work can be explained developmentally. Additionally, differences in response to a demyelinating toxin imply that the cellular environment of the LOT is more conducive to myelin repair. It is possible that a larger microglial and/or precursor cell population contributes to more efficient remyelination. Future research should specify the mechanisms by which remyelination proceeds differently between these two related tracts in order better understand what CNS environments are most conducive to remyelination. Finally, reciprocal innervation of the AON should be investigated to better understand the role of the AON in integrating olfactory information.

Literature Cited

Aggarwal, S., Yurlova, L., & Simons, M. (2011). Central nervous system myelin: structure, synthesis and assembly. *Trends in cell biology*, *21*(10), 585-593.

Bartolomei, J. C., & Greer, C. A. (1998). The organization of piriform cortex and the lateral olfactory tract following the loss of mitral cells in PCD mice. *Experimental neurology*, *154*(2), 537-550.

Brunjes, P. C., Illig, K. R., & Meyer, E. A. (2005). A field guide to the anterior olfactory nucleus (cortex). *Brain research reviews*, *50*(2), 305-335.

Demerens, C., Stankoff, B., Logak, M., Anglade, P., Allinquant, B., Couraud, F., ... & Lubetzki, C. (1996). Induction of myelination in the central nervous system by electrical activity. *Proceedings of the National Academy of Sciences*, *93*(18), 9887-9892.

Gibson, E. M., Purger, D., Mount, C. W., Goldstein, A. K., Lin, G. L., Wood, L. S., ... & Barres, B. A. (2014). Neuronal activity promotes oligodendrogenesis and adaptive myelination in the mammalian brain. *Science*, *344*(6183), 1252304.

Haberly, L. B., & Price, J. L. (1978). Association and commissural fiber systems of the olfactory cortex of the rat. I. Systems originating in the piriform cortex and adjacent areas. *Journal of Comparative Neurology*, *178*(4), 711-740.

Kikuta, S., Sato, K., Kashiwadani, H., Tsunoda, K., Yamasoba, T., & Mori, K. (2010). Neurons in the anterior olfactory nucleus pars externa detect right or left localization of odor sources. *Proceedings of the National Academy of Sciences*, *107*(27), 12363-12368.

Kucharski, D., & Hall, W. G. (1987). New routes to early memories. *Science*, *238*(4828), 786-788.

Luskin, M. B., & Price, J. L. (1983). The topographic organization of associational fibers of the olfactory system in the rat, including centrifugal fibers to the olfactory bulb. *Journal of comparative neurology*, *216*(3), 264-291.

Mori, K., & Takagi, S. F. (1978). An intracellular study of dendrodendritic inhibitory synapses on mitral cells in the rabbit olfactory bulb. *The Journal of physiology*, *279*, 569.

Recio, J. S., Weruaga, E., Gomez, C., Valero, J., Brinon, J. G., & Alonso, J. R. (2007). Changes in the connections of the main olfactory bulb after mitral cell selective neurodegeneration. *Journal of neuroscience research*, *85*(11), 2407-2421.

Schwob, J. E., Haberly, L. B., & Price, J. L. (1984). The development of physiological responses of the piriform cortex in rats to stimulation of the lateral olfactory tract. *Journal of Comparative Neurology*, *223*(2), 223-237.

Shusterman, R., Smear, M. C., Koulakov, A. A., & Rinberg, D. (2011). Precise olfactory responses tile the sniff cycle. *Nature neuroscience*, *14*(8), 1039-1044.

Wilson, D. A., Kadohisa, M., & Fletcher, M. L. (2006, August). Cortical contributions to olfaction: plasticity and perception. In *Seminars in cell & developmental biology* (Vol. 17, No. 4, pp. 462-470). Academic Press.